MSc in Biomedical Science (Research)

The Development of Novel Hydrogel Composites for Use in Bone Tissue Engineering

Daniel Ward

September 2020

Division of Biomedical & Life Sciences

Faculty of Health and Medicine

Lancaster University

Contents

Acknowledgements

First, I would like to thank my supervisors, Dr. Timothy Douglas and Dr. Nigel Fullwood, for their continued patience, guidance and support throughout the completion of this project. I would also like to thank Aleksandra Benko (AGH University of Science and Technology, Poland), Valerie Vanhoorne (Ghent University, Belgium), Krzysztof Pietryga (AGH University of Science and Technology, Poland), Raechelle D'Sa and Jenny Hanson (University of Liverpool, United Kingdom) and Susan Clarke (Queen's University Belfast, United Kingdom), Radmila Kudlackova (Czech Academy of Sciences, Czech Republic) and Stefanie Riedel (Leibnitz Institute of Surface Modifications, Germany) for their collaborations which made this research possible.

Declaration

This thesis is submitted to Lancaster University in accordance with the requirements of the degree of Master of Science in the department of Biomedical and Life Sciences. I can confirm that this thesis has not been submitted for any other degree of any examining body

List of Tables

List of Figures

Glossary

Abbreviation	Meaning
µl	Microlitre
%	Percent
°C	Degrees Celsius
µm	Micrometre
3D	Three Dimensional
a.u	Absorbance Units
ALP	Alkaline Phosphatase
ANOVA	Analysis of Variance
ASC	Adipose Tissue derived Stem Cells
ATR	Attenuated Total Reflectance
bFGF	Basic Fibroblast Growth Factor
BMPs	Bone Morphogenetic Proteins
BMUs	Bone Metabolic Units
BTE	Bone Tissue Engineering
Ca^{2+}	Calcium Ions
$CaCl_2$	Calcium Chloride
CaGP	Calcium Glycerophosphate
CaP	Calcium Phosphate
CDHA	Calcium Deficient Hydroxyapatite
CFU	Colony Forming Unit
cm	Centimetre
cm^{-1}	Reciprocal centimetre (wavenumber)
CNTs	Carbon Nanotubes
Co	Cobalt
CO_2	Carbon Dioxide
CO_3^{2-}	Carbonate
CPEG	Catechol-derivatized Polyethylene Glycol
Cr	Chromium
ddH_2O	Double Distilled Water
DMEM	Dulbecco's Modified Eagle's Medium
DNA	Deoxyribonucleic Acid
ECM	Extracellular Matrix
FBS	Foetal Bovine Serum
Fe	Iron
FGFs	Fibroblast Growth Factors
FT-IR	Fourier-Transform Infrared Spectroscopy
GA	Gallic Acid
GP	Glycerophosphate
GTA	Glutaraldehyde
H_2O	Water
HA	Hydroxyapatite
HMDS	Hexamethyldisilazane
HNO_3	Nitric Acid
HPO_4^{2-}	Monohydrogen Phosphate
ICP-OES	Inductively Coupled Plasma Optical Emission Spectrometry
IGF	Insulin-Like Growth Factor

IL-1	Interlukin-1
IL-6	Interlukin-6
IU/ml	International units per Millilitre
IV	Intravenous
KBR	Potassium Bromide
kGy	KiloGrays
M	Molar
mA	Milliampere
mg	Milligram
MG-63	Human Osteosarcoma Cell Line (Osteoblast-like cells)
MIR	Middle Infrared Region
ml	Millilitre
mm	Millimetre
MMPs	Matrix Metalloproteinases
Mo	Molybdenum
MSCs	Mesenchymal Stromal Cells/Mesenchymal Stem Cells
MTS Assay	Cell Proliferation Assay
mW	Megawatt
MWCNTs	Multi-walled Carbon Nanotubes
N	Newton
Na_2HPO_4	Sodium Phosphate
Ni	Nickel
nm	Nanometre
NPs	Nanoparticles
P	Phosphorus
PBS	Phosphate Buffered Saline
PCL	Poly-Caprolactone
PDGF	Platelet Derived Growth Factor
PEG	Polyethylene Glycol
PFA	Paraformaldehyde
PG	Phloroglucinol
PGA	Poly Glycolic acid
PGs	Proteoglycans
pH	Potential of Hydrogen
PHEMA	Poly-2-hydroxyethylmethacrylate
PLA	Poly Lactic Acid
PLLA	Poly L-Lactic Acid
PO_4^{2-}	Phosphate
PS	Polystyrene
PTH	Parathyroid Hormone
RGD	Arginine-glycine-aspartate tr-amino acid sequence
rpm	Revolutions per Minute
SBDs	Segmental Bone Defects
SBF	Simulated Body Fluid
SEM	Scanning Electron Microscopy
SWCNTs	Single-walled Carbon Nanotubes
TCP	Tricalcium Phosphate
TEM	Transmission Electron Microscopy
TGF- β	Transforming Growth Factor Beta
Ti	Titanium

TNF-α	Tumour Necrosis Factor Alpha
UV	Ultraviolet
VEGFs	Vascular Endothelial Growth Factors
w/v	Weight/Volume
WPI	Whey Protein Isolate
α-LA	Alpha-Lactalbumin
β-LG	Beta-Lactoglobulin
σC	Compressive Stress

Abstract

Objectives

Hydrogels are gaining interest as biomaterials in bone tissue engineering (BTE). However, hydrogels must be mechanically stable, receptive to mineralisation, non-cytotoxic and support adhesion and growth of bone forming cells. Ease of sterilisation and antibacterial activity are also desirable.

This study evaluated the extent to which three hydrogels fulfilled these criteria:

1. Electron irradiated Gelatin hydrogels supplemented with Alkaline Phosphatase (ALP)
2. Whey Protein Isolate (WPI) hydrogels supplemented with Phloroglucinol (PG)
3. WPI hydrogels supplemented with Carbon Nanotubes (CNTs)

Methods

Gelatin hydrogels were crosslinked using electron beam irradiation and subject to ALP-mediated mineralisation. Mineralisation was evaluated by spectroscopic and microscopical techniques. Mechanical properties were examined via compressive testing. Cytocompatibility was assessed using osteoblast-like MG-63 cells.

Similarly, 40% WPI solution was supplemented with CNTs or PG prior to simultaneous hydrogel fabrication and sterilisation by autoclaving. Antibacterial properties of WPI-CNT hydrogels were assessed using *Staphylococcus aureus.* Cell viability was assessed against Human Foetal Osteoblast (hFOB; WPI-CNT only) and MG-63 cells. Surface topography and molecular structures were evaluated microscopically and spectroscopically. The effect of CNT/PG supplementation on mechanical properties was also evaluated.

Results

Calcium phosphate (CaP) deposits were successfully formed in gelatin-ALP hydrogels, which coincided with an elevated compressive modulus. Importantly, electron beam-crosslinked hydrogels, both mineralized and unmineralized, supported MG-63 cell adhesion and proliferation.

Both CNTs and PG were successfully incorporated into WPI hydrogels. CNTs interacted with WPI and increased stiffness, but not compressive strength, of hydrogel composites. PG concentration had little impact on hydrogel mechanical properties. Importantly, WPI-CNT hydrogels exhibited antibacterial activity and supported growth of MG-63 cells. However, MG-63 viability appeared to reduce with increasing PG concentration.

Conclusions

The successful supplementation of hydrogels with additives to confer desirable properties, coupled with the practicality of simultaneous fabrication and sterilisation, demonstrates their applicability in BTE and future research in this space.

Chapter 1: Introduction

1.0 Introduction

In the past, surgery conducted on the human body primarily took place in the absence of additives, such as implants, which are now available to facilitate surgical interventions. Since then, advancements in the understanding of human anatomy, coupled with the identification of materials compatible with the body, has driven an increase in the demand for medical implants (Axinte et al.,2019; Saptaji et al., 2018). These materials, termed Biomaterials, are either natural or engineered substances that can interact with biological systems to therapeutic effect. Implanted materials may be utilised as short term, long term, or permanent aids to treat, repair, or replace biological tissue in numerous applications including drug delivery systems, the cardiovascular system, and orthopaedics, which is the focus of the present study (Bartolo et al., 2012; Khan et al., 2014; Mitsuishi et al., 2013).

1.1 Bone Tissue - A Natural Composite

As the average life-expectancy and chronological age of the worldwide population increases, the incidence of bone related disorders and conditions has elevated considerably. This is of particular significance in populations where obesity and insufficient physical activity coincides with aging. Even though bone is a dynamic vascularised tissue with the capability to heal naturally in response to damage, hundreds of millions of surgical procedures are performed globally, each year, to correct severe bone lesions (Maisani et al., 2017). Recently, research into bone tissue engineering (BTE) has led to improvements in both surgical techniques and orthopaedic implants. However, skeletal conditions remain undertreated.

Bone, along with muscles, ligaments, tendons, the nervous system and other soft tissue forms the musculoskeletal system. These components work synergistically to perform the primary functions of this system – mechanical support, facilitation of regular movement, and the protection of vital organs. Specifically, bone is a natural living connective tissue which, by

weight, is comprised of approximately 30% matrix, 60% mineral and 10% water (Athanasiou et al., 2000). Typically, this cellularised composite is split into two main components: inner spongy bone and outer dense bone. These are known as cancellous or trabecular bone and cortical bone, respectively. In the skeletal system, the relative mass ratio of these two types of bone is 20% to 80% in favour of cortical bone.

1.1.1 Cortical Bone

The basic structural units which comprise cortical, or compact, bone are cylindrical structures with approximate diameters and lengths of 200μm and 400μm, respectively. These structures are known as osteons, or haversian systems, and possess channels within them (haversian canals) which contain blood vessels encompassed by concentric lamellae of mineralised matrix. Lacunae, small cavities within the mineralised matrix, each with an osteocyte present, are connected to the haversian canals by a network of small channels known as canaliculi. This facilitates cell-to-cell interactions and allows the exchange of nutrients and metabolites (Maisani et al, 2017).

1.1.2 Cancellous Bone

Like cortical bone, cancellous bone is composed of lamellae. However, in contrast, the lamellae of cancellous bone are organised into a honeycomb-like network, loosely structured and void of internal canals and blood vessels. In fact, only 15 to 20% of trabecular bone volume is occupied by bone tissue. Most of the trabecular network is occupied by bone marrow which, itself, consists of blood vessels, nerves, and several other cell types that provide nutrients to trabecular osteocytes (Maisani et al, 2017).

1.1.3 Bone Extracellular Matrix (ECM)

The bone extracellular matrix (ECM) is broadly characterised by an organic protein phase and an inorganic mineral containing phase. Despite the presence of calcium carbonate, calcium fluoride and magnesium fluoride, the inorganic mineral component of bone tissue consists

primarily of embedded hydroxyapatite (HA; $Ca_{10}(PO_4)_6(OH)_2$) crystals, which confers stiffness and compressive strength to bone. Additionally, the inorganic component of bone is implicated strongly in the homeostasis of ions, as up to 99% of calcium and 88% of phosphate in the human body is encompassed within it (Driessens et al., 1978; Sasaki et al., 1989).

The organic phase is comprised primarily (approximately 90%) of type I collagen organised into a network of triple helices, which subsequently form fibrils. The remaining 10% consists of supplementary proteins, such as proteoglycans (PGs), growth factors, and glycoproteins. Whereas the mineral component imparts compressive strength, the organic ECM provides numerous structural roles. It regulates the shape of bone by controlling the nucleation and direction of HA crystals, is responsible for fracture resistance and tensile strength (Maisani et al., 2017; Sheikh et al., 2015), and, importantly, acts as a reservoir for cytokines and growth factors which are necessary for the repair and remodelling of bone tissue.

In addition to these primary components, the previously mentioned non-collagenous proteins confer important functions to bone tissue. For example, PGs impart the ability to resist compressive stress as they form a highly hydrated, swollen gel-like matrix. They also fulfil roles in the binding and storage of growth factors and in the regulation of fibrillogenesis (Lamoureux et al., 2007). Glycoproteins of the bone ECM, such as alkaline phosphatase (ALP), osteocalcin and osteopontin, provide similarly important roles, as they are involved directly in the process of bone mineralisation (Maisani et al., 2017).

1.2 Natural Bone Healing

As previously stated, bone is a dynamic tissue. As such, it continually adapts during vertebrate life to first achieve, and subsequently maintain, skeletal size, shape, structural integrity, and to regulate mineral homeostasis (Raggatt and Partridge, 2010). This continual adaptation is underpinned by two processes: modelling and remodelling.

1.2.1 Bone Modelling

Bone modelling occurs primarily during childhood and adolescence, as it is the process responsible for bone growth and the coordination of mechanically induced transformations in bone shape. For this to happen, it is necessary for the processes of bone formation and bone resorption to occur independently, at discrete locations (Maisani et al., 2017; Raggatt and Partridge, 2010).

1.2.2 Bone Remodelling

Bone remodelling is a continuous process which occurs in response to damaged bone. This includes the removal, repair and renewal of bone tissue to maintain the strength and integrity of the skeletal system, whilst ensuring mineral homeostasis (Raggatt and Partridge, 2010). This process is tightly regulated by the synergistic action of an ensemble of cell types including bone forming osteoblasts and bone resorbing osteoclasts, arranged within temporary bone remodelling structures named basic multicellular units or bone metabolic units (BMUs; Maisani et al., 2017; Raggatt and Partridge, 2010).

1.2.2.1 Activation Phase

Bone remodelling can be initiated in response to numerous signals. Stimulatory signals can originate from structural damage resulting from direct mechanical strain, or via hormonal stimuli in response to systemic fluctuations in homeostasis (Raggatt and Partridge, 2010). Mechanical stimuli are detected by osteocytes which, ultimately, translate it into biological signals that result in bone remodelling initiation (Bonewald, 2007). Specifically, damage, such as damage to the bone matrix or limb immobilisation, results in osteocyte apoptosis and increased osteoclastogenesis (Aguirre et al., 2006; Verborgt et al., 2002). Osteoclastogenesis, under basal conditions, is inhibited by the secretion of transforming growth factor β (TGF- β) by osteocytes. Following focal apoptosis of osteocytes, local TGF- β levels fall below the minimum inhibitory concentration. Therefore, osteoclastogenesis signals can stimulate osteoclast formation (Heino et al., 2002). Hormonal initiation of bone

remodelling can involve hormones such as oestrogen or the parathyroid hormone (PTH), which maintains calcium homeostasis. Similarly, inactive osteoblasts located in bone lacunae function as sensors of mechanical strain. In response to this stress, they release paracrine signals which stimulate active osteoblasts and osteoclasts and direct the turnover of bone tissue (Maisani et al., 2017).

1.2.2.2 Resorption Phase

Following the initiation of the activation phase, osteoblasts respond to the bone remodelling signals produced as a result of the aforementioned processes. This response includes the production of cytokines necessary for osteoclastogenesis, the recruitment of osteoclast precursors, and the stimulation of these precursors to differentiate into multinucleated osteoclasts that ultimately initiate the bone resorption phase. Following stimulation by these cytokines, fusion of the mononuclear precursors of the haematopoietic lineage, from which osteoclasts are derived, produce large multinucleated cells (Teitelbaum and Ross, 2003). Osteoblasts also secrete matrix metalloproteinases (MMPs) in response to the remodelling signals (Partridge et al., 1987; Yang et al., 2004). MMP activity is necessary to allow the attachment of osteoclasts to mineralised bone. First, MMPs expose the RGD adhesion sites present in mineralised bone by degrading the unmineralized osteoid that lines its surface. Once exposed, osteoclasts can bind to these RGD sites, generating an isolated microenvironment below the cell (the sealed zone). Once established, hydrogen ions are pumped through membrane proton pumps into the sealed zone to create an acidic environment (ca. pH 4.5). This results in the dissolution of the mineral component of the matrix and the production of the resorptive pit (Howship's lacunae; Teitelbaum, 2000). Subsequently, cathepsin K, along with other collagenolytic enzymes, degrades the organic ECM. The Howship lacunae, however, remains covered with demineralised collagen matrix (Everts et al., 2002). These remnants are removed by mononuclear cells of a still unclear

lineage (reversal cells), that are substituted for osteoclast cells as they undergo apoptosis. Reversal cells then prepare the bone surface for new bone tissue deposition (Delaisse, 2014).

1.2.2.3 Reversal and Formation Phases

Following this process, the resorptive pit houses osteocytes released from the resorbed bone matrix, pre-osteoblasts enlisted from the medullary cavity, mesenchymal stromal cells (MSCs) and a fibrous membrane which covers the exterior of bone. This membrane is populated by mature osteoclasts, reversal cells, progenitor cells and signals released from the previously degraded matrix (Maisani et al., 2017). Numerous growth factors, including TGF-β, fibroblast growth factor (FGF) and bone morphogenetic proteins (BMPs) stimulate the differentiation of progenitor cells into mature osteoblasts, which, in turn, synthesise new bone ECM. Subsequently, these mature osteoblasts pursue one of three possible fates: undergo apoptosis, remain embedded in the newly formed mineralised tissue and transition to the osteocyte phenotype, or, finally, become a quiescent osteoblast with a flat morphology, known as a bone lining cell, and inhabit non-remodelling bone surfaces (Miller et al., 1989).

1.2.2.4 Termination Phase

The process of bone remodelling is terminated when the remodelling machinery is stimulated to conclude its work as a result of largely unknown signals that communicate that an equal quantity of resorbed bone has been replaced. Finally, the resting bone surface environment is achieved and maintained until bone remodelling is initiated again upon receipt of subsequent stimuli (Raggatt and Partridge, 2010).

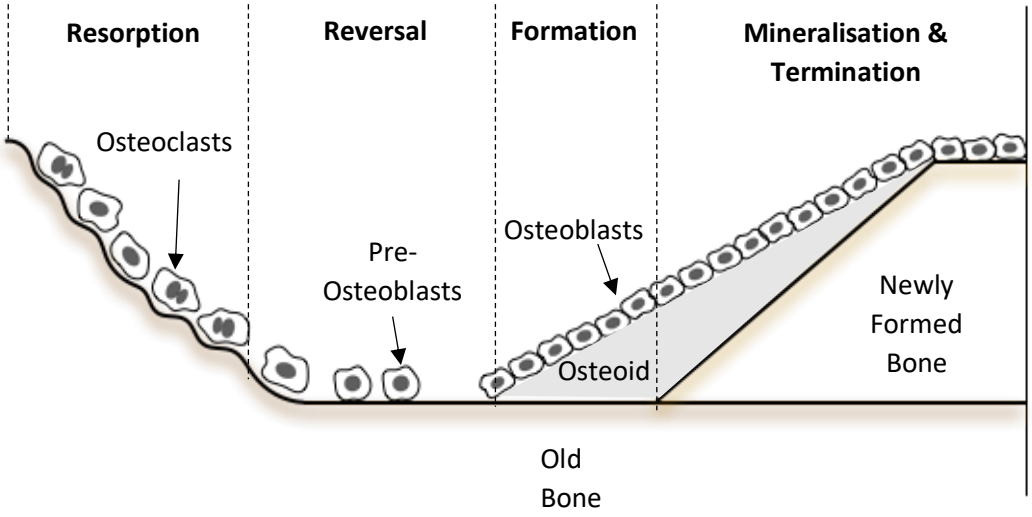

Figure 1: A representation of the physiological process of bone remodelling. *Adapted from Siddiqui and Partridge (2016).*

1.2.3 Bone Healing

Bone tissue also possesses the intrinsic ability to respond to damage and repair itself. Following damage, such as a fracture, there is a resultant disruption in the bone vascular network which minimises nutrient and oxygen exchange and affects the structure of bone marrow. Ultimately, this leads to local loss of skeletal integrity (Baldini et al., 2009). Immediately following trauma of this nature, the first of three main phases of fracture healing begins (Inflammatory/reactive phase, reparative/regenerative phase, and the remodelling phase; Oryan et al., 2012).

1.2.3.1 Inflammatory Phase

As the name suggests, the inflammatory phase begins with local inflammation and the formation of a haematoma within 12 to 14 hours after damage occurs. This haematoma supplies a matrix which facilitates the migration of cells involved in the acute inflammatory response: inflammatory cells, endothelial cells and fibroblasts. Neutrophils are the first responders to the fracture site, before they are substituted for macrophages, lymphocytes

and plasma cells. Macrophages remove necrotic tissue and debris by phagocytosis and, along with platelets and bone cells, release cytokines and growth factors responsible for the initiation of the healing process (Doblare et al., 2004; LaStayo et al., 2003; Moshiri and Oryan, 2012). Amongst these are TGF-β, platelet derived growth factor (PDGF), vascular endothelial growth factors (VEGFs), fibroblast growth factors (FGFs), Interlukin-1 and 6 (IL-1 and IL-6), BMPs, tumour necrosis factor α (TNF-α), and macrophage colony stimulating factor (Moshiri and Oryan, 2013; Parizi et al., 2011; Webb and Tricker, 2000). The release of these factors initiates the migration of multipotent mesenchymal stem cells (primarily originating from bone marrow and the periosteum) and stimulate their differentiation into fibroblasts, angioblasts, chondroblasts and osteoblasts, that are necessary for the angiogenesis and synthesis of the ECM (Moshiri and Oryan, 2013; Oryan and Moshiri, 2012). Ultimately, this results in the formation of transient granulation tissue with low stiffness and tensile strength (Schindler et al., 2008).

1.2.3.2 Reparative Phase

The reparative phase consists primarily of the formation of the fracture-callus. The fibrin-rich granulation tissue produced prior to this stage is used as a natural scaffold to produce a soft callus which stabilises the fracture site. This occurs via one of two methods of ossification: endochondral or intramembranous ossification. Endochondral ossification relies on the deposition of a cartilaginous callus across the fracture site, which is subsequently vascularised and calcified. However, at this stage, the callus remains mechanically weak, as it is characterised by a random organisation of collagen fibres (Maisani et al., 2017). Intramembranous ossification is characterised by high partial pressure of oxygen and a functional capillary network (Marzona and Pavolini, 2009). In this case, cartilage deposition is not required. Instead, osteoblasts directly synthesise compact and trabecular bone.

Progressively, osteoblasts replace the calcified cartilage with woven bone. Once this occurs, the mechanical properties increase with the formation of a hard callus. Calcified cartilage stimulates the recruitment of osteoclasts which allow the woven bone to replace the cartilage matrix, and osteoblasts into the fracture site, in addition to inducing angiogenesis (Marsell and Einhorn, 2011).

1.2.3.3 Remodelling Phase

In the final phase, the woven bone is remodelled into new cortical or trabecular bone tissue with a lamellar structure. The duration of this phase can often be months or years, until the original biomechanical properties and integrity of the fractured bone is restored. This is achieved, briefly, by the deposition of bone by osteoblasts to replace the callus which is resorbed by osteoclasts within previously mentioned BMUs (Marsell and Einhorn, 2011).

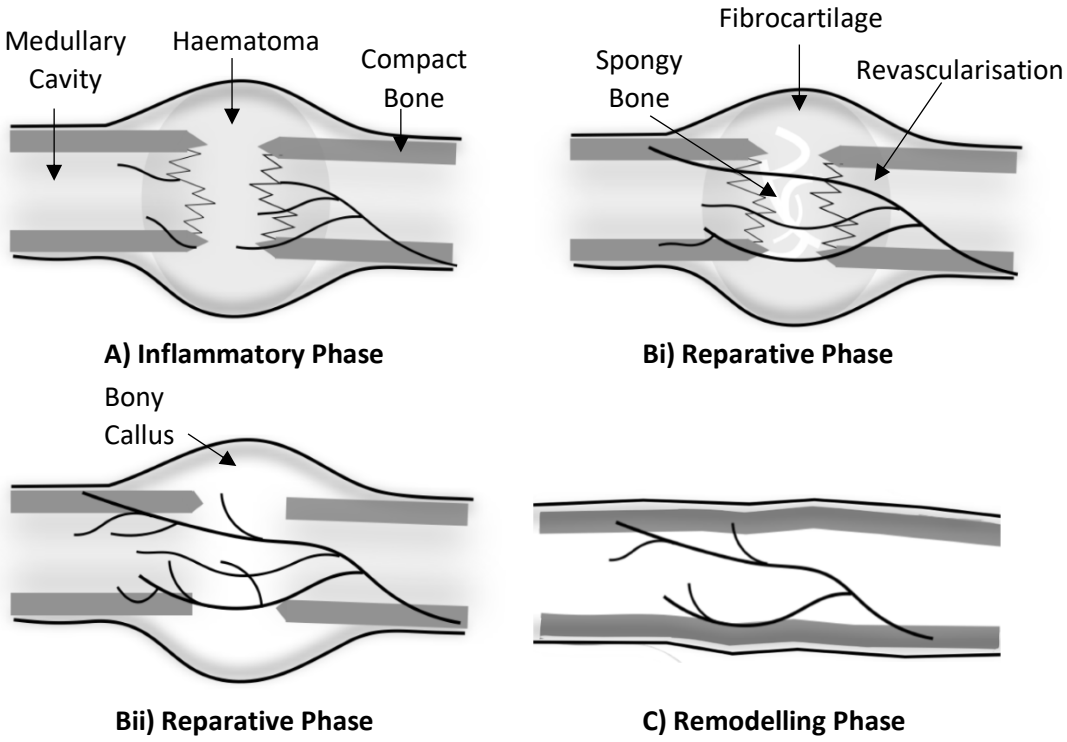

Figure 2: A representation of the three phases of fracture repair. *Adapted from Sfeir et al. (2005).*

1.3 Bone Defects

Intrinsic bone healing is often insufficient. This issue occurs in relation to segmental bone defects (SBDs) – bone injuries resulting in a section of bone tissue being completely shattered or absent. If the loss of bone tissue is large enough, or, specifically, more than two and a half times the radius of the bone, this defect is termed a critical sized defect. In these cases, bone is incapable of regenerating without medical intervention (Pilia et al., 2013; Schroeder and Mosheiff, 2011). Similarly, medical intervention and corrective surgery is necessary when a defect results in a non-union (pseudoarthrosis) or malunion and, ultimately, a loss of function. A malunion occurs when the natural healing process can form a bridge to attempt to reconnect the damaged ends of bone tissue, but this results in misalignment and resultant mechanical vulnerability. Whereas a non-union is the term used for the case in which the two ends of bone tissue cannot be reconnected, and a critical defect is formed (Pilia et al., 2013).

SBDs, broadly, are brought about by one of three causes, the first of which is trauma. Trauma related causes can be further divided into fractures, sport injuries, and blast injuries. Blast injuries, as expected, are most prevalent amongst military personnel because of explosive detonations. These are the most severe cause of trauma related SBDs since other tissue, such as muscle and nervous tissue, is also affected. Fractures and sports injuries are less severe; however, they are characterised by the necessitated need for the surgical removal of shattered/fragmented pieces of bone (Pilia et al., 2013).

The second significant cause is disease. Specifically, disease resulting in the abnormal weakening of bone tissue or the need for surgical removal to prevent disease transmission. This includes osteosarcoma, osteoporosis, osteoarthritis (Baino et al., 2009) congenital deformity corrections, generic infections, pathological degenerative bone destruction and numerous degenerative diseases (Kang et al., 2011 and Pilia et al., 2013). This links with the

third significant cause - aging. Increasing chronological age is accompanied by increased risk, and increased severity, of the prior significant causes of SBDs occurring.

If SBDs remain untreated, complications, in the form of malunion, can mean the new bone will remain susceptible to fractures. This is frequently observed in undiagnosed fractures and can lead to a reduction in bone function (Pilia et al., 2013). Similarly, non-union can occur if the ends of the bone are not secured in place sufficiently, therefore allowing excessive movement and preventing the ossification of the callus. In both cases, surgical intervention is required to minimise further decline in functionality (Pilia et al., 2013).

Therefore, coinciding with the aging population, orthopaedic trauma and resultant orthopaedic surgery is becoming more frequent. This trend of increasing orthopaedic needs is expected to continue in the coming years, therefore, increasing the need for cost efficient and effective treatments (Pilia et al., 2013).

1.4 Current Treatment Methods

Currently, except for blood, bone is the most frequently transplanted tissue (Eddy et al., 2013). Conventional therapeutic approaches to the treatment of bone tissue defects include autografts, allografts, xenografts, and the implantation of exogenous materials, such as metal or ceramics.

1.4.1 Autografts

Bone transplant procedures ordinarily involve the transplantation of small fragments, to induce osteogenesis, or large fragments, to compensate for the loss of larger sections of bone tissue.

Autologous bone grafts remain the ‘gold standard’ to augment bone tissue healing. Grafts of this nature mean that the recipient is also the donor. Autologous cancellous and corticocancellous tissue, or even vascularised bone tissue segments, are isolated from the

patient, most frequently from the iliac bone, or the fibula. These are subsequently implanted back to the patient at the defect site (Gomez-Barrena et al., 2015; Schroeder and Mosheiff, 2011). In addition to the absence of an elicited immune response, as the tissue is autologous, autografts possess the necessary characteristics to stimulate the growth of new bone tissue. They provide an osteoconductive scaffold, possess osteoprogenitor cells (and therefore osteogenicity), and the ability to induce the osteogenic differentiation of local stem cells (Goldberg, 2000; Shen et al., 2005; Urist, 1980). However, due to the autologous nature, the supply of appropriate bone is limited. Similarly, there are multiple other concerns including donor site morbidity, surgical limitations and elevated bone resorption during healing (Banwart et al., 1995; Sheikh et al, 2015).

1.4.2 Allografts and Xenografts

Allografts, the transfer of bone tissue sourced from a genetically different human donor, and xenografts, the transfer of bone tissue sourced from a different species, are alternative approaches. These methods negate the concerns regarding donor site morbidity and allow greater quantities of bone tissue to be transplanted. However, due to the necessary sterilisation and purification processes that must precede transplantation, the osteoinductive properties that accompany autografts are lost (Schroeder and Mosheiff, 2011). Additionally, both methods (particularly xenografts), elicit a significant immune response in the host tissue, ultimately leading to rejection unless immunosuppressive medication is received. Similarly, grafts of this nature are accompanied by the risk of bacterial, viral, and prion transmission (Mankin et al., 2005). Finally, allografts/xenografts rarely integrate fully with host tissue. Most transplants result in only the periphery of the graft substituting successfully, leading to a subsequent graft fracture in as many as 60% of cases after 10 years (Wheeler and Enneking, 2005).

1.4.3 Metals and Metal Alloys

The use of large prostheses, such as metals and metal alloys, is an additional method to remedy bone tissue defects. Metallic materials such as stainless steel, cobalt and chromium-based alloys (Co-Cr), titanium (Ti) and titanium alloys have been widely used to produce bone plates, complete hip joints, dental components, pins, screws, and numerous load-bearing implants for decades (Mediaswanti et al., 2013; Poinern et al., 2013). The reason for this is because their fracture resilience and high compressive and tensile strength mean they are equipped for high load-bearing applications (Poinern et al., 2013). However, prostheses of this kind are usually a temporary solution, with 30% of recipients requiring a revision 7 years after the original procedure (Mittermayer et al., 2001). This is because metal/metal alloy implants lack a biological interface. As they do not interact, either chemically or biologically, with the surrounding tissue, there is minimal osteointegration or interfacial bonding. Therefore, over time, chronic wear or loosening renders the implant ineffective (Schroeder and Mosheiff, 2011). One of the primary disadvantages associated with metallic implants is 'stress shielding'. This occurs due to the mismatch in mechanical properties between metallic implants and natural bone tissue which means, instead of transferring mechanical forces/loads onto the healing bone, it is retained by the implant. Ultimately, this results in unwanted bone resorption and implant loosening (Alexander and Theodos, 1993). Further disadvantages include: the risk of the implant damaging host tissue due to its weight and robustness, the release of toxic ions and particles via corrosion, allergic reactions and inflammatory cascades (Mediaswanti et al., 2013; Poinern et al., 2013). Even though metallic implants, particularly Ti alloys, with a higher resistance to corrosion and a reduced elastic modulus compared to previous metallic implants are now available, improvements are still necessary.

1.4.4 Polymers

Polymers are an additional category of biomaterials utilised as exogenous implants for bone tissue repair. They consist of many repeated units of small chemical monomers forming long chain molecules. These can be natural or synthetic, both of which have implications in numerous applications due to their properties: flexibility, low density, resilience and surface modifiability (Cooke et al., 1996). In terms of bone repair, polymers have been utilised as tissue scaffolds, bases for dentures, hip joint and cartilage replacements and as bone pins, screws and plates (Silver, 1994). Natural biodegradable polymers can be protein based, such as fibrin gel or collagen, or polysaccharide based, such as chitosan or hyaluronic based polymers (Poinern et al., 2013). Both of which have been used extensively in tissue engineering, particularly as scaffolds that allow cell attachment. Synthetic biodegradable polymers, including poly lactic acid (PLA), poly (L-lactic acid) (PLLA), poly-caprolactone (PCL) and poly glycolic acid (PGA), can be manufactured under controlled conditions to yield scaffolds with desired mechanical and physical properties. Furthermore, the degradation rate of synthetic polymers can be more easily controlled, while toxicity is also reduced (Poinern et al., 2013). Most commonly, PGA and PLA polymers are used clinically and can be manufactured with the most appropriate structure (disks, pellets, films or fibres) to satisfy specific applications (Poinern et al., 2013). Despite this, the mechanical strength of polymer implants is significantly lower than that of metallic implants. Their use in high load bearing applications is therefore limited, instead, their primary use is in soft tissue engineering (Poinern et al., 2013). Additional disadvantages associated with polymeric implants include disrupted or uneven integration of the surrounding tissue due to the irregular degradation of the scaffold and induction of the inflammatory response. Natural polymers also come associated with further risks surrounding the potential for disease transmission, like those associated with allo/xenografts.

1.4.5 Ceramics

Biological ceramics also have implications in bone tissue regeneration. These are inorganic, non-metallic materials that display chemical and thermal stability, durability, good wear resistance and physical strength (Hench and Wilson, 1993). They can also be sterilised with ease, are biocompatible, nontoxic, non-immunogenic and are readily available, which confers significant advantages in tissue regeneration. Furthermore, they can be shaped to fit a specific defect site or application (Hench, 1991).

There are different categories of ceramics, each with slightly different applications. Bioinert ceramics, such as alumina, don't interact with the surrounding tissue and are most used in dental implants (Best et al., 2008). Bioactive ceramics, such as bioactive glasses and hydroxyapatite (HA), directly interact with the adjacent tissue to elicit osteointegration (Gbureck, 2003). This property prompted the use of bioactive ceramics to coat metallic implants, such as Ti alloys, to increase post-implantation osteointegration (Shi and Jiang, 1998). The third type, resorbable ceramics such as tricalcium phosphate (TCP), directly form a scaffold which promotes the proliferation of bone cells. This scaffold is slowly resorbed and replaced with the proliferating bone tissue (Campbell, 2003; Tancret et al., 2006). Finally, porous ceramics, such as HA coated metal implants, allow the infiltration of the surrounding tissue at the porous sites (Poinern et al, 2013). Again, however, there are multiple disadvantages associated with bioceramics. Primarily, these are associated with their low fracture toughness, tendency to be brittle and their lack of resilience (Poinern et al, 2013).

Despite the varying advantages which accompany each of these conventional techniques, their overall effectiveness remains inadequate. In the USA alone, projections for the demand of hip and knee implants were estimated to increase by 174% and 673%, respectively, between 2005 and 2030 (Kurtz et al., 2007). Similarly, in Australia, primary and revision hip surgery numbers were elevated by approximately 17% in 2008 compared to the previous

year (Mediaswanti et al, 2013). Therefore, highlighting the need for more effective, long lived, biomechanically and biocompatible materials for use in orthopaedic applications.

1.5 Foundation of Bone Tissue Engineering

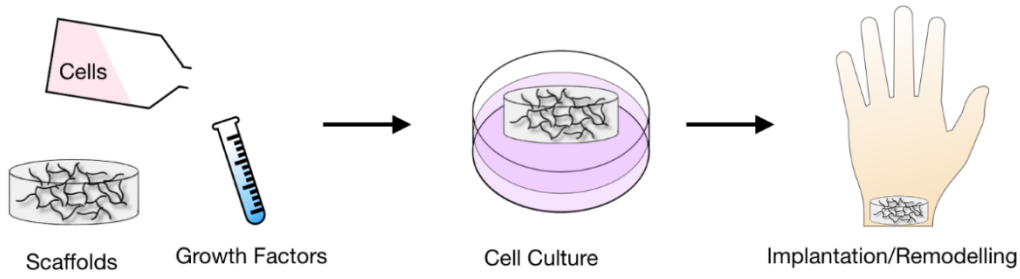

Figure 3: Diagrammatic representation of the preparation and application of a scaffold for bone tissue engineering. *Adapted from Drosse et al. (2008).*

Consequently, novel treatment options which address the existing issues with current orthopaedic treatments and offer all key elements of fracture healing and bone tissue regeneration are necessary. The ideal, or 'holy grail', treatment would be biocompatible (not elicit an adverse immune response upon implantation into the host), osteoinductive (promote stem cell differentiation), osteoconductive (promote the attachment, migration and proliferation of cells), capable of osteogenecity (production of new bone) when osteoprogenitor cells are present and promote vasculogenesis (Pilia et al., 2013 and Lu et al., 2012). Additionally, this treatment, or synthetic material, would break down at the same rate that bone tissue is formed and would mimic the structural architecture and mechanical properties of natural bone tissue (Pilia et al., 2013).

Tissue engineering strategies are currently being utilised to create such a treatment. Generally, this is a multifactorial approach combining metabolically active cells with a structurally supportive three-dimensional (3D) scaffold and molecular signals, such as growth

factors, to achieve tissue growth (Drosse et al., 2008; Gomez-Barrena et al., 2015). Following the production of a 3D scaffold matching the geometry of the defect site, the appropriate cells and growth factors are loaded into it. Then, the scaffold is maintained in cell culture conditions to facilitate the proliferation of the loaded cells. Subsequently, the product of this procedure is implanted into the patient at the defect site to stimulate the regeneration of bone tissue (Drosse et al., 2008).

The most compatible material to produce scaffolds of this nature, of course, is autologous bone. However, the previously discussed issues related to allografts necessitate the need for an alternative material. Preferably available in unrestricted quantities (Schieker et al., 2006). Numerous synthetic osteoconductive bone substitutes fitting the necessary criteria are available. These include bioactive glasses, calcium phosphate-based materials such as calcium hydroxyapatite and TCP, and other proteinaceous and carbohydrate-based substrates (Paderni et al., 2009).

Similarly, multiple cell types have been investigated for their ability to enhance the efficiency of bone tissue engineering treatments. Bone marrow stromal cells, periosteal cells and osteoblasts have all been investigated, however, adult mesenchymal stem cells (MSCs) appear to be the most appropriate (Groger et al., 2003 and Stangenberg et al., 2005). MSCs appear to have the largest implications for multiple reasons: ease of isolation, ease of expansion (*in-vitro*), and the ability to manipulate their progression from immature progenitor cells to specific cell types belonging to osteogenic, chondrogenic or adipogenic lineages (Drosse et al., 2008; Pittenger, 1999).

Finally, many of the growth factors present in the matrix and osteoid of the skeletal system, involved in the natural processes of bone tissue regeneration, metabolism and overall function have been investigated to establish potential implications in the treatment of bone defects. Specifically, TGF-β, Insulin-like growth factor (IGF), PDGF, basic fibroblast growth

factor (bFGF) and BMPs. For example, the proliferation of bone marrow stromal cells was stimulated by fibroblast growth factor Two (FGF-2) *in-vitro*. When these stromal cells were seeded onto a bio-ceramic scaffold, cell differentiation was stimulated and bone tissue was formed *in-vivo* (Martin et al., 1997).

Similarly, four patients suffering with SBDs were treated using a bioceramic scaffold loaded with autologous MSCs (previously isolated from the respective patients' bone marrow and cultured *in-vitro*). This appeared to result in the integration of the scaffold with bone tissue without any negative implications, up to 7 years following the procedure.

1.6 Hydrogels

An alternative approach for the percutaneous delivery of cells and biomaterials to increase the efficacy of bone tissue regeneration is the use of hydrogels - an increasingly important class of highly hydrated polymers.

Specifically, hydrogels are 3D, hydrophilic, crosslinked polymeric materials capable of absorbing large quantities of water or biological fluids without dissolving. This high-water content, partnered with porosity and soft consistency means that hydrogels replicate natural living tissue more accurately than other classes of synthetic biomaterials (Peppas, 2000).

Hydrogels can be categorised according to numerous criteria: origin (natural or synthetic), preparation method (homopolymer, co-polymer, multipolymer or interpenetrating hydrogels), ionic charge and physical structure (amorphous, semi-crystalline, or hydrogen bonded structures; Gkioni et al., 2010).

1.6.1 Natural

Natural hydrogels, generally, are biodegradable, biocompatible, and promote the attachment and proliferation of cells in the absence of cytotoxic effects (Ghasemi-Mobarakeh, 2015). This category of hydrogels primarily consists of polysaccharides such as

chitosan, alginate, pullulan and agarose, and proteins, such as collagen, gelatin, and fibrin (Ghasemi-Mobarakeh, 2015). However, as natural hydrogels are synthesised using materials from living organisms, the previously mentioned immunological risks surrounding viral/prion transmission apply. Similarly, the speed at which natural hydrogels degrade and the degree of variability between batches are also problematic (Maisani et al., 2017).

1.6.2 Synthetic

Synthetic hydrogels negate these immunological concerns, as well as providing greater reproducibility of their physiochemical characteristics. Furthermore, as they are synthetically produced, they are available in unlimited quantities and can be modified to allow a more precise fit to applications (Maisani et al., 2017). Synthetic polymers used for hydrogel production include polyesters such as PGA, PLA, polyethylene glycol (PEG), polyphosphoesters, and synthetic peptides (Maisani et al., 2017). Despite their advantages, synthetic hydrogels of this nature lack cellular binding sites that are present in natural hydrogels, such as those composed of collagen or gelatin.

1.6.3 Preparation

In the absence of crosslinking hydrogels are known as hydrosols, which is a liquid state. Crosslinking of the hydrophilic polymers is therefore necessary for the fabrication of hydrogels. This can be via physical or chemical crosslinking.

1.6.3.1 Physical Crosslinking

Physical crosslinking involves intra and intermolecular interactions between polymers. Specifically, the polymeric chains are connected by non-covalent interactions such as ionic interactions, hydrogen bonds, hydrophobic effects, or via direct entanglement of polymeric chains (Ahmed, 2015). Crosslinking of this nature relies upon factors such as pH or temperature changes for initiation. Therefore, the cytocompatibility of resultant hydrogels is not affected by the use of cytotoxic initiators and chemical crosslinkers (Rajan et al., 2006).

1.6.3.2 Chemical Crosslinking

Chemical crosslinking, unlike physical crosslinking, involves the formation of irreversible covalent bonds between polymeric chains (Ahmed, 2015). Numerous techniques have been utilised to achieve covalent crosslinking, including free radical polymerisation, click chemistry, photo-crosslinking, Michael-type addition and enzymatic crosslinking (Gasperini et al., 2014; Maisani et al., 2017; Sivashanmugam et al., 2015). The commonality between these methods is the provision of specific chemical and physical conditions which stimulate the reaction between polymeric chains. However, to be considered in bone tissue engineering applications, potentially toxic precursors, initiators and crosslinkers must be removed entirely prior to use. Additionally, chemical crosslinking may result in the undesirable alteration of the original biological properties of the polymers (Maisani et al., 2017).

1.6.4 Biomedical Applications

The first synthetic, biocompatible, hydrogel was formulated from poly-2-hydroxyethylmethacrylate (PHEMA), intended for applications as contact lenses (Wichterle and Lim, 1960). Since then, the versatile nature of hydrogels, and the multitude of advantages which they possess, have been elucidated. These advantages include: injectability, precise fitting to defect sites and the incorporation of cells and bioactive substances, such as growth factors and enzymes, with relative ease (Douglas et al, 2012). As a result, hydrogels have numerous applications. For example, in controlled drug delivery (Hoffman, 2002) and in biosensors (Gawel et al., 2010). Importantly, in terms of bone tissue engineering, hydrogels can be used to synthetically replicate the architecture of the extracellular matrix (ECM), provide a structurally supportive temporary scaffold for cells and ensure efficient nutrient and gas exchange is maintained (Geckil et al., 2010). Therefore, hydrogels possess the ideal micro-environment to support the proliferation and

differentiation of bone cells, to ultimately restore functionality to defect sites (Kondiah et al., 2016).

However, as hydrogels gain interest as biomaterials for utilisation in BTE, their mechanically stability, receptiveness to mineralisation, non-cytotoxicity and ability to support adhesion and growth of bone forming cells are increasingly important. Ease of sterilisation and antibacterial activity are also desirable properties of hydrogels in this space. Importantly, these properties can be enhanced by the incorporation of additives into the hydrogel. For example, Travan et al (2009) demonstrated the antimicrobial activity of a hydrogel supplemented with nanoparticles, while ceramics and carbon nanotubes have been used to increase the mechanical properties of hydrogels (Tozzi et al., 2002).

1.7 Research Aims

The aim of the present study was to investigate novel biomaterials for use in bone-tissue engineering. Specifically, three hydrogel materials were evaluated:

1. Electron irradiated Gelatin hydrogels supplemented with Alkaline Phosphatase (ALP)
2. WPI hydrogels supplemented with Carbon Nanotubes (CNTs)
3. WPI hydrogels supplemented with Phloroglucinol (PG)

The alkaline phosphatase enzyme (ALP) was incorporated into electron beam-crosslinked gelatin hydrogels to attempt to induce their mineralisation with Calcium phosphate (CaP). Both physiochemical and biological properties of the resultant gels were then evaluated to establish the effects of this process, and the suitability of these hydrogels for bone tissue engineering.

CNTs and PG were incorporated into WPI hydrogels to investigate their influence on properties relevant for bone tissue engineering. Specifically: antibacterial properties, mechanical properties, and cell viability.

Chapter 2: Gelatin Hydrogels

2.0 Introduction

2.1 Biomaterial Mineralisation

Hydrogels possess several inherent disadvantages when examined as materials to satisfy applications in bone tissue engineering. Their generally weak mechanical properties are one of the primary disadvantages, as this limits their use in non-load bearing sites (Griffith, 2000; Hoffman, 2002). Furthermore, hydrogels are generally unable to mineralise with calcium phosphate (CaP) and form durable interactions with tissues such as bone. Previously, the most common strategy to remedy this was the inclusion of inorganic particles, such as CaP ceramics, into the hydrogel matrices to act as nucleation sites and enable mineralisation (Douglas et al., 2012). However, this strategy usually results in the aggregation of CaP particles. It is often necessary, therefore, to use techniques to improve dispersion, such as the direct formation of CaP in the hydrogel (Leeuwenburgh et al., 2007), or the utilisation of dispersants such as citrate (Leeuwenburgh et al., 2010). Finally, sterilisation is often difficult (Neumann and Epple, 2006).

As discussed by Douglas et al (2012), a multitude of advantages are predicted to accompany mineralisation. The presence of the CaP mineral can enhance the biological performance of bone-substituting materials by a phenomenon of bioactivity, where a chemical bond is formed with the adjacent bone tissue following implantation (Le Geros, 1991). Additionally, CaP ceramics possess an intrinsic affinity for biologically active proteins, such as growth factors, which are necessary for the natural healing process of bone tissue (Ruhe et al., 2005). Furthermore, as previously mentioned, one of the primary disadvantages associated with hydrogels are weak mechanical properties, meaning that, without reinforcement, their implications are somewhat restricted to soft tissue engineering. However, the mechanical reinforcement brought about by mineralisation enables them to be considered for hard

tissue engineering purposes, such as bone tissue regeneration (Douglas et al., 2013). Furthermore, mineralisation is anticipated to improve the compatibility of hydrogels with bone tissue, as both stiffer and rougher surfaces are known to promote the differentiation of cells towards the osteoblastic phenotype. Therefore, the development of mineralised hydrogels is desirable.

2.1.1 Mineralisation by Incorporation of Nanoparticles

One method to mineralise hydrogels is by directly incorporating inorganic phase nanoparticles. Upon integration, these inorganic phases provide nucleation sites for the formation of HA, in addition to adhesion sites that permit integration with adjacent bone tissue (Cao and Hench, 1996; Rea et al., 2004). As well as the previously mentioned benefits that accompany mineralisation, the incorporation of inorganic nanoparticles allows the manipulation of the rate at which the hydrogels degrade (Ara et al., 2002; Neumann and Epple, 2006). Additionally, the combination of ceramic biomaterials with hydrogels allows easier implantation into bone defects as the elastic properties of the hydrogel shield the ordinarily brittle ceramic particles (Kretlow and Mikos, 2007).

Numerous bioactive inorganic materials can fulfil the role of mineralising hydrogels. However, calcium phosphates and bioglasses are used most frequently. Specifically, HA, amorphous calcium phosphate, and β-tricalcium phosphate as they closely resemble the native mineral phase of bone tissue (Dorozhkin and Epple, 2002). The incorporation of HA into cyclic acetal hydrogels resulted in increased expression of osteogenic signals, which ultimately enhanced the differentiation of bone marrow stromal cells. Therefore, implicating these composites in hard tissue engineering (Patel et al., 2010).

An additional method by which hydrogel mineralisation can be achieved is via biomimetic mineralisation in solutions containing calcium and phosphate ions. This can be further split into two methods based on whether mineralisation occurs prior to, or following, gel

formation. Both methods, however, result in CaP crystals occupying the hydrogels, acting as nucleation sites, and stimulating posterior crystal growth (Douglas et al., 2013).

2.1.2 Immersion in Calcium/Phosphate Ion Containing Solutions

Immersion strategies are dependent on the ability of ions to enter hydrogels (which is permitted by their hydrated structure). Traditionally, as it is thought to replicate the *in-vivo* mineralisation behaviour of a biomaterial, simulated body fluid (SBF) was the most common solution used to achieve mineralisation of biomaterials (Douglas et al., 2013). Following treatment with calcium chloride solution, immersion in SBF for 14 days resulted in successful, homogenous, mineralisation of a cellulose based hydrogel (Hong et al., 2006).

Alternative approaches include alternate soaking – the sequential immersion of hydrogels in solutions containing supraphysiological ion concentrations, first in a calcium ion (Ca^{2+}) containing solution and then in a solution containing phosphate (PO_4^{3-}), or vice versa. This technique does not replicate *in-vivo* mineralisation conditions; however, mineral is formed quicker, and the ability to manipulate both ion concentration and the temperature at which this process occurs allows the mineralisation process to be optimised. For example, Du et al (2000) utilised the alternate soaking method to mineralise collagen matrices. This study also demonstrated that various crystal polymorphs could be formed by manipulating the method. Numerous additional studies have validated this technique, for example, Hutchens et al (2006) identified the formation of calcium deficient HA, comparable to the apatite crystals present in natural bone, in cellulose hydrogels exposed to this technique. The addition of biomacromolecules which stimulate the mineralisation process has also been found to enhance this process. However, the resultant mineral phase formed by alternate soaking is primarily located on the surface, rather than the interior, as it relies on diffusion (Douglas et al., 2013).

2.1.3 *In-situ* Formation of Calcium Phosphate Nanocrystals

Adaptation of the aforementioned method can increase the homogeneity of hydrogel mineralisation. CaP nanocrystals are formed, *in-situ*, during hydrogel formation. Subsequently, these nanocrystals act as nucleation sites to promote further crystal formation following incubation in a mineralisation solution. For example, as discussed by Douglas et al., (2013) and Douglas et al., (2016), amorphous CaP and brushite was formed in the central interior of a gelatin hydrogel as a result of a double diffusion method – calcium chloride ($CaCl_2$) and sodium phosphate (Na_2HPO_4) diffused into the hydrogel via separate reservoirs, on opposite sides of the hydrogel. This hydrogel was then incubated in SBF, which induced the formation of HA from the mineral phase (Douglas et al., 2016).

2.1.4 Enzymatic Mineralisation

However, despite the increased homogeneity of this strategy, the aggregation of CaP particles remains an issue. An alternative to the incorporation of CaP particles is the use of Alkaline phosphatase (ALP) - an enzyme involved in the mineralisation of bone in the human body by cleavage of phosphate from organic phosphate (Orimo, 2010). Specifically, ALP catalyses the hydrolysis of organic phosphoesters, increases the concentration of inorganic phosphate groups, locally, and ultimately results in the formation of carbonated apatite deposits. ALP can, therefore, be used to induce homogenous mineralisation of hydrogels and simultaneously increase their mechanical strength and suitability for applications in bone replacement.

Previously, the successful mineralisation of poly(hydroxyethyl methacrylate) hydrogels and artificial self-assembling peptide amphiphile hydrogels by ALP was demonstrated (Spoerke et al, 2009). Furthermore, mineralisation was induced in dentine-derived collagen sheets, both *in-vitro* and *in-vivo*, by covalent linkage with ALP (Beertsen and Van den Bos, 1992; Van den Bos and Beertsen, 1994). More recently, a study was conducted by Douglas et al (2012) in

which ALP was used to induce mineralisation in one natural and two synthetic hydrogel materials, thus, demonstrating the applicability of this approach to a wide range of hydrogels. The implications of ALP as a hydrogel component to directly increase bone tissue regeneration have been evaluated. Specifically, following covalent linkage to a fibrin gel, ALP induced mineral formation was observed *in-vitro*. Subsequently, this scaffold enhanced bone tissue formation in a mouse calvarial defect *in-vivo* (Osathanon et al., 2009).

The basic principle of ALP mediated hydrogel mineralisation begins with the entrapment of the enzyme into the hydrogel during gelation. Once incorporated, the hydrogel is soaked in a solution containing glycerophosphate (GP) and Ca^{2+} (substrates for ALP). These substrates diffuse into the hydrogel, where ALP cleaves the phosphate (P) from GP. Subsequently, free P reacts with Ca^{2+} ions to form insoluble CaP which remains within the hydrogel (Douglas et al, 2012).

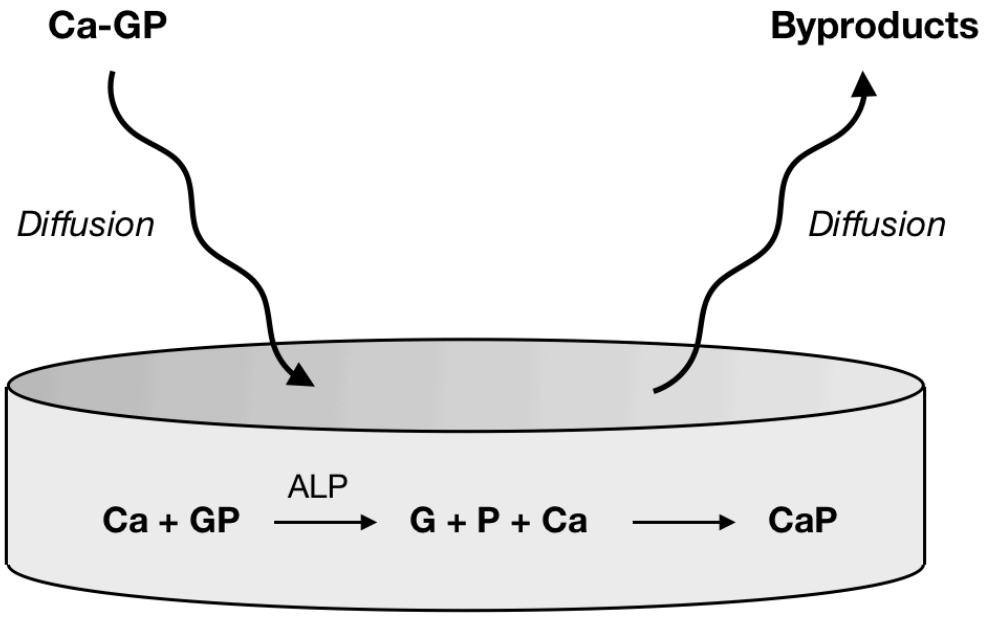

Figure 4: The process of enzymatic mineralisation of hydrogels with Calcium Phosphate. *Ca-GP diffuses into hydrogels supplemented with ALP resulting in cleavage of glycerophosphate (GP) to phosphate (P) by ALP. Free P then reacts with Calcium ions to form insoluble Calcium Phosphate (CaP). Adapted from Douglas et al. (2012)*

2.2 Gelatin

The present study utilised this ALP mediated approach to mineralise hydrogels comprised of gelatin. Previously, gelatin based materials have shown promise as biomaterials for applications in bone tissue engineering. Gelatin is a mixture of proteins obtained by either acid or alkaline hydrolysis of collagen – the primary component in the ECM, skin, tendons and all other connective tissues (Harrington and Von Hippel, 1962). Therefore, it is inexpensive and widely available in nature. Moreover, it has exceptional biocompatibility, is not immunogenic, is biodegradable and has the capacity to be modified at the amino acid level (Liu et al, 2009). The ability of gelatin to promote cellular growth has also been previously established (Wisotzki et al., 2016). All of which make gelatin an ideal biomaterial for tissue engineering.

However, gelatin hydrogels lose integrity at body temperature without crosslinking. Thus, providing an obstacle for its applications in bone tissue engineering. Conventional crosslinking methods involve the use of potentially toxic chemical crosslinkers, such as glutaraldehyde (GTA), which detract from the previously mentioned advantages. Specifically, unreacted GTA, as well as GTA released via degradation, has been demonstrated to increase cytotoxicity and reduce cellular growth (Jayakrishnan and Jameela, 1996; van Luyn et al., 1992). Reagent free crosslinking methods are, therefore, desirable. Both gamma and ultraviolet (UV) radiation have been implicated, however, negatives such as uneven transmission through the gelatin layers (UV) and the long exposure time required to achieve high doses (gamma) accompany these techniques (Wisotzki et al., 2014). More recently, crosslinking via electron irradiation has been elucidated as a quick yet effective crosslinking technique. Further advantages include the manipulation of penetration depth by altering electron energy, and the fact that electron irradiation, even at low doses (several KiloGrays [kGy]), simultaneously sterilises (Wisotzki et al., 2014; Wisotzki et al., 2016).

Specifically, Wisotzki et al (2016) evaluated the potential cytotoxicity of electron irradiated gelatin hydrogels on fibroblast cells. No significant increase in cell death was observed, even at doses of 60kGy. However, cell viability and proliferation rates were reduced slightly, in a dose-dependent manner. Therefore, overall, implicating gelatin hydrogels crosslinked by this method in tissue engineering.

Thus, the present study combines the previously elucidated method of ALP mediated mineralisation with electron irradiation to produce gelatin hydrogel composites with increased suitability for applications in bone tissue engineering. Specifically, mechanical strength, mineralisation and cytocompatability were evaluated.

3.0 Methods

3.1 Hydrogel Preparation

Hydrogel preparation was carried out by Stefanie Riedel (Leibnitz Institute of Surface Modifications, Germany). First, type I gelatin powder (G2500; Sigma-Aldrich Chemie GmbH, Germany) was dissolved in deionised water, resulting in a concentration of 8mg/ml. Alkaline phosphatase (ALP; P7640; Sigma-Aldrich, Germany) was then added (with concentrations of 0, 1.25, or 2.5 mg/ml). Subsequently, the gelatin-ALP solution was left to swell for one hour at room temperature before being heated to 37°C with simultaneous stirring to ensure the solution was dissolved homogenously. The solution was then poured into the desired moulds and left to polymerise for 12 hours, at 6°C.

3.2 Hydrogel Preparation ‘Thick’ and ‘Thin’

To evaluate whether the thickness of mineralised gelatin hydrogels influences their suitability for bone tissue engineering, this process was repeated to produce ‘thick’ and ‘thin’

gelatin hydrogels. Different moulds were used to produce samples 8mm and 2mm in height, respectively.

3.3 Electron Irradiation

Electron Irradiation was carried out by Stefanie Riedel (Leibnitz Institute of Surface Modifications, Germany). Following polymerisation, samples were prepared for electron irradiation. Briefly, they were inserted into airtight bags which were flushed with nitrogen and sealed. Simultaneous crosslinking and sterilisation of samples was subsequently carried out, as they were irradiated with electrons by a linear electron accelerator (MB10-30MP; Mevex, Ontario, Canada) with doses ranging from 5 to 40kGy, in steps of 5 kGy. The electron accelerator was operated with a moving state at a repetition rate of 180Hz, a scanning frequency of 3Hz, and an electron pulse length of 8µm. During this process, samples were cooled by an air draft to prevent heating. The irradiation dose was verified (to an accuracy of 10%) by a graphite dosimeter.

3.4 Mineralisation of Hydrogels

Hydrogel mineralisation was performed by Stefanie Riedel (Leibnitz Institute of Surface Modifications, Germany). Resultant hydrogels were mineralised in accordance with the previously published protocol by Douglas et al (2012). Briefly, resultant hydrogels were incubated in 0.1M calcium glycerophosphate (CaGP) in H_2O for 6 days – medium was changed every 24 hours. Ultrapure H_2O was then used to rinse the hydrogels three times, before incubating them for 24 hours, to remove residual CaGP.

3.5 Dry Mass Percentage:

To determine the ratio of mineralised material, samples were weighed in the hydrated state, dried for 24 hours at 60°C, and weighed again. Dry mass percentage was then calculated using the following equation.

$$\text{Dry mass \%} = \left(\frac{Weight\ in\ dry\ state}{Weight\ in\ hydrated\ state}\right) \text{x } 100$$

3.6 Compression Modulus Analysis

The compressive modulus of samples was determined by Stefanie Riedel (Leibnitz Institute of Surface Modifications, Germany) using a universal testing machine (Inspekt mini; Hegewald & Peschke Meß- und Prüftechnik GmbH, Germany), with a 100 Newton (N) load cell to measure the applied force. The displacement rate was set at 2mm per minute until sample failure was reached. Compressive stress (σC) was then determined using the applied force and the cross-sectional area: $\sigma C = F/A$. Then, the compression modulus can be determined by the gradient of the linear-elastic range of the stress-strain curve for small strains.

3.7 Raman Spectroscopy

Raman spectroscopy was utilised to provide a structural fingerprint of the gelatin hydrogels, to allow subsequent identification of their molecular structures and chemical composition. Raman spectra were collected using a Renishaw inVia Raman Spectrometer (Renishaw Plc., UK) using an excitation wavelength of 785 nm. The laser power was ~15 megawatts (mW) at the sample, and spectral acquisition time was 5 seconds x 12, resulting in a total exposure time of 1 minute. For each sample, spectra were collected in triplicate.

To compare spectra directly, cosmic ray removal, baseline correction and smoothing were carried out using MATLAB software (The MathWorks, USA). Smoothing was applied using a triangular sliding average and baseline correction was applied using an asymmetric least squares algorithm.

3.8 Fourier-Transform Infrared Spectroscopy (FT-IR)

The molecular structure of the gelatin hydrogels was examined using an Agilent Technologies Cary 630 FT-IR machine, equipped with a diamond crystal, in attenuated total reflectance mode (ATR) and using microlab software. Spectra were recorded over a wavenumber range of 500cm^{-1} to 4000cm^{-1}.

3.9 Scanning Electron Microscopy (SEM)

SEM analysis was performed using a 7800F JEOL SEM instrument.

Prior to SEM analysis, samples were mounted on aluminium stubs (Agar scientific Ltd, UK) using carbon adhesive pads (Agar Scientific Ltd, UK) and coated with a thin layer of gold (ca. 10nm) using a Q150RES sputter coater (Quorum Technologies Ltd).

3.10 Cell Culture Sample Preparation for Scanning Electron Microscopy

Following cell culture, samples were also visualised by SEM to allow a more detailed evaluation of the surface topography of the hydrogels, cell morphology and attachment to the surface of the samples.

First, at the relevant time points (1, 4 and 7 days), the samples were fixed for a minimum of 2 hours, in 4% Glutaraldehyde. Samples were then subject to a series of dehydration steps with ethanol (Fisher Scientific, UK). Samples were placed in 70%, 80%, 90% ethanol, sequentially, and then in 100% ethanol twice, for 20 minutes each. Subsequently, samples were submerged in Hexamethyldisilazane (HMDS; Agar Scientific, UK) for 1 hour, before

being placed in fresh HMDS and left in the fume cupboard in an open vial, to allow the HMDS to sublimate.

Once dry, samples were mounted on aluminium stubs (Agar scientific Ltd, UK), using carbon adhesive pads (Agar Scientific Ltd, UK), and coated with a thin layer of gold using an S150A sputter coater. Coating was carried out at 40mA, under 1.5 bars of pressure for 5 minutes. Samples were subsequently examined using a JEOL JSM-5600 instrument (JEOL Ltd, Japan). A spot size of 14, and an acceleration voltage of 15 was used.

3.11 Inductively Coupled Plasma Optical Emission Spectrometry (ICP-OES)

Since ICP-OES is a more reliable method to evaluate the elemental composition of the mineralisation product, the Calcium and Phosphorus concentrations, as well as the calcium to phosphorus ratio, were determined using a 5100 Synchronous Vertical Dual View optical emission spectrometer (Agilent Technologies, USA). Prior to analysis, hydrogels were dried, dissolved in 3ml of 14 Molar (M) Nitric acid (HNO_3; Fisher Scientific, UK), then further diluted (1 in 100) using 0.3 M HNO_3. 7 standard solutions, with calcium (Fisher Scientific, UK) and phosphorus (Alfa Aesar, UK) concentrations ranging from 0 to 250mg/L, were used to calibrate the instrument. Additionally, all solutions contained Yttrium (Sigma-Aldrich, USA), which was utilised as an internal standard to account for exogenous effects. Measurements were taken in triplicate.

3.12 Cell Culture

To evaluate the interaction of the gelatin hydrogels with bone cells, a human osteosarcoma (MG-63) cell line (Sigma-Aldrich, USA) was seeded on to the hydrogels. At intervals of 1, 4 and 7 days, the adhesion, proliferation, and morphology of cells was assessed by fluorescent microscopy, while cell viability was evaluated via the MTS assay.

Specifically, MG-63 cells were cultured in Dulbecco's modified Eagle's medium (DMEM) supplemented with 10% foetal bovine serum (FBS; Nemecko, Germany), Penicillin and

Streptomycin (50-100IU/ml and 50-100µg/ml, respectively), at 37°C, with 90% humidity and 5% atmospheric pressure of carbon dioxide (CO_2).

Hydrogels were cut into thin slices and placed into 48-well plates (Corning Incorporated, USA). Subsequently, 1ml of DMEM culture media containing 5000 cells was added to each well (5263 cells/cm^2 growth area). Once the cells were seeded, the hydrogels were incubated at 37°C, with 90% humidity and 5% atmospheric pressure of CO_2 once again.

3.12.1 Fluorescent Microscopy

At the appropriate time point (1, 4 and 7 days) samples were washed with phosphate buffered saline (PBS), and subsequently fixed with 70% ethanol (Fisher Scientific, UK) at -20°C for 10 minutes. Samples were then washed again with PBS before staining.

Samples were stained with Hoechst and Texas red (both Sigma-Aldrich, USA) diluted in PBS at concentrations of 500ng/ml and 50ng/ml, respectively, for 15 minutes in dark conditions. Hoechst binds to the minor groove of double DNA, with affinity for adenine and thymine rich sequences. Thus, Hoechst is used to stain the cell nucleus. The Hoechst stain is excited in the UV range (approximately 361nm) and emits blue fluorescence around 497nm. Texas Red is used to stain the cytoplasm, as it binds to reduced thiol groups which are present in cytoplasmic proteins. The maximal excitation is approximately 596nm, while the optimal emission is around 615nm (observed as red).

After staining, samples were washed twice with PBS and subsequently visualised on an Axio Scope.A1 microscope (Zeiss, Germany) using a digital camera and Zeiss software.

3.12.2 Proliferation (MTS) Assay

The MTS assay was used to assess the proliferation of MG-63 cells on each of the hydrogel sample groups at the appropriate time points (1, 4 and 7 days). Briefly, this method indirectly measures proliferation, cell viability and cytotoxicity since viable, metabolically active cells convert a soluble tetrazolium salt into insoluble formazan. This is achieved by a

mitochondrial dehydrogenase enzyme named succinate tetrazolium reductase produced by metabolically active cells. The concentration of this insoluble formazan can then be quantified by spectrophotometry

DMEM, without phenol red, and supplemented with 10% FBS was used to dilute the MTS Cell Titer 96 Aqueous one solution cell proliferation assay kit (Promega, USA) by a factor of 1:6. Three independent samples for each sample group and time interval were included in the assay, along with a polystyrene plate (Corning Incorporated, USA) as a control sample. One sample without cells for each sample group and time interval was used to measure a background of the materials. First, samples were washed with PBS, transferred to a new well plate to remove interference from cells attached to the base of the polystyrene plate wells, and then incubated for 2 hours at 37°C with 90% humidity and 5% atmospheric pressure of CO_2, in 0.5ml of the diluted MTS solution.

After the 2-hour incubation, 100 µl of the solution from each well was transferred, in triplicate, to a 96-well plate to allow the extent of the yellow tetrazolium dye reduction to violet formazan to be quantified by a spectrophotometer (Tecan Infinite M200 Pro, Switzerland), at a wavelength of 490nm.

4.0 Results

Sample Abbreviation	Description
0mg/ml ALP in ddH_2O	Electron irradiated Type I gelatin (40kGy unless stated otherwise), 0mg/ml ALP, incubated in ddH_2O.
0mg/ml ALP in CaGP	Electron irradiated Type I gelatin (40kGy unless stated otherwise), 0mg/ml ALP, incubated in 0.1M CaGP for 6 days prior to rinsing.
1.25mg/ml ALP in CaGP	Electron irradiated Type I gelatin (40kGy unless stated otherwise), 1.25mg/ml ALP incubated in 0.1M CaGP for 6 days prior to rinsing.
2.5mg/ml ALP in CaGP	Electron irradiated (40kGy unless stated otherwise) Type I gelatin, 1.25mg/ml ALP incubated in 0.1M CaGP for 6 days prior to rinsing.
Thick	As above, 8mm in height
Thin	As above, 2mm in height

Table 1: The different sample groups examined in Chapter 2

4.1 Dry Mass Percentage:

The percentage of hydrogel mass, not consisting of water, for gelatin hydrogels with ALP concentrations of 0, 1.25 and 2.5 mg/ml, exposed to radiation doses of 0, 5, 10, 15, 20 and 40 kGy, is illustrated in figure 5.

The dry mass percentage of samples at each concentration of ALP increased due to electron irradiation. Statistically significant increases in dry mass percentage were observed, for each sample group (0mg/ml ALP in ddH_2O, 0mg/ml ALP in CaGP, 1.25mg/ml ALP in CaGP, and 2.5mg/ml ALP in CaGP) when the irradiation dose was raised from 0kGy to 40kGy. From 0kGy to 5kGy, and 5kGy to 10kGy, this increase followed a somewhat linear trend. After this point, however, the increase started to plateau. This was more apparent in the samples containing higher concentrations of ALP (1.25 and 2.5 mg/ml). For example, there was no significant difference in the dry mass percentages of 1.25 mg/ml ALP samples exposed to electron irradiation doses of 10, 15, or 20kGy.

However, statistically significant increases in the dry mass percentages were observed when ALP concentrations were raised from 0 to 1.25 mg/ml, and again from 1.25 to 2.5 mg/ml, at each dose of electron irradiation (0, 5, 10, 15, 20, and 40 kGy).

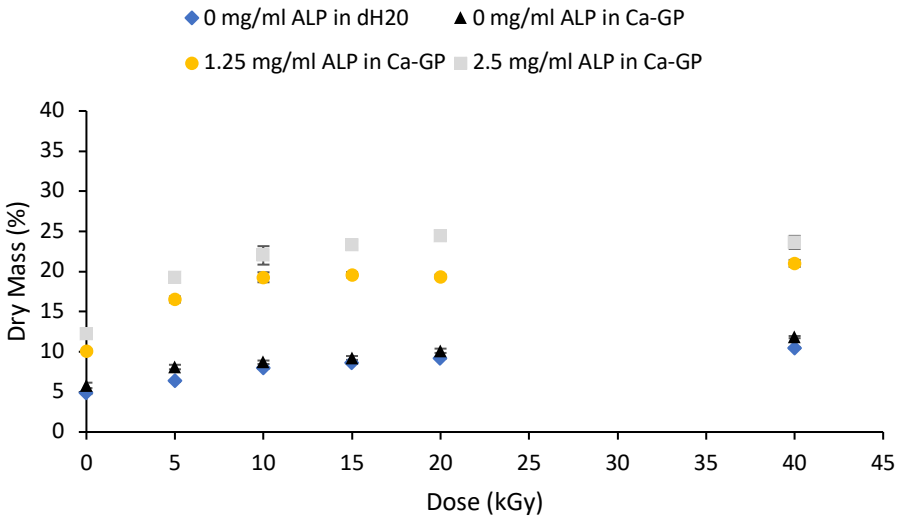

Figure 5: Dry Mass percentages of gelatin hydrogels with ALP concentrations of 0, 1.25 and 2.5mg/ml, at electron irradiation doses ranging from 0 to 40 kGy, mineralised for 6 days as per method*. Error bars show standard deviation.*

4.2 Compression Modulus

The compression modulus of gelatin hydrogels with ALP concentrations of 0, 1.25 and 2.5 mg/ml, exposed to radiation doses of 0, 5, 10, 15, 20 and 40 kGy, is illustrated in figure 6. Hydrogels were subject to compressive testing until failure. The compressive stress was calculated, and the compression modulus was subsequently determined.

Although the compression modulus of both the 0 mg/ml in ddH_2O, and 0 mg/ml in CaGP increased alongside each subsequent elevation of the electron irradiation dose (0 to 40 kGy), a one-way ANOVA with Tukey's post hoc analysis identified no statistical significance. For the 1.25 and 2.5 mg/ml ALP samples, however, a statistically significant increase in the compression modulus was identified when the samples were exposed to 40 kGy compared to the 0 kGy control (increases of 11,486 and 11,266 kPa, respectively).

However, for both the 1.25 and 2.5 mg/ml ALP samples, an increase in radiation from 10 kGy to 15 or 20 kGy resulted in a decrease in the compression modulus. For 1.25 mg/ml ALP samples, those exposed to 10 kGy displayed a statistically significant elevation in compression modulus compared to the 40 kGy exposed group. This trend was not shown in the 2.5 mg/ml ALP samples, as compression modulus recovered from the reduction displayed at 15 and 20 kGy to demonstrate an increase (although not significant) of 870 kPa when compared to the 10 kGy samples.

At each dose of electron irradiation, 0 mg/ml ALP samples in ddH_2O displayed higher compression moduli than the 0 mg/ml samples in CaGP, although these discrepancies were not deemed statistically significant. Raising the ALP concentration from 0 mg/ml to 1.25 mg/ml resulted in a statistically significant increase in the compression modulus observed for the samples at all the electron irradiation doses examined, apart from 0 kGy (5, 10, 20 and 40 kGy); while the highest concentration (2.5 mg/ml) resulted in a statistically significant increase at all doses.

Although the compression moduli of samples at 2.5 mg/ml ALP were elevated compared to the 1.25 mg/ml ALP samples at doses of 0 and 40 kGy of electron irradiation, no statistical significance was identified. However, at the remaining irradiation doses (5, 10, 15 and 20 kGy), the compression moduli of samples containing ALP at concentrations of 1.25 mg/ml were elevated, in a statistically significant manner, compared to those containing 2.5 mg/ml.

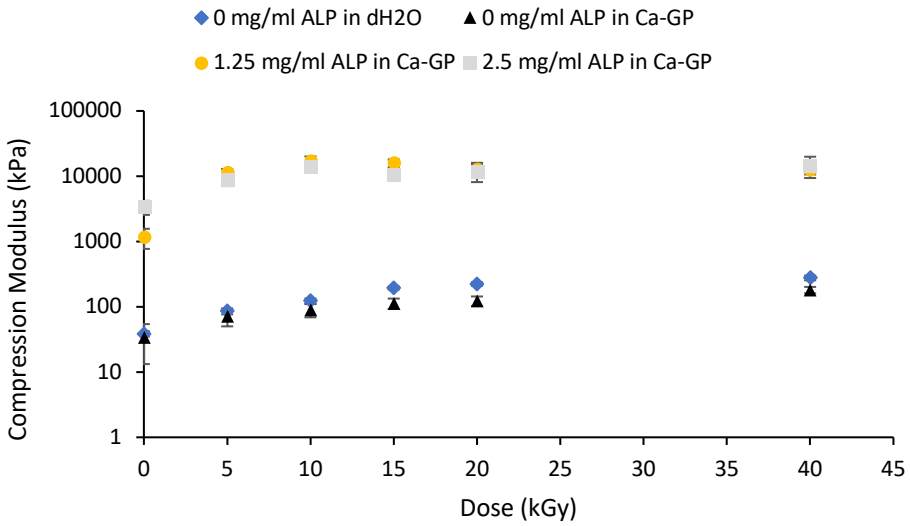

Figure 6: Compression modulus of gelatin hydrogels with ALP concentrations of 0, 1.25 and 2.5mg/ml, at electron irradiation doses ranging from 0 to 40 kGy*. Subject to compressive testing following 6 days of enzymatic mineralisation. Error bars show standard deviation*

4.3 Raman Spectroscopy

Raman spectroscopy utilises vibrational, rotational, and other low frequency modes in a system to provide a structural fingerprint which enables molecular identification.

No significant bands, typical of molecules of interest, were detected via the Raman spectra (figure 7) for the gelatin control samples (0 mg/ml ALP in ddH_2O). Similarly, the spectra for the 0 mg/ml ALP in CaGP group were unremarkable, except for a relatively low intensity peak at approximately 1035 cm^{-1}, typical of $_{v1}PO_4^{3-}$. However, high intensity bands typical of PO_4^{3-} groups were detected for both gelatin samples containing ALP (1.25 and 2.5 mg/ml ALP in CaGP).

Specifically, Raman bands characteristic of the v1 stretching of PO_4^{3-} groups were detected at approximately 957 cm^{-1}. The intensity of this band approximately doubled when ALP concentration was increased from 1.25 mg/ml to 2.5 mg/ml. Additional bands were detected at around 1242 cm^{-1}, characteristic of Amide III groups – specifically the protein β-sheet and random coils, and ~1446 cm^{-1}, characteristic of protein CH_2 deformation; both of which were more intense at 2.5 mg/ml ALP. Furthermore, bands characteristic of collagen proline (v(C-C)/(C–C–H) were detected at approximately 853 cm^{-1}.

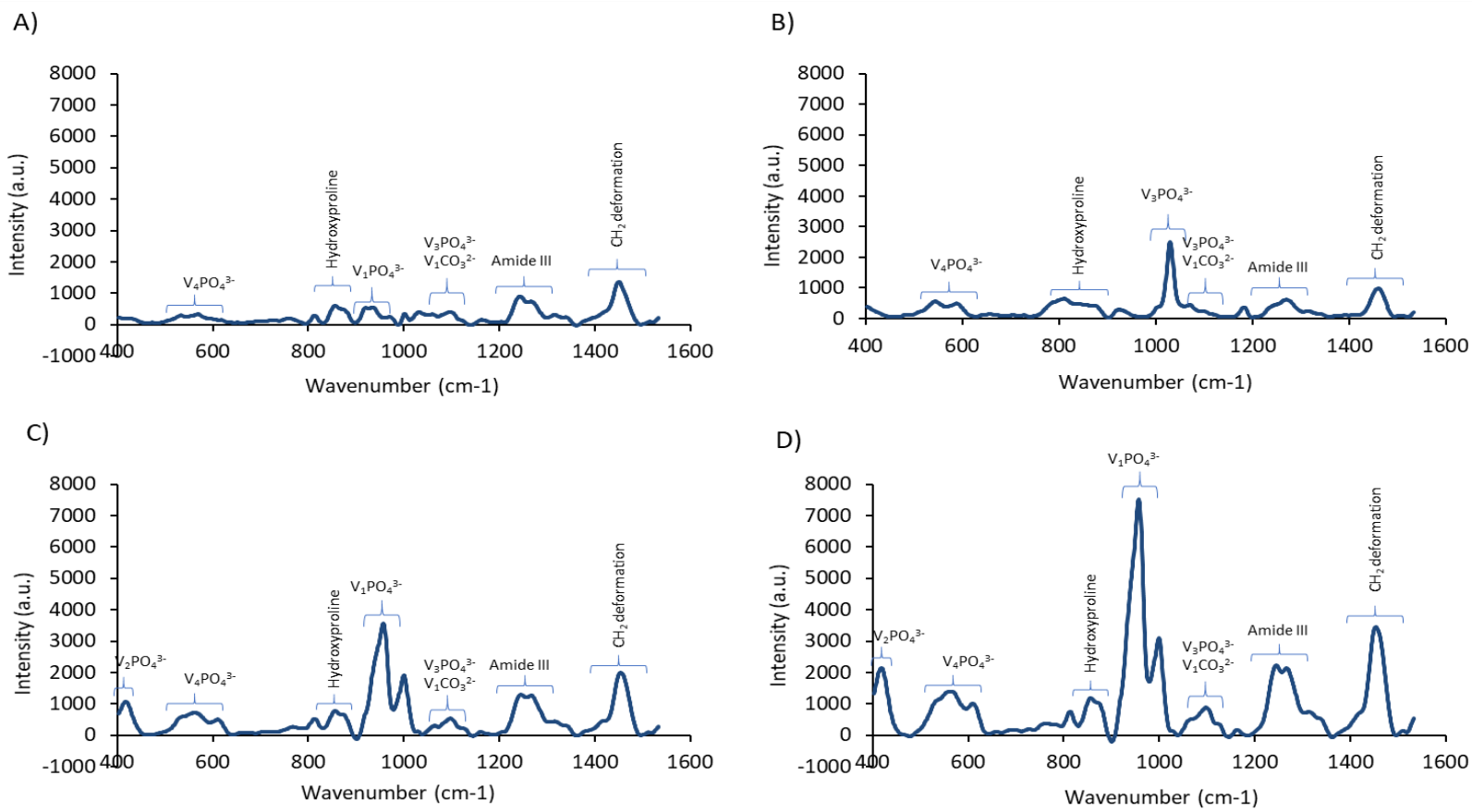

Figure 7: Baselined-corrected Raman Spectra of gelatin hydrogels electron irradiated at doses of 40kGy, with ALP concentrations of 0, 1.25 and 2.5mg/ml, subject to enzymatic mineralisation for 6 days. (A) 0mg/ml in ddH2O, B) 0mg/ml in CaGP, C) 1.25mg/ml, D) 2.5mg/ml).

4.4 Fourier Transmission Infrared Spectroscopy (FT-IR)

FT-IR spectra for all composites subject to incubation in CaGP displayed double bands characteristic of the v4 vibrations of PO_4^{3-} groups in the region of 563-603cm^{-1}, which were absent in the control (0mg/ml in ddH_2O). This double band is more obvious at ~540cm^{-1}, with the second band at ~600cm^{-1} less apparent. Strong absorption bands characteristic of PO_4^{3-} stretching were also present at ~970 cm^{-1} and between 1045 to 1100cm^{-1} in the spectra for samples containing ALP but absent in the control. However, the spectra for the CaGP control (0mg/ml ALP) displayed two bands in this region. A weak band at ~870cm^{-1} derived from the v5 P-O(H) deformation of HPO_4^{2-} groups was also present in both ALP supplemented composites (1.25 and 2.5mg/ml) but did not appear to be present in either of the control groups (Van Den Vreken et al., 2006).

Strong bands in the region of ~1200-1700cm^{-1} representative of overlapping signals of N-H bending and C=O and C-N stretching typical of the Amide I and Amide II bands found in proteins were observed in the 0mg/ml ALP ddH2O control. These bands were far less pronounced in the remaining sample groups.

It was also noted that the relative intensities presented on the spectra was unexpected, with both the 0mg/ml ALP CaGP and 1.25mg/ml ALP samples exhibiting elevated absorbance compared to the sample group with increased ALP concentration.

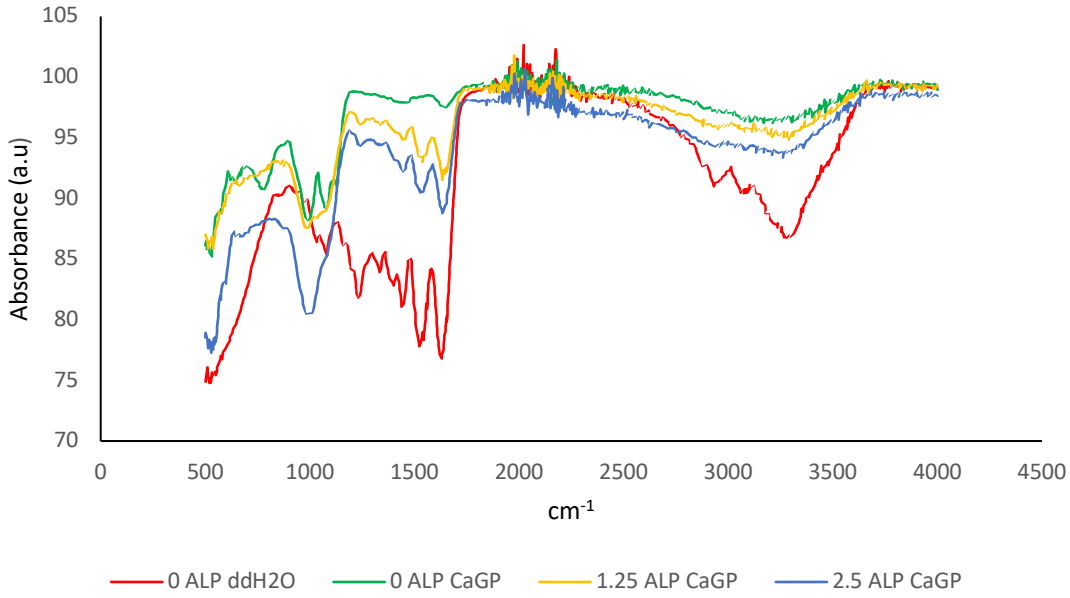

Figure 8: FTIR spectra of Electron Irradiated Gelatin hydrogels incorporated with ALP, presented in the region between 4000-500 cm-1.

4.5 Scanning Electron Microscopy (SEM)

SEM was utilised to analyse differences in the surface topography of gelatin hydrogels with ALP concentrations ranging from 0 to 2.5 mg/ml, following 6 days of mineralisation in CaGP (figure 9).

The unmineralized ALP/CaGP-free gelatin control samples (A) displayed a consistently smooth surface topography. The surfaces of the 0 mg/ml ALP in CaGP samples were also relatively smooth in appearance. However, their surface displayed a less consistent morphology as sporadic deposits and 'rougher' sections could be visualised (figure 9B). Despite this, both ALP-free sample groups were markedly different to the ALP mineralised samples, which presented a considerably rougher surface morphology.

SEM imaging of both 1.25 and 2.5 mg/ml ALP samples demonstrated successful ALP-induced mineralisation. Mineral deposits of irregular shapes and sizes were tightly compact and

distributed homogenously across the surface of the gelatin samples, with typical diameters of 100 to 500 nm.

SEM was perhaps insufficient to allow the elucidation of morphological discrepancies between samples containing 1.25 and 2.5 mg/ml ALP, as no obvious differences could be identified.

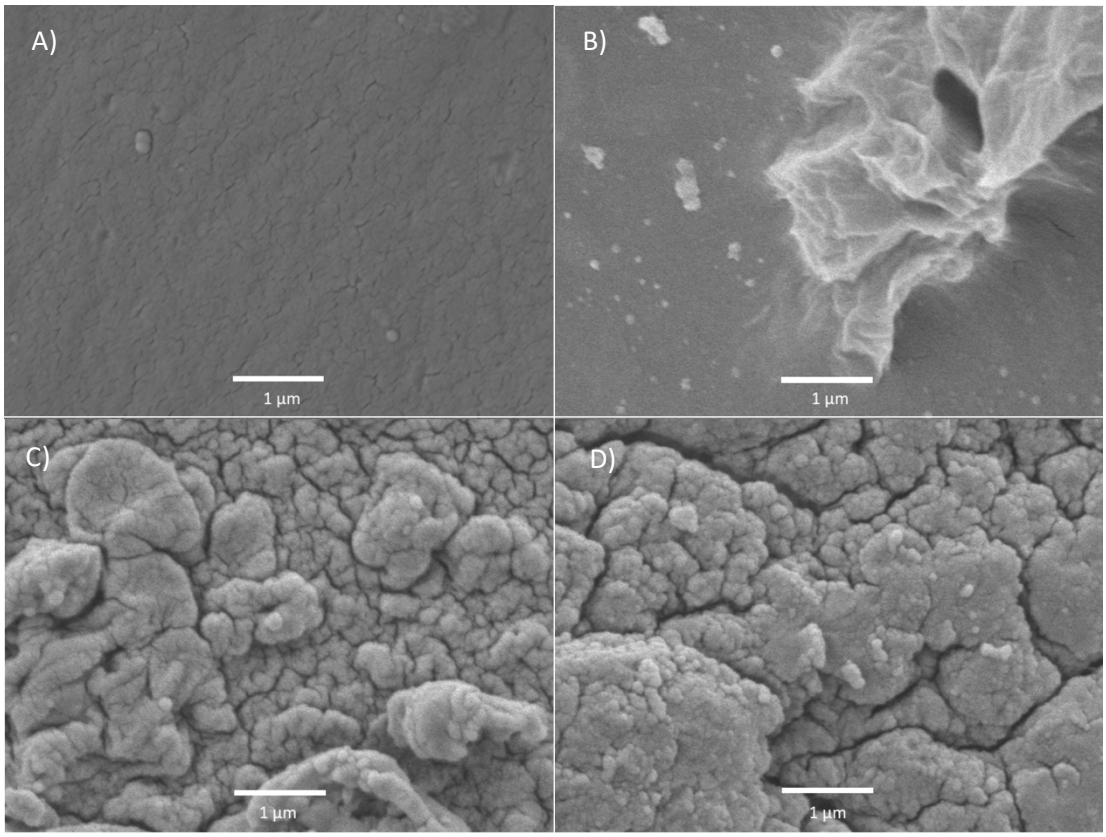

Figure 9: SEM Images of gelatin hydrogels containing ALP concentrations of 0 mg/ml in ddH2O (A), 0 (B), 1.25 (C) and 2.5 (D) mg/ml mineralised for 6 days in CaGP. *Images show scale bars representing 1 µm.*

4.6 Cell culture Scanning Electron Microscopy

To allow a more detailed assessment of the morphology and attachment of cells onto the hydrogel samples following cell culture, samples were visualised by SEM (as illustrated in figure 10). Following 7 days of cell culture, confluent layers of cells could be visualised on the control (0 mg/ml ALP in ddH_2O samples [Ai and Aii]). Cells were spread with clearly defined borders and visible filopodia present, suggesting effective attachment. Similarly, large areas with complete cell coverage were observed in the remaining ALP-free sample group (0 mg/ml ALP in CaGP [Bi and Bii]). Again, filopodia could be seen, and attachment to the hydrogel surface appeared to be good. However, areas of the hydrogel without cell coverage could also be observed.

As the ALP concentration increased, first to 1.25 (Figure 10 Ci and Cii) and then 2.5 mg/ml (Di and Dii), the areas of the hydrogels with cell coverage became more sporadic. On the 1.25 mg/ml hydrogels, layers of cells which appear to have been (previously) confluent could be observed. Spread cells could still be observed, but they were also accompanied by a greater proportion of cells which appeared to be peeling from the surface, or cells which appear to have been lysed (Cii). These observations remained consistent when the 2.5 mg/ml samples (Di and Dii) were imaged. However, the proportion of cell coverage was again reduced, while the number of cells demonstrating an 'unhealthy' morphology increased.

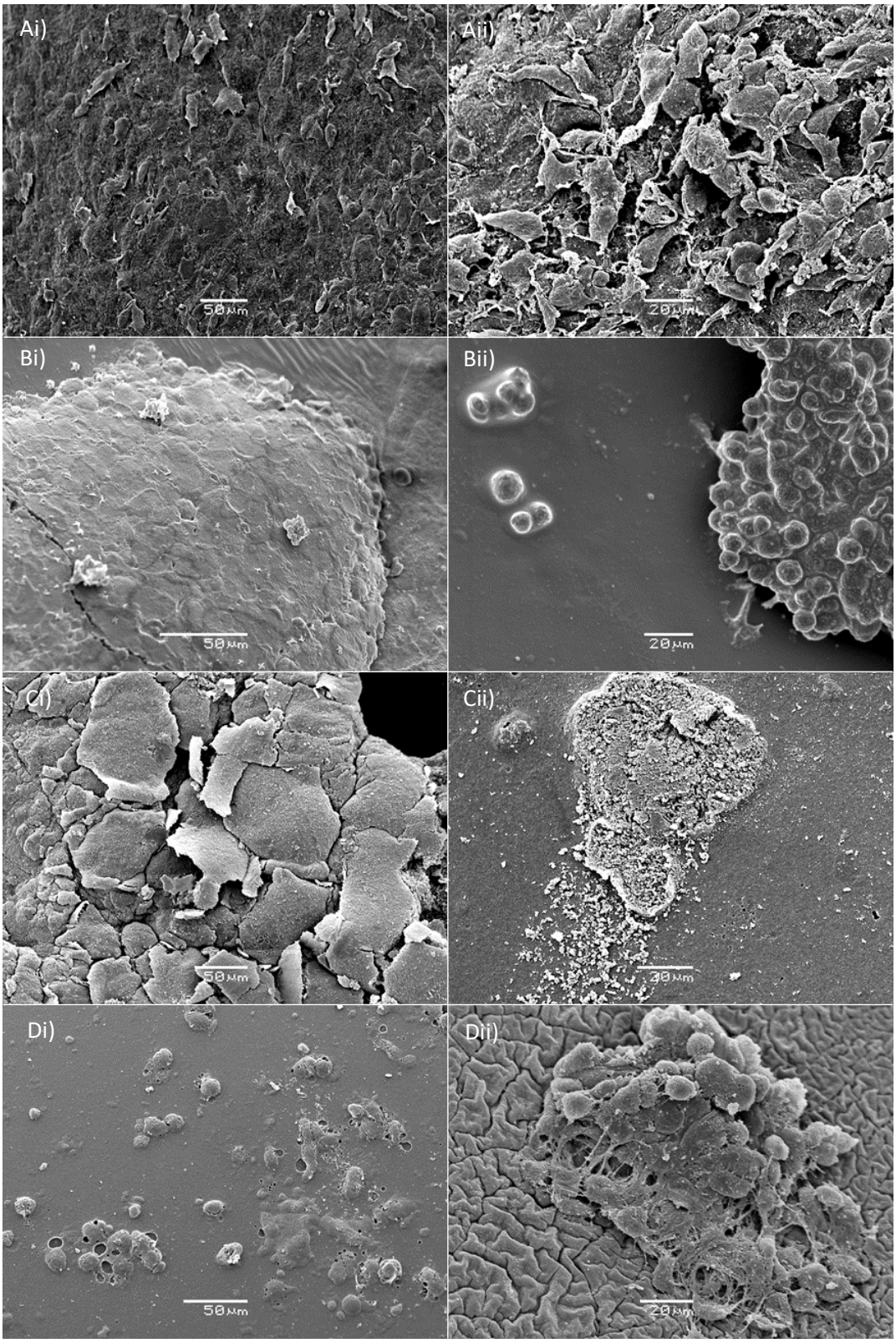

Figure 10: SEM images of gelatin hydrogels containing ALP concentrations of 0 mg/ml in ddH2O (Ai and Aii), (Bi and Bii), 1.25 (Ci ad Cii) and 2.5 (Di and Dii) mg/ml mineralised for 6 days in CaGP, after the 7th day of cell culture. *Images show scale bars (Left = 50µm, Right= 20µm)*

4.7 Inductively Coupled Plasma Optical Emission Spectrometry (ICP-OES)

ICP-OES was utilised to obtain a more accurate determination of the extent to which mineralisation had been successfully induced by ALP. The elemental composition of the mineralisation product, P and Ca concentrations, and the Ca:P ratio was determined.

4.7.1 Phosphorus Concentration

Only negligible traces of elemental P were detected in the ALP/CaGP-free gelatin control group. A statistically significant increase ($p<0.05$) in elemental P concentration was observed when the ddH_2O was replaced with CaGP, even when the ALP concentration remained at 0 mg/ml. However, when the concentration of ALP was raised to 1.25 mg/ml, and further to 2.5 mg/ml, statistically significant increases ($p<0.001$) in the mean elemental P concentration of samples was observed (83.15mgP/g and 93.35mgP/g, respectively). Although the observed P concentration of samples containing 2.5 mg/ml ALP was elevated compared to 1.25 mg/ml ALP samples, this increase was not statistically significant (figure 11).

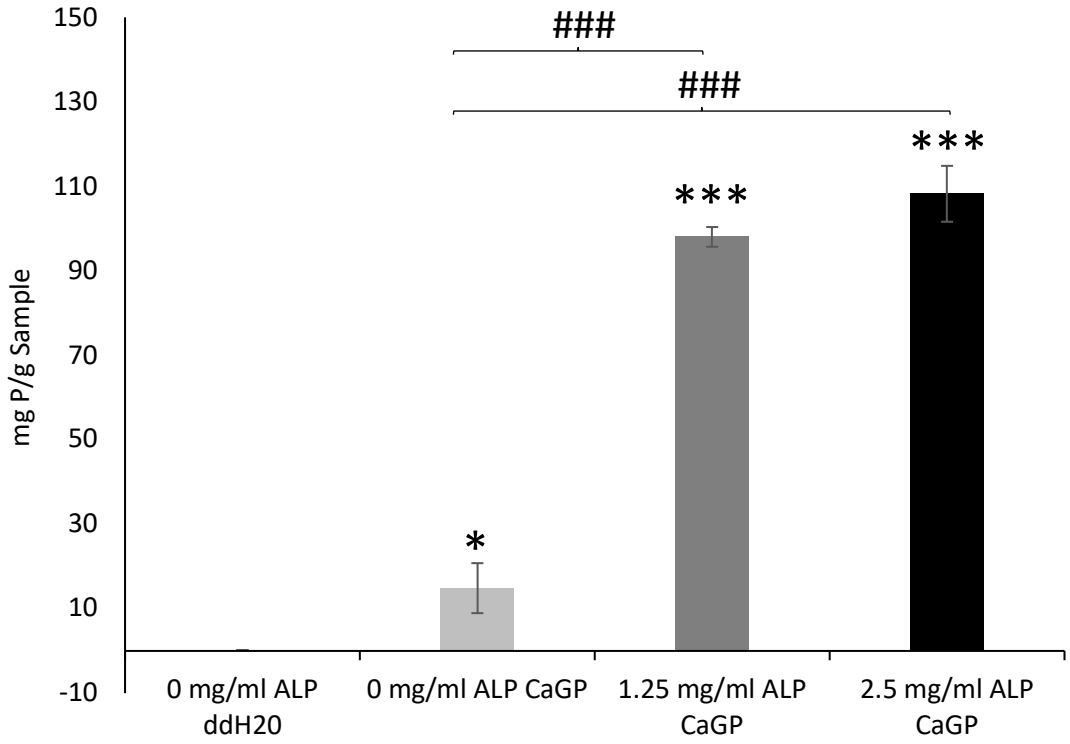

Figure 11: ICP-OES determination of Phosphorus concentrations of gelatin hydrogels with ALP concentrations of 0, 1.25 and 2.5mg/ml, electron irradiated at 40kGy, following 6 days of enzymatic mineralisation*. One-way ANOVA was performed. Results expressed as means ± standard deviation. Differences considered significant if p≤0.05. '*' relates to the significant difference between groups exposed to CaGP and the ddH_2O control (*** P<0.001, * P<0.05). '#' relates to the significant difference between experimental groups (### P<0.001).*

4.7.2 Calcium Concentration

The same trend was observed for elemental Ca concentration (figure 12). No notable concentration of Ca was identified in 0mg/ml ALP in ddH_2O samples. This increased, in a statistically significant manner ($p<0.05$), to a mean Ca concentration of 20.54 mg/g in 0 mg/ml ALP in CaGP samples. Similarly, mean Ca concentrations displayed statistically significant increases ($p<0.001$) when ALP concentrations were raised to 1.25 and 2.5 mg/ml (155.91 and 177.30 mg/g sample, respectively). The mean increase of 21.39 mg/g observed

when ALP concentration was elevated from 1.25 to 2.5 mg/ml, was also statistically significant ($p<0.05$).

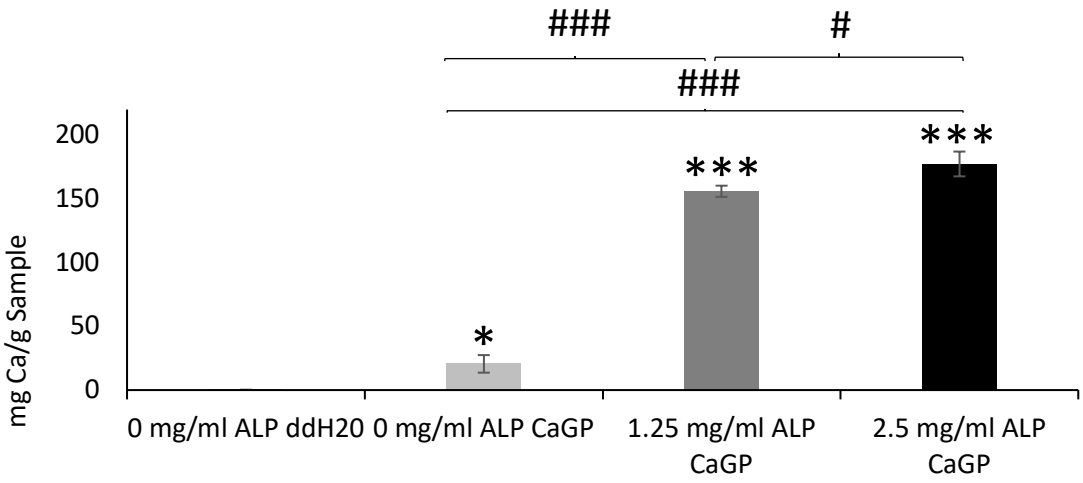

Figure 12: ICP-OES determination of calcium concentrations of gelatin hydrogels with ALP concentrations of 0, 1.25 and 2.5mg/ml, electron irradiated at 40kGy, following 6 days of enzymatic mineralisation*. One-way ANOVA was performed. Results expressed as means ± standard deviation. Differences considered significant if p≤0.05. '*' relates to the significant difference between groups exposed to CaGP and the ddH_2O control (*** P<0.001, * P<0.05). '#' relates to the significant difference between experimental groups (### P<0.001, # p<0.05).*

4.7.3 Molar Ratio

The molar Ca:P ratio, determined by ICP-OES, is illustrated in figure 13. All observed Ca:P ratios were lower than that of stoichiometric hydroxyapatite (1.67).

ALP/CaGP-free samples displayed a mean Ca:P ratio of 0.82. This increased to 1.11 in ALP free samples soaked in CaGP and increased further in samples containing 1.25 and 2.5 mg/ml ALP (1.23 and 1.27, respectively), all of which displayed statistical significance ($p<0.05$) compared to the ALP/CaGP free control. However, differences in the molar ratios between the remaining samples showed no statistical significance.

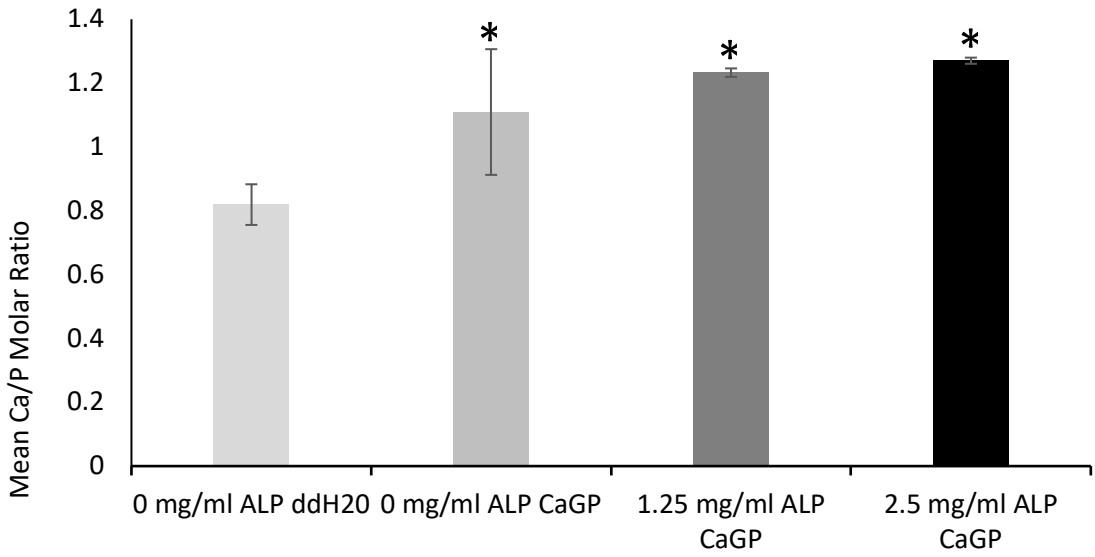

Figure 13: ICP-OES determination of Ca/P molar ratio of gelatin hydrogels with ALP concentrations of 0, 1.25 and 2.5mg/ml, electron irradiated at 40kGy, following 6 days of enzymatic mineralisation*. One-way ANOVA was performed. Results expressed as means ± standard deviation. Differences considered significant if p≤0.05. '*' relates to the significant difference between groups exposed to CaGP and the ddH_2O control (P<0.05).*

4.8 Fluorescent Microscopy (Experiment One)

The interaction of gelatin hydrogels, containing ALP and mineralised for 6 days, with a human osteosarcoma (MG-63) cell line was evaluated at intervals of 1, 4 and 7 days. The adhesion, proliferation, and morphology of cells was assessed by fluorescent microscopy, as illustrated in figure 14. Cell nuclei were successfully stained (blue) with Hoechst, while the cytoplasmic regions of cells were successfully stained (red) with Texas Red.

No definitive conclusions can be drawn from the results of fluorescent microscopy, as expression levels were not quantified, p-values were not obtained, and therefore no statistical significance can be suggested. However, as illustrated in figure 14, after 24 hours of cell culture, it was observed that MG-63 cells had been successfully cultured on each of

the sample groups (ALP/CaGP control, 0, 1.25 and 2.5 mg/ml ALP in CaGP hydrogels). On each group, both the cytoplasm and nuclei of cells were well defined, while cells portrayed a healthy, well spread morphology. However, cells appeared more numerous in the gelatin control sample, where an almost confluent layer of cells was observed. The number of cells visible by microscopy appeared to reduce, first when ddH_2O was substituted with CaGP, and then further with each increase of sample ALP concentration.

These observations appeared consistent at both 4 and 7 days of cell culture. In both sample groups for which ALP was absent, the number of visible cells seemed to remain relatively consistent from the first to the seventh day of cell culture. Similarly, the nuclei and cytoplasm of the visualised cells remained well defined. However, for samples containing ALP (1.25 and 2.5 mg/ml), the number of cells visible via fluorescent microscopy appeared to decrease further with each consecutive time point, with minimal cell coverage after 7 days, particularly in the samples containing 2.5 mg/ml ALP. Additionally, the observed cells presented a more rounded phenotype.

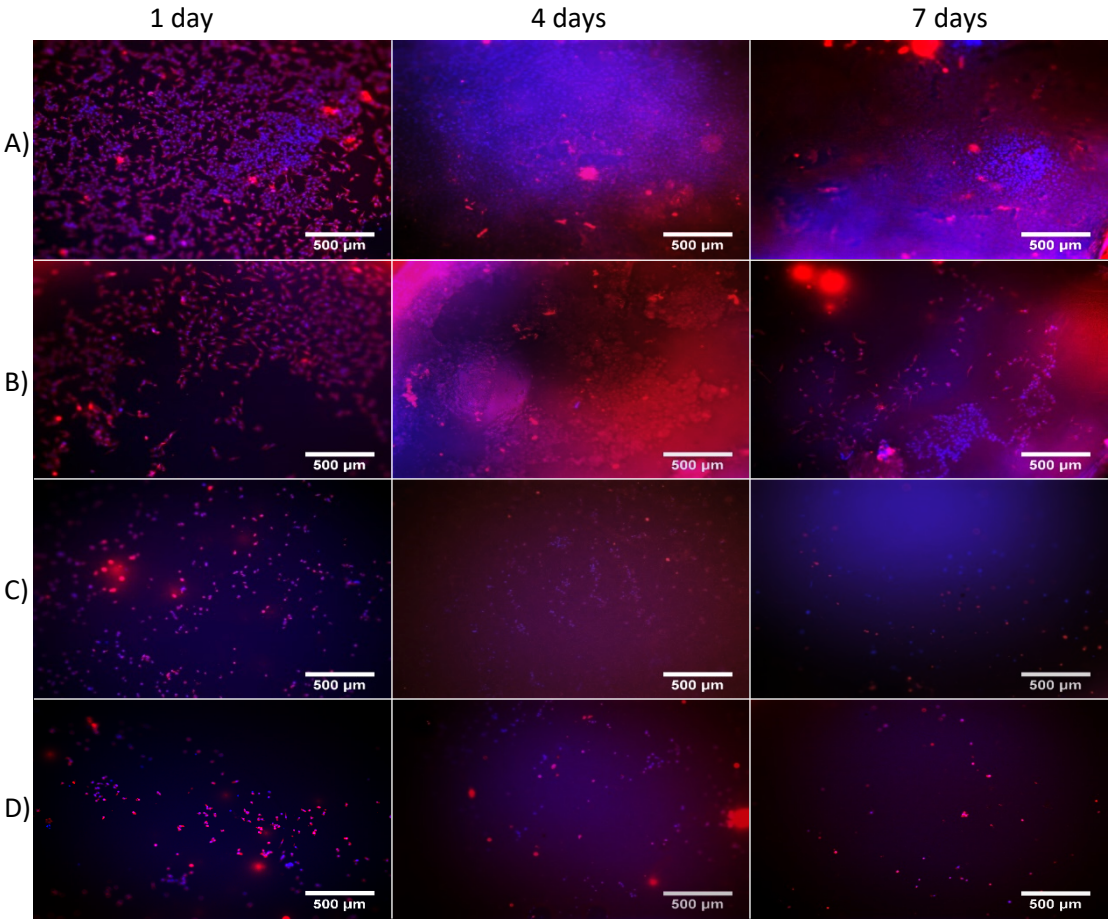

Figure 14: Fluorescent microscopy of MG-63 osteoblast-like cells cultured on gelatin hydrogels with varying ALP concentrations. *A) 0mg/ml + H_2O, B) 0mg/ml , C) 1.25mg/ml (D) 2.5mg/ml. Samples (B,C,D) mineralised in CaGP solution and electron irradiated at 40kGy at 1, 4 and 7 days. Cells stained by Hoechst (nuclei, blue) and Texas Red (cell cytoplasm, red). Scale bar indicates 500µm.*

4.9 Proliferation (MTS) Assay (Experiment One)

The MTS assay (figure 15) was utilised to allow a quantitative evaluation of the previously discussed cell culture results, by measuring the extent to which metabolically active cells have converted a soluble tetrazolium salt into insoluble formazan – thus, indirectly measuring proliferation and cell viability, and cytotoxicity of the samples.

As illustrated in figure 15, a statistically significant reduction in metabolic activity from MG-63 cells was observed for each of the sample groups compared to the polystyrene control, at each time point (1, 4 and 7 days). After 24 hours of cell culture the absorbance due to the insoluble formazan was almost identical for the ALP-free samples (in ddH_2O & in CaGP), measured at 0.0227 and 0.0229 a.u, respectively. Although this was approximately 11 times lower than the polystyrene control at the same time point. The absorbance reduced further with increasing ALP concentration, to 0.00586 at 1.25 mg/ml, and 0.00508 a 2.5 mg/ml ALP. In fact, no significant difference in metabolic activity was observed between 1.25 and 2.5 mg/ml ALP at 1, 4 and 7 days, and both ALP-free samples after 1 day. Despite this, the absorbance displayed a statistically significant increase for both ALP-free samples after 4 days. The maximum absorbance recorded for experimental samples was recorded at 0.277 a.u for the 0 mg/ml ALP samples in CaGP after 7 days – a significant increase from that observed after 4 days. However, this showed no statistically significant increase compared to the polystyrene control after only 24 hours.

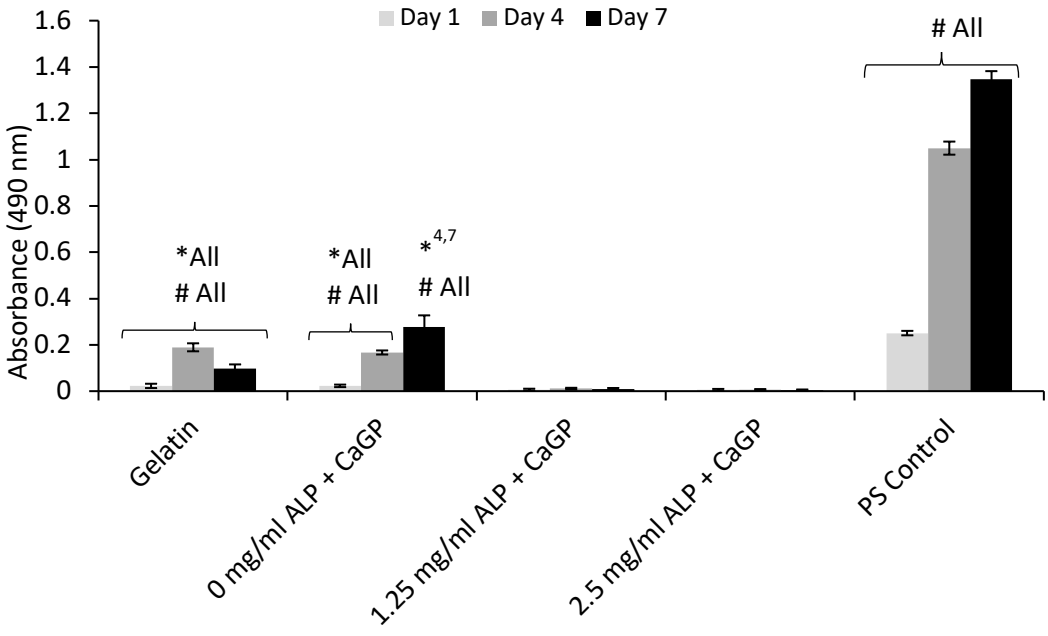

Figure 15: Proliferation of MG-63 osteoblast-like cells on gelatin hydrogels with ALP concentrations of 0, 1.25 and 2.5mg/ml, mineralised in CaGP solution and electron irradiated at 40kGy*. Assessed at 1, 4 and 7 days, via the MTS assay (as per method). Hydrogels were placed in 500µl of MTS solution and incubated for 2 hours. Absorbance was then measured via a spectrophotometer (at 490nm). # All indicates statistical significance within sample groups (P<0.05). *All/4,7 indicates statistical significance compared to the Polystyrene control at the corresponding time periods (P<0.05). Error bars show standard deviation.*

4.10 Fluorescent Microscopy (Experiment Two)

To supplement the previously discussed analysis of the interaction between mineralised gelatin hydrogels with the MG-63 cell line, the experiment was repeated using both 'thick' and 'thin' hydrogels, to elucidate any potential effects that hydrogel thickness may have on the adhesion, proliferation and morphology of cells. As illustrated in figure 16 the nuclei of cells were successfully stained (blue) with Hoechst stain, and the cytoplasm of cells were successfully stained (red) with Texas Red.

Figure 16 depicts fluorescent microscopy images taken from samples on the seventh day of cell culture. Successfully cultured MG-63 cells were observed on all sample groups (ALP/CaGP control, 0, 1.25 and 2.5 mg/ml ALP in CaGP hydrogels), both 'thick' and 'thin', after 7 days of cell culture. However, cell coverage appeared to be superior on the 'thin' samples, where a seemingly confluent layer of cells appeared to cover the surface of the hydrogels for each sample group, including the 1.25 and 2.5 mg/ml ALP samples. Cells appeared to display a spread morphology, with clearly defined nuclei. The gelatin control hydrogels in the 'thick' category also displayed good cell coverage (although not confluent as with the thin samples), similarly, with a seemingly healthy morphology. However, increasing the ALP concentration to 1.25 and 2.5 mg/ml appeared to have a negative effect on cell proliferation, as fewer cells were observed, more sporadically, the higher the concentration of ALP. Additionally, the morphology of the observed cells appeared less spread and well defined when compared to the cells cultured on the 'thin' counterparts.

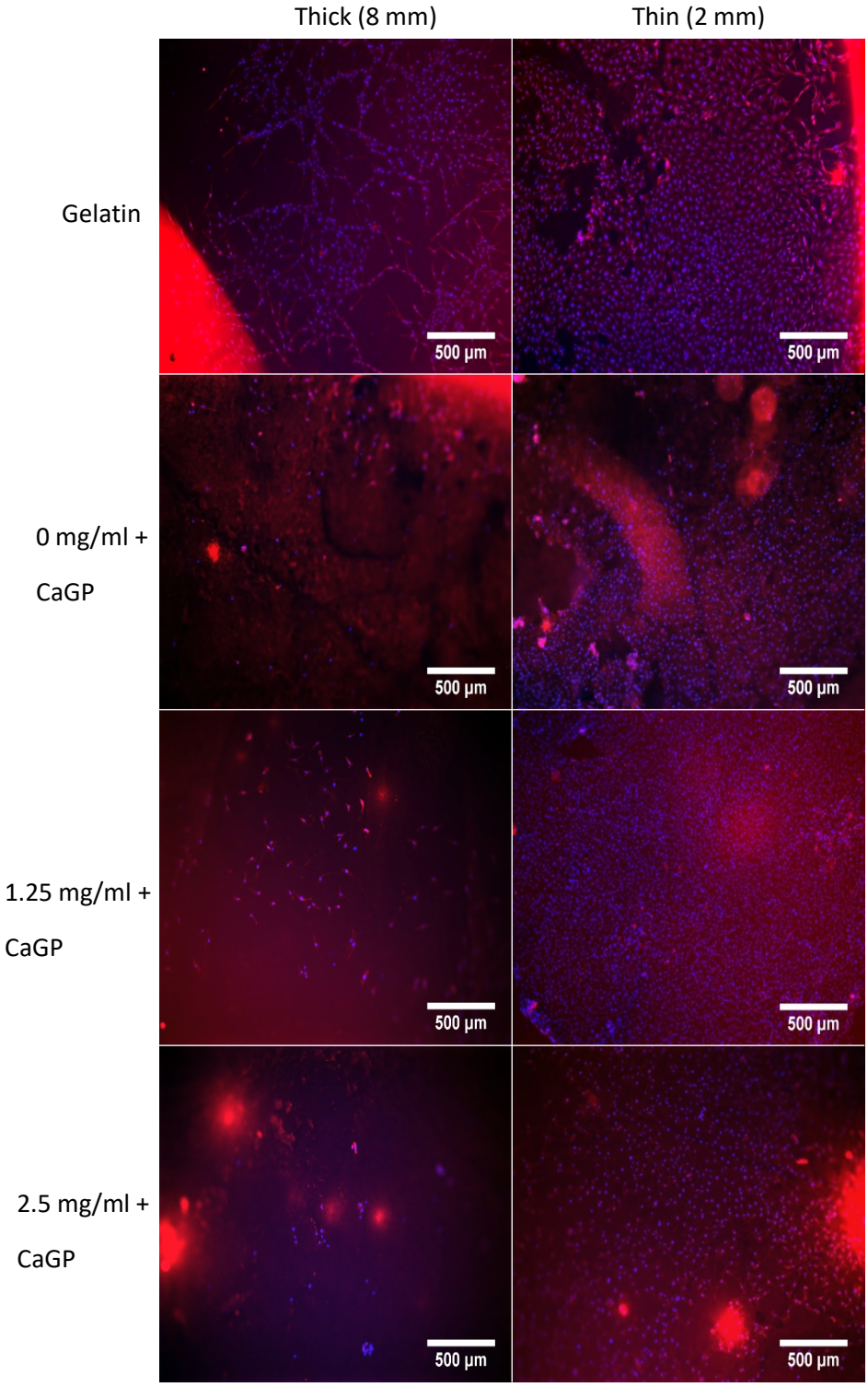

Figure 16: Fluorescent microscopy of MG-63 osteoblast-like cells cultured on 'Thick' and 'Thin' gelatin hydrogels with ALP concentrations of 0, 1.25 and 2.5mg/ml.

Mineralised in CaGP solution and electron irradiated at 40kGy following 7 days of cell culture. Cells stained by Hoechst (nuclei, blue) and Texas Red (cell cytoplasm, red). Scale bar represents 500µm.

4.11 Proliferation (MTS) Assay (Experiment Two)

Again, the MTS assay (figure 17) was utilised to evaluate the proliferation, cell viability and cytotoxicity of 'thick' and 'thin' gelatin hydrogel samples, in a quantitative manner.

As illustrated in figure 17, no statistically significant difference ($p<0.05$) in metabolic activity from cultured MG-63 cells was observed between any of the sample groups, or the polystyrene control, after 24 hours. The observed absorbance due to insoluble formazan increased for each sample group from day 1 to day 4 of cell culture. Again, the values observed for both 0 mg/ml ALP in ddH_2O (0.431 a.u) and 0 mg/ml ALP in CaGP (0.462 a.u) 'thin' samples displayed no statistically significant difference compared to the polystyrene control after 4 days of cell culture (0.519 a.u). However, the absorbance for all remaining sample groups (1.25 and 2.5 mg/ml ALP in CaGP, both 'thick' and 'thin' and ALP-free 'thick' samples) demonstrated a statistically significant reduction compared to the polystyrene control. For the 'thin' samples, increasing the ALP concentration from 1.25 to 2.5 mg/ml reduced the observed absorbance from 0.264 to 0.239 a.u, although this was not statistically significant. Both observed values were increased compared to their 'thick' counterparts. 1.25 mg/ml ALP samples demonstrated a negligible 0.007 increase in the 'thin' samples compared to the thick. A statistically significant increase was observed in the 2.5 mg/ml ALP samples, however, which increased by 0.159 from 0.0796 ('thick') to 0.239 ('thin'). After 7 days of cell culture, all sample groups, both 'thick' and 'thin' displayed a statistically significant reduction in metabolic activity compare to that of the polystyrene control at the same time point. Unexpectedly, the results observed for MTS following 7 days of cell culture contrast those of previous time points, along with the assumptions drawn from fluorescent microscopy. The metabolic activity observed from each sample group was increased in the 'thick' hydrogels than in its 'thin' counterpart, all of which were statistically significant increases, except for the 1.25 mg/ml ALP sample group, which was almost identical at both thicknesses.

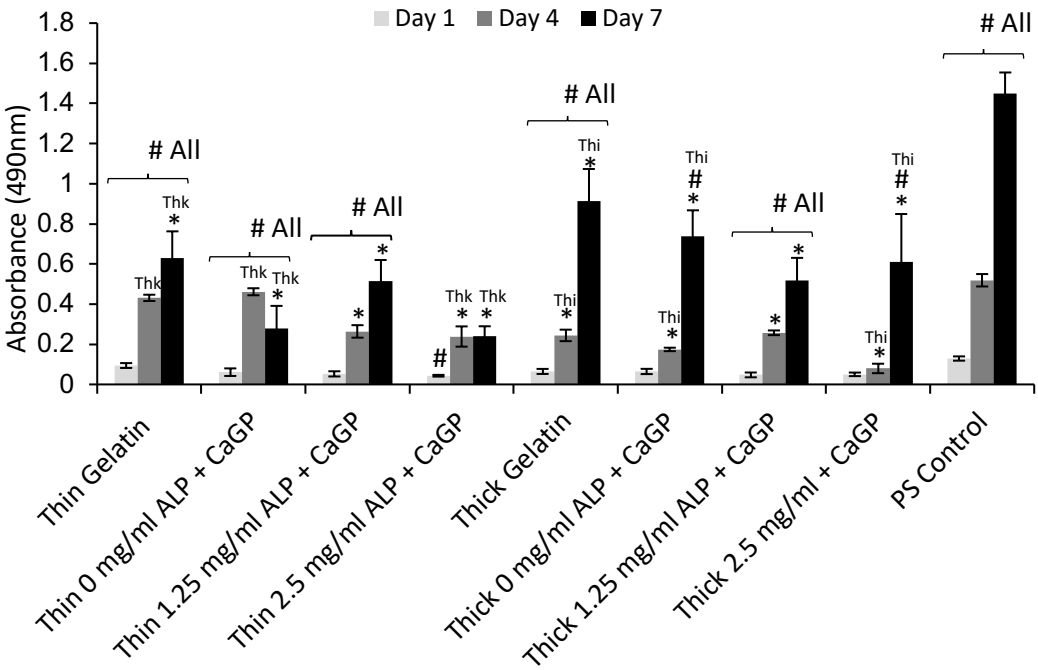

Figure 17: Proliferation of MG-63 osteoblast-like cells on both 'thick' and 'thin' gelatin hydrogels with ALP concentrations of 0, 1.25 and 2.5mg/ml, electron irradiated at 40kGy*. Assessed at 1, 4 and 7 days, via the MTS assay (as per method). Hydrogels were placed in 500µl of MTS solution and incubated for 2 hours. Absorbance was then measured via a spectrophotometer (at 490nm). # indicates statistical significance for values within sample groups (P<0.05). * indicates a statistically significant difference compared to the polystyrene control (P<0.05). 'Thi' and 'Thk' indicate a statistically significant difference between the Thick sample group and their 'Thin' counterpart, at the corresponding time point. Error bars show standard deviation.*

5.0 Discussion

As previously stated, hydrogels have numerous potential advantages in tissue engineering. One of which is the ease of incorporation of bioactive substances such as enzymes. Gelatin is a promising biomaterial, being inexpensive, biocompatible, non-immunogenic, and biodegradable. However, in the absence of crosslinking, hydrogels comprised of gelatin lose structural integrity at body temperature. This study aimed to demonstrate the utilisation of electron beam irradiation to simultaneously crosslink and sterilise gelatin hydrogels, while avoiding the use of cytotoxic chemical crosslinkers such as glutaraldehyde. Furthermore, in this study, the enzyme ALP was incorporated into the electron beam-crosslinked gelatin hydrogels to induce their mineralisation with CaP and elicit the numerous advantages associated with this. Mineral formation itself, along with its effects on both the morphology and mechanical properties of the electron irradiated gelatin hydrogels, was evaluated.

Gelatin hydrogels were successfully formed, and simultaneously sterilised, by electron irradiation at each of the experimental doses.

Consistent with the findings of Douglas et al., (2012), who demonstrated that cPEG, collagen and OPF hydrogels could be successfully mineralised via the incorporation of ALP, and subsequent incubation in a solution containing glycerophosphate (GP) and Ca^{2+} (ALP substrates), successful mineralisation of the electron irradiated gelatin hydrogels exposed to this method was confirmed by numerous techniques.

5.1 Dry Mass

The statistically significant increase in dry mass percentage for each of the sample groups when the irradiation dose was elevated from 0 to 40kGy confirmed the relevance of this technique to crosslink gelatin hydrogels in the absence of toxic chemical crosslinkers, as previously discussed by Wisotzki et al (2014) and Wisotzki et al (2016). As expected, the increase in dry mass attributable to the increasing dose of electron irradiation was greater

when moving from 0 to 5kGy, and from 5 to 10kGy, after which the increase in dry mass began to plateau with subsequent increases in the irradiation dosage, presumably due to crosslinking nearing saturation point. This plateau was more severe in the sample groups containing 1.25 and 2.5mg/ml of ALP.

Importantly, the ALP induced mineralisation of the 1.25 and 2.5mg/ml ALP hydrogels resulted in a dry mass percentage increase that overshadowed that attributable to the crosslinking effect of increasing the dose of electron irradiation. Thus, demonstrating the successful formation and incorporation of the mineral phase in the hydrogels.

5.2 Raman Spectroscopy

Raman spectroscopy provided direct evidence to reinforce the indirect indication of successful ALP induced mineralisation provided by dry mass analysis. Raman spectroscopy utilises vibrational, rotational, and other low frequency modes in a system to provide a structural fingerprint which enables the molecular structure and chemical composition of samples to be elucidated.

Typically, the Raman spectra of bone is reported for a window from approximately 400cm^{-1} to 1750cm^{-1} as this is the region which presents bands characteristic of both bone mineral and bone matrix (Mandair and Morris, 2015). The present study adhered to this norm in order to confirm successful ALP induced mineralisation of the gelatin hydrogels.

The absence of bands representative of bone mineral observed in the control sample group (0mg/ml ALP in ddH_20) was expected, due to the absence of exposure to the mineralisation process. Similarly, the low intensity bands representative of Amide III and CH_2 deformation characteristic of the hydrogels gelatinous nature were expected. However, the peak of relatively low intensity, representative of phosphate, observed in the spectra of the 0mg/ml ALP Ca-GP group was not expected. As this group was not exposed to the ALP induced

mineralisation procedure, this can most likely be explained by residual CaGP in the hydrogels due to incomplete washing out.

The Raman spectra for both experimental groups (1.25 and 2.5mg/ml ALP in Ca-GP) changed dramatically. The presence of a phosphate band in Raman spectra representative of carbonated apatite's is the most common mineral band used to confirm bone mineralisation. Therefore, this band was expected in the Raman spectra for both sample groups exposed to ALP. Instead, bands characteristic of the v1 stretching of PO_4^{3-} were observed at approximately 957cm^{-1}. As discussed by Mandair and Morris (2015), the exact position of the band characteristic of carbonated apatite's (959cm^{-1}) is susceptible to change due to the carbonate (CO_3^{2-}) and monohydrogen phosphate (HPO_4^{2-}) content of samples. A high HPO_4^{2-} content, as possessed by newly deposited or immature bone mineral, is known to shift this band to a lower wavenumber, as observed in the present study (Crane et al., 2006; Kazanci et al., 2006). Thus, the presence of this band in both sample groups exposed to ALP (1.25mg/ml and 2.5mg/ml) provides further evidence for successful ALP induced CaP mineralisation of gelatin hydrogels. Similarly, as the intensity of this band approximately doubled when the ALP concentration of the hydrogels was increased from 1.25mg/ml to 2.5mg/ml, ALP induced mineralisation is shown to be dose dependent.

5.3 Fourier Transform-Infrared Spectroscopy (FT-IR)

FT-IR spectra also evidenced successful ALP mediated mineralisation. Like the Raman spectra, in addition to both ALP supplemented hydrogels, bands representative of Phosphate were observed in the IR spectra for the 0mg/ml ALP Ca-GP control. This supports the theory, initially drawn from Raman spectroscopy, that residual Ca-GP remains in the hydrogels due to incomplete washing out. Additionally, bands indicative of Amide groups in the gelatin component of the hydrogel were pronounced in the 0mg/ml ALP ddH_2O control and decreased considerably in the ALP supplemented sample groups. This demonstrates that the

protein (gelatin) phase of the hydrogels accounted for a lower overall proportion of the sample mass, therefore indicating the presence of another (mineral) phase.

Specifically, the band present at ~970cm^{-1} in the spectra for ALP supplemented samples may indicate that calcium deficient hydroxyapatite (CDHA) is present. This is common in aqueous solutions, where stoichiometric hydroxyapatite (HA; Ca:P = 1.67) does not generally form. However, CDHA containing composite hydrogels have demonstrated more efficient biodegradation and elevated cellular activity when compared with stoichiometric hydroxyapatite (Guo et al., 2009).

The presence of CDHA is also suggested by the double bands in the region of 563-603cm^{-1} in spectra for sample groups. As the second band is less apparent, the spectra imply that the mineral formed is not highly crystalline and that amorphous CaP is also present. Alternatively, this may be explained by a decrease in the absorbance below ~600cm^{-1} which is caused by the apparatus itself. Specifically, the crystal used in attenuated total reflection (ATR) mode is known to absorb infrared radiation below this wavelength and decrease the intensity of the bands displayed in the spectra.

The use of FT-IR in ATR mode may also be implicated in the difference in intensities observed between sample groups. Increased mineralisation is expected to be accompanied by similarly elevated intensity in FT-IR spectra. However, in the present study, both 0mg/ml ALP CaGP and 1.25mg/ml ALP sample groups presented intensities higher than those observed for the sample group supplemented with the highest concentration of mineralising enzyme. This may be explained by the need to ensure quality contact between the sample and the crystal in ATR mode, since the attenuation of the IR radiation that passes into the space immediately above the crystal during reflection is being measured. With increasing ALP concentration, hydrogels were noticeably ‘harder’. This made the process of pressing the sample into the crystal increasingly difficult in practice, which may have resulted in poorer

contact. Although the preparation of samples is more laborious, further analysis should be conducted in transmission mode to circumvent issues with sample-crystal contact and auto-absorbance under 600cm^{-1}.

5.4 Scanning Electron Microscopy (SEM)

SEM was utilised to provide a visual representation of the effects of ALP induced mineralisation upon the surface topography of the gelatin hydrogels following 6 days of mineralisation in CaGP. As expected, the smooth surface observed for the ALP/CaGP-free control samples illustrated the absence of mineralisation in this group. Similarly, as the majority of the surface of the 0mg/ml ALP CaGP group was consistent with that of the ddH_2O control, the sporadic deposits and 'rougher' sections which were observed support the previous suggestion that residual CaGP remains in the hydrogels and was not washed out completely, rather than providing evidence of mineralisation.

The rougher surface morphology presented by both sample groups containing ALP (1.25mg/ml and 2.5mg/ml) provides visual confirmation of successful ALP induced mineralisation. Consistent with the findings of Douglas et al (2012), mineralisation appeared to manifest as homogenously distributed globular deposits with diameters like those induced by ALP in cPEG, collagen and peptide amphiphile gels (Douglas et al, 2012; Spoerke et al, 2009). Despite this, further cross-sectional imaging of the hydrogels is necessary to enable the extent of successful mineralisation of the sub-surface regions to be evaluated.

5.5 Inductively Coupled Plasma Optical Emission Spectrometry (ICP-OES)

ICP-OES was utilised to elucidate the elemental composition of the mineralisation product. This technique verified the presence of Calcium and Phosphorus in significantly increased quantities for both ALP containing hydrogels (1.25 and 2.5mg/ml) compared to ALP-free hydrogels – both soaked in CaGP and ddH_2O.

The Ca:P molar ratios of all the hydrogel groups, the highest of which was identified as 1.27 (2.5mg/ml ALP), were found to be considerably lower than that of stoichiometric hydroxyapatite (1.67). This may be a result of the mineralisation medium (CaGP) possessing a Ca:P molar ratio of one, whereas media possessing greater molar ratios were used in studies reporting successful hydroxyapatite formation (Douglas et al, 2012; Spoerke et al, 2009). Additionally, as discussed by Douglas et al (2012), varying concentrations of ALP and CaGP, as well as the type of hydrogel itself, may yield different mineral compositions. In this case, CDHA or a mixture of amorphous and crystalline calcium phosphate may be responsible for the reduced Ca:P molar ratio observed by ICP-OES; which supports the findings of FT-IR analysis.

5.6 Compression Modulus

The effect of ALP-induced mineralisation on the compressive modulus of each of the hydrogel groups was evaluated. Increases in the dosage of electron irradiation, as well as increases in ALP concentration, was hypothesised to result in an elevated compression modulus.

For both ALP-free sample groups, although not statistically significant, the compression modulus increased with each increase in electron irradiation. This trend was not shared with the ALP containing hydrogels, where, despite a statistically significant increase in the compression modulus of samples exposed to 40kGy of electron irradiation compared to the 0kGy control, increasing the dose from 10kGy to 15 or 20kGy resulted in a decreased compressive modulus.

Hydrogels containing ALP (1.25mg/ml and 2.5mg/ml) demonstrated elevated compressive moduli, across the range of electron irradiation doses examined, compared to the 0mg/ml ALP hydrogels. Interestingly, however, while the compression moduli of samples at 2.5 mg/ml ALP were elevated compared to the 1.25 mg/ml ALP samples at doses of 0 and 40 kGy

of electron irradiation, the compression moduli of hydrogels containing 1.25mg/ml were superior to those of the 2.5mg/ml group at the intermediate doses of electron irradiation. This suggests that, although mineralisation imparts increased mechanical properties onto the hydrogels, this is not proportional to the amount of mineral formed (represented by the dry mass percentage). Specifically, a statistically significant increase in dry mass percentage was displayed when ALP concentrations were raised from 1.25 mg/ml to 2.5 mg/ml, but this was not mirrored in the compression moduli. This suggests the absence of strong interactions between the mineral phases and polymeric phases of the mineralised gelatin hydrogels following ALP-induced mineralisation (Douglas, 2012).

5.7 Cell Culture

Irrespective of mineralisation or compressive strength, the ability of the gelatin hydrogels to support the adhesion and proliferation of cells is a crucial aspect which must be evaluated if this material is to have potential implications in bone tissue regenerative applications.

As previously stated, gelatin itself is known to be biocompatible and has been proven to promote cellular growth (Wisotzki et al., 2016). In contrast to conventional methods used to crosslink gelatin which are known to elevate cytotoxicity and reduce cellular growth on gelatinous material gelatin hydrogels exposed to electron irradiation doses, exceeding those used in the current study (60kGy), had no significant impact on fibroblast cell death (Jayakrishnan and Jameela, 1996 and van Luyn et al., 1992).

The present study evaluated the interaction of gelatin hydrogels, containing ALP and mineralised for 6 days, with a human osteosarcoma (MG-63) cell line. Although successfully cultured MG-63 cells were visible on all of the sample groups after 24 hours, the cell coverage was most numerous in the gelatin control samples (0mg/ml ALP in ddH_2O), with observable decreases seen when ddH2O was substituted with CaGP, and then further with each increase of sample ALP concentration. While cell coverage appeared to remain

consistent for both of the ALP-free sample groups at both of the subsequent time points visualised (4 and 7 days), cell coverage on samples containing ALP (1.25mg/ml and 2.5mg/ml) appeared to decrease with each consecutive time point, with minimal coverage observed after 7 days.

These observations were supported by the MTS assay – an indirect method to measure proliferation and cell viability by measuring the extent to which metabolically active cells have converted a soluble tetrazolium salt into insoluble formazan. The absorbance, and therefore metabolic activity, of samples containing ALP showed no significant increase from day 1 to day 7, with a significant reduction observed compared to both ALP-free samples at 4 and 7 days.

As stated by Wisotzki et al. (2016), even though no significant increase in fibroblast cell death was observed for electron irradiated gelatin hydrogels, cell viability and proliferation rates reduced slightly, in a dose dependent manner. This effect may have been present in the ALP-free gelatin hydrogels, however, as cell culture was only conducted on samples exposed to 40kGy of electron irradiation due to time constraints, additional testing with the remaining doses would have to be carried out to confirm this.

Furthermore, it is unlikely that the reduction in cell coverage observed in the hydrogels which had been subject to ALP-induced mineralisation was a consequence of ALP mediated cytotoxicity. This method was utilised to mineralise a fibrin gel, *in-vitro,* which later enhanced bone tissue formation *in-vivo* (Osathanon et al.,2009). Therefore, it was hypothesised that these effects on cell growth could be attributed to an accumulation of Calcium which is released from the hydrogels – an issue which would be self-moderating in an *in-vivo* system.

To examine this theory, a subsequent round of cell culture was carried out with ‘Thick’ (8mm in height) and ‘Thin’ gelatin hydrogels (2mm in height). It was hypothesised that the ‘thin’

samples would demonstrate elevated cell coverage compared to the ‘thick’ samples, as the concentration of calcium would be lower.

Following 7 days of cell culture, fluorescent microscopy illustrated a seemingly confluent layer of cells on each of the ‘Thin’ sample groups, superior to that observed on the ‘Thick’ counterparts. Imaging of the ‘Thick’ samples returned results consistent with the first round of cell culture. Specifically, the gelatin control displayed good cell coverage, which was reduced considerably in samples containing 1.2 and 2.5mg/ml ALP.

The MTS assay conducted for this round of cell culture, unlike the first round of cell culture, demonstrated an increase in absorbance, and thus cell metabolic activity, in all groups for day 7 compared to day 1. However, after 4 days, the MTS assay supported the observations made via fluorescent microscopy. All ‘Thin’ samples displayed elevated absorbance values compared to their ‘Thick’ counterparts, with a statistically significant increase demonstrated for the ‘Thin’ 2.5mg/ml ALP hydrogels compared to the ‘Thick’. However, contrary to the results observed for fluorescent microscopy, the metabolic activity observed from each sample group was increased in the ‘Thick’ hydrogels compared to their ‘thin’ counterparts. These discrepancies may be explained by several reasons. For example, the cells on the ‘Thin’ hydrogels may have reached confluency and ceased to be metabolically active due to contact inhibition (Leontieva et al., 2014). Whereas the cells on the ‘Thick’ hydrogels continued to proliferate as they reached confluency at a later stage. Alternatively, as the layer of cells becomes more brittle when it reaches confluency, the cells could have been lost due to the manipulation of samples (pipetting and washing in particular) prior to the MTS assay being conducted.

5.8 Cell Culture Scanning Electron Microscopy

Supplementary to fluorescent microscopy and the MTS assay, SEM of hydrogel samples fixed after 7 days of cell culture provided a more detailed insight into the morphology and attachment of the cultured cells. The confluent layers of cells visualised on the control hydrogels (0 mg/ml ALP in ddH_2O) possessed clearly defined borders and visible filopodia, suggesting effective attachment. Similarly, large areas with complete cell coverage were observed in the remaining ALP-free samples. Again, filopodia could be seen, and attachment to the hydrogel surface appeared to be good.

However, consistent with fluorescent microscopy and the MTS assay, the areas of the hydrogels with cell coverage became sporadic when ALP concentration was increased to 1.25 and 2.5mg/ml. Layers of cells which appeared to have been confluent and subsequently peeled from the surface could be observed, while peeling cells and cells that appeared to have been lysed were also observed.

Unfortunately, cell culture SEM was only carried out for the first round of cell culture. Therefore, as the results were observably different in the second round where both 'Thick' and 'Thin' samples were examined, SEM of these samples should be imaged to enable the morphology and attachment of the cultured cells to be evaluated. Similarly, one of the primary limitations of this study is the restriction of most of the analytical techniques to gelatin hydrogels exposed to one dose of electron irradiation (40kGy). Thus, the variation attributable to electron irradiation dosage is hard to compare. However, the results of the dry mass percentage, coupled with the compressive moduli analysis suggest that a lower dosage of electron irradiation may still be enough to produce the desired effects, in the absence of any negative implications. Therefore, this should be examined further.

6.0 Conclusion

Typically, the ability of hydrogels to satisfy requirements for use in bone tissue engineering is restricted by their generally weak mechanical properties and inability to mineralise with CaP in order to form durable interactions with bone tissue. Furthermore, the sterilisation of these materials is a common hurdle that must be overcome.

In the present study, the previously elucidated method of ALP mediated mineralisation was coupled with electron irradiation to produce crosslinked gelatin hydrogel composites which circumvent these restrictions. Dry mass percentage, SEM, Raman, FT-IR and ICP-OES illustrated the successful formation of CaP (CDHA) in these hydrogels. As expected, this mineralisation coincided with an elevated compressive modulus, although this was not proportional to the amount of mineral formed. Importantly, preliminary *in-vitro* studies demonstrated that electron beam-crosslinked hydrogels, both mineralised and unmineralized, supported MG63 cell adhesion and proliferation of human osteoblast-like MG-63 cells.

Ultimately, electron irradiation coupled with ALP mediated mineralisation demonstrates applicability to produce sterile hydrogels with properties compatible for use in bone tissue engineering applications. Specifically, with respect to the widely available in nature and inexpensive gelatin. However, further *in-vitro* and *in-vivo* studies are necessary to identify the extent of their potential for use in bone tissue engineering applications.

Chapter 3: Carbon Nanotube - Whey Protein Isolate Hydrogels

7.0 Introduction

7.1 Antibacterial Properties

In addition to providing hydrogels with a mineralisation source, and the advantages which accompany this process, the incorporation of alternate nanoparticles may elicit additional advantages. Namely, enhanced mechanical reinforcement, antibacterial properties, and further promotion of bone-forming cell proliferation.

Implant-related microbial infections, caused by bacteria and fungi, remain one of the primary causes of wound healing complications and, ultimately, failure of orthopaedic implants (Salomé Veiga and Schneider, 2013 and Romano et al., 2015). Specifically, the pathogenicity of infections with *Escherichia coli*, *Pseudomonas aeruginosa*, *Staphylococcus aureus*, *Staphylococcus epidermis* and species of *Candida* can lead to tissue morbidity or, in extreme cases, sepsis. Wound healing is compromised, and orthopaedic implants can fail because of pathogenicity at the tissue-implant interface (Salomé Veiga and Schneider, 2013). This is accompanied by increased socio-economic cost as the removal and subsequent replacement of the implants is necessary. The occurrence, and extent, of infections related to orthopaedic implants is a multifactorial issue. It is therefore necessary to consider: the surgical procedure itself, bacterial load, type of implant, microbial type, the host's condition (immunocompromised etc) and the type of antibacterial prophylaxis prior to surgery (Romano et al., 2015).

Complications of this nature have been significantly reduced in number due to current perioperative methods to prevent infection (such as antibacterial prophylaxis). Despite this, it has been reported that approximately 2.5% of primary hip and knee joint surgeries and 10% of revision arthroplasties are still subject to complications induced by infections (Lentino, 2003). Additionally, as discussed by Dale et al (2009), these figures may represent

an underestimation of cases, which continue to rise. Importantly, pathogens that possess multi-resistance are also frequently isolated from complication sites (Aggarwal et al., 2014).

Therefore, implantable biomaterials which possess antimicrobial activity, and thus, the ability to prevent/treat infections at implantation sites are desirable. Hydrogels can satisfy these criteria via various methods: antimicrobial agents can be directly encapsulated within or covalently immobilised onto the hydrogels, or the hydrogel itself can be obtained using materials that possess indigenous antimicrobial activity (Salomé Veiga and Schneider, 2013).

Previous studies have utilised silver nanoparticles (NPs), which are known to possess antimicrobial properties against a wide range of bacteria and fungi, to increase the antibacterial properties of hydrogels (Salomé Veiga and Schneider, 2013). For example, Travan et al (2009) encapsulated NPs inside a hydrogel and subsequently demonstrated that this product displayed microbial activity towards *Escherichia coli*, *Pseudomonas aeruginosa*, *Staphylococcus aureus*, *Staphylococcus epidermis.*

7.2 Mechanical Properties

Besides antimicrobial enhancement, mechanical reinforcement is the primary advantage bestowed upon hydrogels by the incorporation of particles. The mechanical integrity of orthopaedic tissue engineering scaffolds for implantation is a necessity. To avoid previously mentioned complications, such as stress shielding, re-fracture and implant related osteopenia, the mechanical properties of implants must also replicate those of the native tissue as closely as possible (Amini et al., 2012; Byrne et al., 2007). For hydrogels to successfully provide scaffolds for bone tissue engineering, their ordinarily weak mechanical properties must, therefore, be improved. As previously stated, mineralisation contributes to this increase in structural integrity. Similarly, as discussed by Nichol et al (2010), the type and extent of crosslinking, as well as the concentration of hydrogel precursors, can be manipulated to increase the structural integrity of hydrogels (Fedorovich et al., 2007).

However, these alterations may also detract from the original benefits that accompany hydrogels. For example, gaseous and nutrient exchange, which is necessary for the successful healing of bone tissue, may be restricted (Ulubayram et al., 2002). Therefore, numerous composites have been evaluated with the aim of increasing mechanical properties while maintaining their inherent advantages. The majority of these include: bioceramics such as hydroxyapatite and TCP, bioglasses and carbon nanotubes (Tozzi et al., 2002).

7.3 Carbon Nanotubes

Carbon nanotubes (CNTs) were first discovered by Iijima (1991), who observed a hollow tube-like structure, measuring only a few nanometres in diameter and up to a few millimetres in length, on the end of a graphite electrode. Since their discovery, CNTs have been the subject of a vast amount of research which has elucidated their unique structural, mechanical, electrical, electromechanical and chemical properties – each of which implicate CNTs in numerous applications.

CNTs are allotropes of carbon. They are comprised of planar sheets of hexagonal bonded carbon forming honeycomb crystal lattices (graphene), rolled into cylindrical sheets. Depending on the number of graphene sheets folded to form these cylindrical structures, single walled CNTs (SWCNTs) or multi walled CNTS (MWCNTs) can be formed, each with unique properties. SWCNTs are cylindrical monolayers of graphene ranging in diameter from 0.4 to 2nm, depending on the temperature during synthesis (Madani et al., 2013). Although they consist of one layer, the cylindrical honeycomb lattice structure of SWCNTs can be arranged in multiple ways, known as: armchair, zigzag and chiral arrangements. MWCNTs are comprised of multiple, cylindrical, graphene layers. Ordinarily, the central layer has a diameter of 1 to 3nm, while the outer cylindrical layer measures between 2 and 100nm in diameter. Like SWCNTs, MWCNTs can be arranged in multiple ways. The first is known as the ‘Russian doll’ structure, which consists of concentric layers of graphene sheets. The second

involves the graphene sheet wrapping around itself to form a parchment-like structure (Madani et al., 2013).

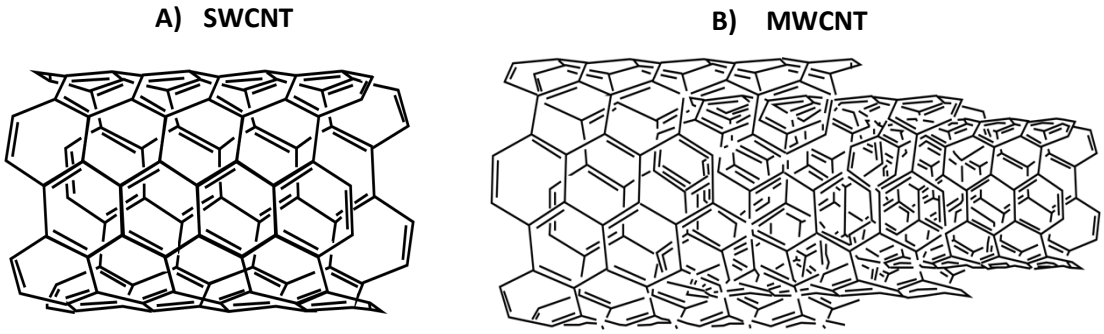

Figure 18: The structure of (A) Single walled carbon nanotubes (SWCNTs) and (B) Multi-walled carbon nanotubes (MWCNTs).

Their ultra-light weight, high surface area and extreme durability implicate CNTs as ideal candidates for use in structural materials, specifically, nanocomposites. Polymers reinforced with CNTs have previously been exploited in numerous applications. For example, nanocomposites have been utilised in bicycles, boat hulls and golf clubs in the sporting industry (De Volder et al., 2013; Saito et al., 2014). Similarly, they have found applications in physics and electronics, where they have been used as components in supercapacitors, actuators, and displays such as television screens (De Volder et al., 2013; Saito et al., 2014). The electrical properties of CNTs have also allowed biomaterials containing them to be evaluated for nerve regeneration (Nunes et al, 2012) and muscle actuation (Baughman et al.,1999). They have also been proposed as drug delivery systems and implicated in the treatment of cancer (Lacerda et al, 2006). In terms of bone tissue engineering, they have been implicated in the production of hydrogels with enhanced mechanical properties,

without detracting from the flexible, porous structure which mimics that of the ECM (Tozzi et al., 2016). Usui et al (2008) demonstrated that, in a mouse model, MWCNTs were biocompatible, permitted bone repair and became integrated with bone tissue. Similarly, Seo et al (2014) found that the integration of 2% functionalised CNTs into chitosan/silica membranes increased both their tensile strength and elastic modulus considerably. This finding is supported by Yasmeen et al (2014) who observed an increase in compressive strength when chitosan gels were supplemented with CNTs. Additionally, with potential significance in their use as biomaterials in bone-tissue engineering, Zhao et al (2005) noted that CNTs promoted the formation of mineralised bone, while Yasmeen et al (2014) illustrated that the thermal properties of CNTs reduced the gelation time of chitosan gels from an hour to less than 10 minutes.

Similarly, CNTs are known to possess antimicrobial activity against a broad spectrum of microorganisms. The first evidence of these properties was documented by Kang et al (2007) who observed antimicrobial activity of both SWNTs and MWNTs against *Escherichia coli.* Since this time, numerous studies have implicated CNTs in applications for the inactivation of pathogens (Liu et al., 2018).

However, the use of CNTs in the biomedical field remains somewhat controversial. This is due to concerns regarding their toxicity, which has not yet been fully elucidated. Previous research into this topic has been inconsistent. However, it has also suggested that toxicity varies based upon method of exposure, shape, size, and composition (Madani et al, 2013).

As discussed by Foldvari and Bagonluri (2008), studies have reported only mild inflammation when the route of exposure to CNTs is intravenous (IV) injection, oral, or dermal administration. However, severe inflammation has been reported as a result of inhalation. This may be due to their similar shape to asbestos particles – long, thin, lightweight crystals which are known for their pathogenic effects following inhalation (Lam et al., 2004). Toxicity

directed towards the respiratory system was demonstrated as a result of intratracheal instillation of CNTs, however, this was not confirmed by studies in which CNTs were inhaled directly, which showed no major damage to the respiratory system (Mitchell et al., 2007; Poland et al., 2008).

Similarly, Takanashi et al (2012) evaluated the carcinogenicity of CNTs by injecting MWCNTs into the subcutaneous tissue of mice. Carbon black, a component used in black tattoo ink, was used as a comparison. The histological results demonstrated that injection with MWCNTs did not result in neoplasm formation and, in fact, carbon black implantation resulted in elevated carcinogenicity compared to MWCNTs. Additionally, inflammatory cells, such as lymphocytes and neutrophils were absent from the peripheral tissue following MWCNT injection.

As discussed by Tonelli et al (2012), in terms of the direct effect of CNTs on bone tissue, most studies are conducted *in-vitro*. However, several *in-vivo* studies have been performed. Mostly, these studies examine MWCNTs in combination with polycarbosilane, chitosan, or hyaluronate, and have illustrated that bone tissue growth was improved without a notable immune response being initiated (Abarrategi et al., 2008; Mendes et al., 2010; Saito et al., 2001; Usui et al., 2008; Wang et al., 2007).

Contrastingly, multiple *in-vivo* studies have evaluated the effects of CNTs following dermal contact. For example, Murray et al (2009) examined the effects of non-purified CNTs on mouse skin. The generation of free radicals, oxidative stress, inflammation, and ultimately, dermal toxicity was observed because of this topical exposure. Purity of CNTs, therefore, has been implicated as a factor responsible for CNT toxicity, particularly via the dermal route. Impurities, generally, consist of metals. Cobalt (Co), Iron (Fe), Nickel (Ni), and Molybdenum (Mo) are used as a catalyst during the synthesis of CNTs (Donaldson et al., 2006). As a result, residues of these metals can become encapsulated within the graphene layers and remain as

impurities following CNT synthesis. It has been elucidated that these metal residues can lead to cell death via mechanisms such as mitochondrial destruction and oxidative stress (Pichardo et al., 2012). Therefore, impurities are said to be a primary factor determining CNT toxicity. Purification of CNTs can be achieved via functionalisation (Sharifi et al., 2012). Ultrasonication is one method to accomplish functionalisation of CNTs as it stimulates the release of metallic impurities into solution. Toh et al (2012) demonstrated that CNT mediated toxicity was reduced significantly following ultrasonication for as little as 5 minutes. Another common approach is to directly coat the CNTs with polyethylene glycol (PEG) – a biocompatible polymer which has demonstrated the ability to diminish CNT toxicity *in-vivo* (Bottini et al., 2011).

Importantly, the mechanisms by which hydrogels interact with incorporated particles are yet to be fully understood. Specifically, *in-vitro* studies are insufficient. Therefore, prior to their use in bone tissue engineering applications, the long-term activity of hydrogel composites, specifically *in-vivo*, should be elucidated. Cytotoxicity, biocompatibility, biodegradability and osteogenicity should all be established (Zhao et al. 2015).

The present study aimed to evaluate the mechanical and antibacterial advantages imparted into WPI based hydrogels by the inclusion of CNTs.

7.4 Whey Protein Isolate

Whey protein isolate (WPI) is a protein derived from dairy sources and a by-product when producing foods such as Greek yoghurt. Recently, WPI, particularly in the form of hydrogels, has attracted attention for potential applications in bone tissue engineering.

As the natural function of milk is to sustain the life of a new-born, it is an inherent source of components necessary for the development and regeneration of bone tissue. Milk proteins function as delivery mechanisms for essential micronutrients, such as calcium and phosphate, amino acids, and components of the immune system, such as immunoglobulins

and lactoferrin (Douglas et al., 2018). The primary groups present in milk are caseins, which account for 80% of proteins, and whey protein, which accounts for 20% of all proteins. The primary components of whey protein are β-lactoglobulin (β-LG) and α-lactalbumin (α-LA), while lactoferrin, serum albumin and other proteins are present in reduced quantities (Do et al., 2016). In comparison with caseins, whey proteins possess a higher concentration of amino acids rich in sulphur. Proteins rich in sulphur are said to confer a higher protein efficiency ratio (weight gain to protein intake during a specified time period) and have important implications in immune modulation (Douglas et al., 2018). Furthermore, whey protein enhances protein synthesis in muscle cells, as they consist of branched chain amino acids (Walzem et al., 2002). The primary component of whey protein, β-LG, also possesses a calyx which provides it with the ability to bind to numerous ligands, including hydrophobic molecules (Kontopidis et al., 2004). This ability provides β-LG with functionality as a carrier protein to enhance both the uptake and solubility of hydrophobic molecules (Diarrassouba et al., 2015; Ha et al., 2013)

With respect to bone tissue engineering, WPI hydrogels possess the advantage of simultaneous fabrication and sterilisation, as gelation is induced by heat. Furthermore, a study conducted by Douglas et al (2018) concluded that WPI enhanced the growth of both human osteoblast-like Saos-2 cells, and human neonatal dermal fibroblasts. WPI also stimulated calcium deposition by Saos-2 cells and elevated the expression of type I collagen by fibroblasts. Finally, WPI induced the expression of markers characteristic of osteogenic cell differentiation by human adipose tissue derived stem cells (ASC), in a dose-dependent fashion, as well as increasing the activity of ALP. This, along with the availability and low cost of WPI, implicates it in bone tissue engineering applications. However, their applicability is restricted by susceptibility to bacterial infection.

This, therefore, underpins the decision to supplement WPI based hydrogels with CNTs to attempt to simultaneously increase their mechanical properties (Young's modulus etc) and impart antibacterial activity – properties which are evaluated in the present study.

8.0 Methods

8.1 Whey Protein Isolate – Carbon Nanotube Hydrogel production

Stock solutions of 40% w/v whey protein isolate were prepared by dissolving WPI powder in deionised H_2O. A sonicator was used to facilitate dissolution and minimise foaming. Subsequently, 500µl of stock solution was added to Eppendorf tubes alongside the required amount of multi-walled Carbon Nanotubes (MWNTs; Sunnano Nanotech Ltd, China) to make 0 (control), 2.5, 5, 10, 20 and 40% CNT samples. Once in Eppendorf tubes, samples were sonicated for an additional 30 minutes to aid dispersion of the CNTs.

Next, samples were autoclaved at 134°C for 20 minutes, to simultaneously sterilise and induce gelation of the samples.

8.2 Dry mass percentage

Samples were weighed in the hydrated state, before being dried for 24 hours at 60°C. Dry mass percentage was then calculated using the following equation.

$$\text{Dry mass \%} = \left(\frac{Weight\ in\ dry\ state}{Weight\ in\ hydrated\ state}\right) \text{x } 100$$

8.3 Laser Diffractometry

Valerie Vanhoorne (Ghent University, Belgium) conducted laser diffractometry to measure the size of the CNTs. First, 100mg of CNT powder was added to 10ml of deionised water with

0.2% Tween 80 and vortexed vigorously to suspend the powder. The suspension was then placed in an ultrasonic bath for 10 minutes, before being added to the measuring cell until the obscuration reached 10 to 30%. 5000 scans were taken, using a MS1 small volume dispersion unit, and a 300RF lens with a range of 0.05-800µm, stirred at 1500 rpm.

8.4 Sample Preparation for Scanning Electron Microscopy

Prior to SEM analysis, samples were mounted on aluminium stubs using carbon adhesive pads (both Agar Scientific Ltd, UK). Samples were then subject to sputter coating for 5 minutes in an Edwards S150A sputter coater. Coating was carried out at 40mA, under 1.5 bars of pressure. Samples were subsequently examined using a JEOL JSM-5600 instrument (JEOL Ltd, Japan), with a spot size of 14, and an acceleration voltage of 15.

8.5 Cell Culture Sample preparation for Scanning Electron Microscopy

Following cell culture, samples were also visualised by SEM to allow a more detailed evaluation of the surface topography of the hydrogels. Samples prepared as previously described in chapter 2, section 3.10.

8.6 Fourier Transmission Infrared Spectroscopy (FT-IR)

The molecular structure of the WPI-CNT hydrogels was examined using FT-IR, in collaboration with Aleksandra Benko (AGH University of Science and Technology, Poland). This was performed on a Bruker Tensor 27 spectrometer, in the middle infrared (MIR) region (4000-400cm^{-1}). Samples were lyophilised to remove water residue, and ground to a fine powder using a mortar and pestle prior to analysis. The powder was subsequently mixed with approximately 200mg of KBr and pressed into pellets. Measurements were then taken, in transmission mode, by averaging 128 scans per sample, with a spectral resolution of 4cm^{-1}.

OPUS 7.2 software was utilised for data acquisition and editing. Manual baseline correction of all spectra was performed. In the case of WPI and its composites, deconvolution of the overlapping bands in the 3800-2300 $cm^{-1}$and 2000-800 cm^{-1} was performed to allow the

visualisation of changes in the number of bands and their relative intensities, caused by the presence of CNTs. Band positions were established based on the presence of maxima in the second derivative of the spectra, and fitting to the predetermined bell-type functions (mixed Gaussian/Lorentians) was performed until the value of the root mean square (RMS) of the fitted bands in relation to the starting spectra was lower than 0.0015.

8.7 Cell culture

To evaluate the ability of the WPI-CNT hydrogels to support bone cells, a human osteosarcoma (MG-63) cell line (Sigma-Aldrich, USA) was seeded on to the hydrogels. Hydrogels were cut into thin slices of approximately 2mm and placed into 48-well plates. At intervals of 1, 4 and 7 days, the adhesion, proliferation, and morphology of cells was assessed by fluorescent microscopy, while cell viability was evaluated via the MTS assay.

Specifically, MG-63 cells were cultured in Dulbecco's modified Eagle's medium (DMEM) supplemented with 10% foetal bovine serum (FBS; Nemecko, Germany), Penicillin and Streptomycin (50-100IU/ml and 50-100µg/ml, respectively), at 37°C, with 90% humidity and 5% atmospheric pressure of CO_2.

8.7.1 Fluorescent Microscopy

Hydrogels were cut into thin slices and placed into 48-well plates (Corning Incorporated, USA). Subsequently, 1ml of DMEM culture media containing 10,000 cells was added to each well (10,526 cells/cm^2 growth area). Once the cells were seeded, the hydrogels were incubated at 37°C, with 90% humidity and 5% atmospheric pressure of CO_2 once again.

At the appropriate time point (1, 4 and 7 days) samples were washed with phosphate buffered saline (PBS), and subsequently fixed with 70% ethanol at -20°C for 10 minutes. Samples were then washed again with PBS before staining.

Samples were stained with Hoechst and Texas red (both Sigma Aldrich, USA) diluted in PBS, at concentrations of 500ng/ml and 25ng/ml, respectively, for 15 minutes in dark conditions. Hoechst binds to the minor groove of double DNA with affinity for adenine and thymine rich sequences and is therefore used to stain the cell nucleus. The Hoechst stain is excited in the ultraviolet range (approximately 361nm) and emits blue fluorescence around 497nm. Texas Red is used to stain the cytoplasm, as it binds to reduced thiol groups which are present in cytoplasmic proteins. The maximal excitation is approximately 596nm, while the optimal emission is around 615nm (observed as red).

After staining, samples were washed twice with PBS and subsequently visualised on an Axio ScTope.A1 microscope (Zeiss, Germany) using a digital camera and Zeiss software.

8.7.2 Proliferation Assay (MTS)

The MTS assay was used to assess the proliferation of MG-63 cells on each of the hydrogel sample groups at the appropriate time points (1, 4 and 7 days).

DMEM, without phenol red, and supplemented with L-Glutamine and 10% FBS was used to dilute the MTS Cell Titer 96 Aqueous one solution cell proliferation assay kit (Promega, USA) by a factor of 1:6. For each sample group, 3 repeats and one sample without cells (to allow background to be subtracted) were included in the assay, along with a polystyrene plate control. First, samples were washed with PBS, transferred to a new well plate to remove interference from cells attached to the base of the polystyrene plate wells, and then incubated for 2 hours at 37°C, with 90% humidity and 5% atmospheric pressure of CO_2, in 0.5ml of the diluted MTS solution.

After the 2-hour incubation, 100µl of the solution from each well was transferred, in triplicate, to a 96-well plate, to allow the extent of the yellow tetrazolium dye reduction to violet formazan to be quantified by a spectrophotometer, at a wavelength of 490nm (Tecan Infinite M200 Pro, Switzerland).

8.8 Cell Viability

8.8.1 Human Foetal Osteoblast Cell Line Cell Preparation

The ability of WPI-CNT hydrogels to support cell attachment and proliferation was also tested on a human foetal osteoblast cell line (hFOB; LGC Standards, USA), in collaboration with Doctor Susan A. Clarke at Queen's University, Belfast. The hFOBs were cultured in DMEM/HAM F12 supplemented with 10% FBS, 50 mg/ml Geneticin + 2millimolar L-glutamine. Cells were cultured at 34°C and 5% atmospheric pressure of CO_2. Hydrogels were placed into 24-well plates, before 50µl of cell solution containing 1000 cells was administered to the surface of each sample. Samples were then incubated for 30 minutes to allow cell attachment. Subsequently, 2ml of culture media was added to each well. Culture medium was replaced twice a week.

8.8.2 Cell Proliferation & Differentiation

To quantify the number of viable cells located on the base of the 24 well plates, a Crystal Violet assay was performed. Hydrogel samples were washed with PBS and transferred into a fresh 24 well plates for cell lysis. Cells that remained on the base of the well were fixed using 4% paraformaldehyde (PFA). Crystal Violet dye was applied to each well before washing with distilled water 3 times and treating with 0.5% acidified methanol. Plates were read using a Tecan GENios multi-scan spectrophotometer at a wavelength between 550-620nm.

8.8.3 Statistical Analysis

Differences between groups were analysed using an Independent Samples t-test. Significant if $P<0.05$.

8.9 Anti-bacterial – Colony Forming Unit Assay

To identify potential antibacterial properties of WPI-CNT hydrogels, a CFU assay was conducted in collaboration with Doctor Raechelle D'Sa and Doctor Jenny Hanson at the University of Liverpool.

The CFU assay enumerates the surviving bacterial cells following incubation with a surface/substrate. Bacterial cells were incubated with the WPI-CNT hydrogels, and after 24 hours of contact time, an aliquot of solution was removed and plated on agar to determine the number of bacterial cells remaining in the solution.

An overnight culture of *S. aureus* (1×10^{8}) in Luria broth (LB) was diluted to contain 1×10^{6} CFU/ml (in LB). 1 ml was then applied to each sample. Samples were incubated at 37 ˚C with shaking at 180 rpm for 24 hours. Subsequently, serial dilutions of the bacterial solutions were prepared in LB (up to 10^{-10}), and 10 µl of each dilution was plated, in triplicate, on LB agar using the Miles and Misra method. Following overnight incubation at 37˚C, colonies were counted, and statistical analysis performed using SigmaPlot. Samples groups were 20% and 40% CNT-WPI hydrogels, 0% control WPI hydrogel, and a blank (bacteria and broth without hydrogel).

8.10 Mechanical Testing

To evaluate the extent to which, if any, the addition of CNTs to WPI hydrogels increases their mechanical strength, mechanical testing was conducted in collaboration with Krzysztof Pietryga (AGH University of Science and Technology, Poland). Cylindrical samples, 8mm both in height and diameter were subject to compressive testing using a Zwick 1435 Universal Testing Machine. Test parameters were set at a speed of 10mm per minute, and a test range of 0-95% strain.

8.11 Statistical Analysis

Statistical analysis was performed using the SPSS platform. One-way ANOVA coupled with Tukey's multiple comparison post-hoc test was performed.

9.0 Results

Sample Abbreviation	Description
WPI Control	40% WPI - 0% CNT hydrogel
2.5% CNT	40% WPI - 2.5% CNT hydrogel
5% CNT	40% WPI - 5% CNT hydrogel
10% CNT	40% WPI - 10% CNT hydrogel
20% CNT	40% WPI - 20% CNT hydrogel
40% CNT	40% WPI - 40% CNT hydrogel

Table 2: The different sample groups examined in Chapter 3

9.1 Laser Diffractometry

The size of the CNTs used to supplement WPI hydrogels in this study was elucidated via Laser Diffractometry, in collaboration with Valerie Vanhoorne (Ghent University, Belgium). Analysis illustrated that, on average over three runs, there were no CNTs below 1.95 µm in size and none above 48.27 µm (figure 19). However, only a negligible proportion of CNTs were demonstrated to be between 1.95 and 5.69 µm at the lower end, and between 30.53 and 48.27 µm at the higher end of the CNT sizes analysed. 74.5% of the CNTs analysed displayed a size between 7.72 and 22.49µm, with the highest percentage (12.42%) between 12.21 and 14.22 µm (figure 19).

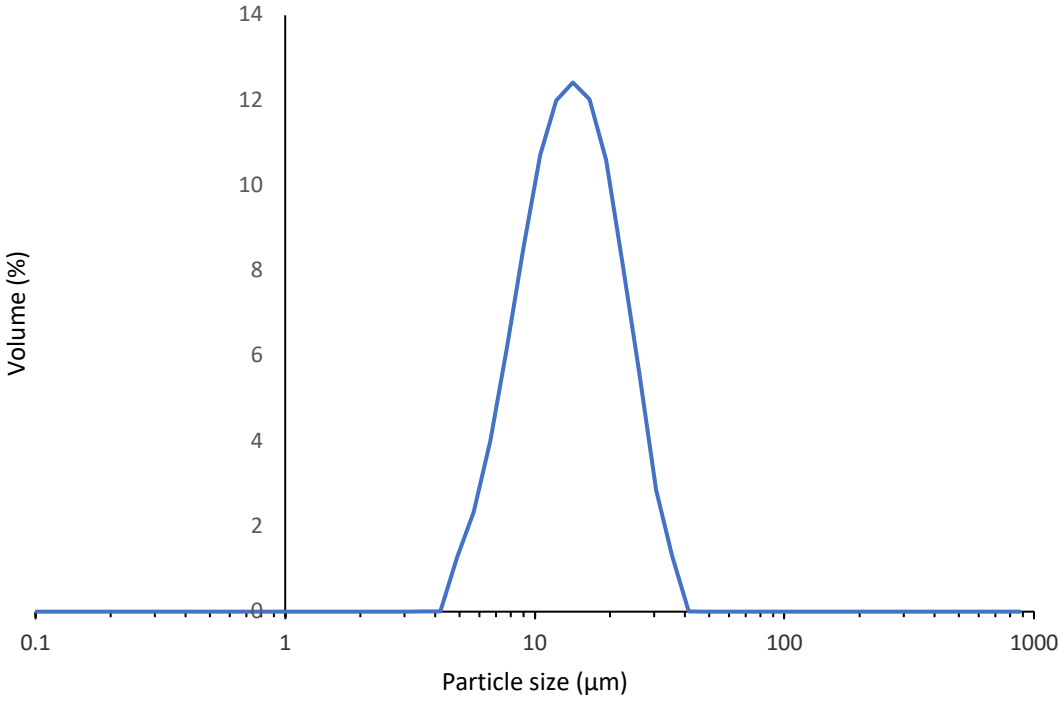

Figure 19: The average particle diameter of CNTs, analysed by Laser Diffractometry using a MS1 small volume dispersion unit.

9.2 Scanning Electron Microscopy (SEM)

SEM was utilised to analyse differences in the surface topography of WPI hydrogels supplemented with CNTs at concentrations at 0, 2.5, 5, 10, 20 and 40% (figure 20). Specifically, this technique was used to allow the evaluation of CNT dispersion and homogeneity within the hydrogels, in addition to their effects on sample integrity.

The WPI control (0% CNT) samples displayed a homogenous, smooth, surface topography (Figure 20A). As hypothesised, the surface became increasingly rough as the CNT concentration was increased. From the lowest concentration, 2.5% CNTs (Figure 20B), CNTs could be observed, encapsulated within the WPI hydrogels and penetrating through the exterior, coated in protein. The frequency of these observations and the roughness of the samples increased with increasing CNT concentration.

At the highest CNT concentrations (20 and 40%), the surface of the hydrogel samples displayed an exceedingly porous topography, with seemingly reduced homogeneity. CNTs which were attached to the hydrogels, but not fully encapsulated in the protein, could also be observed (figure 20F).

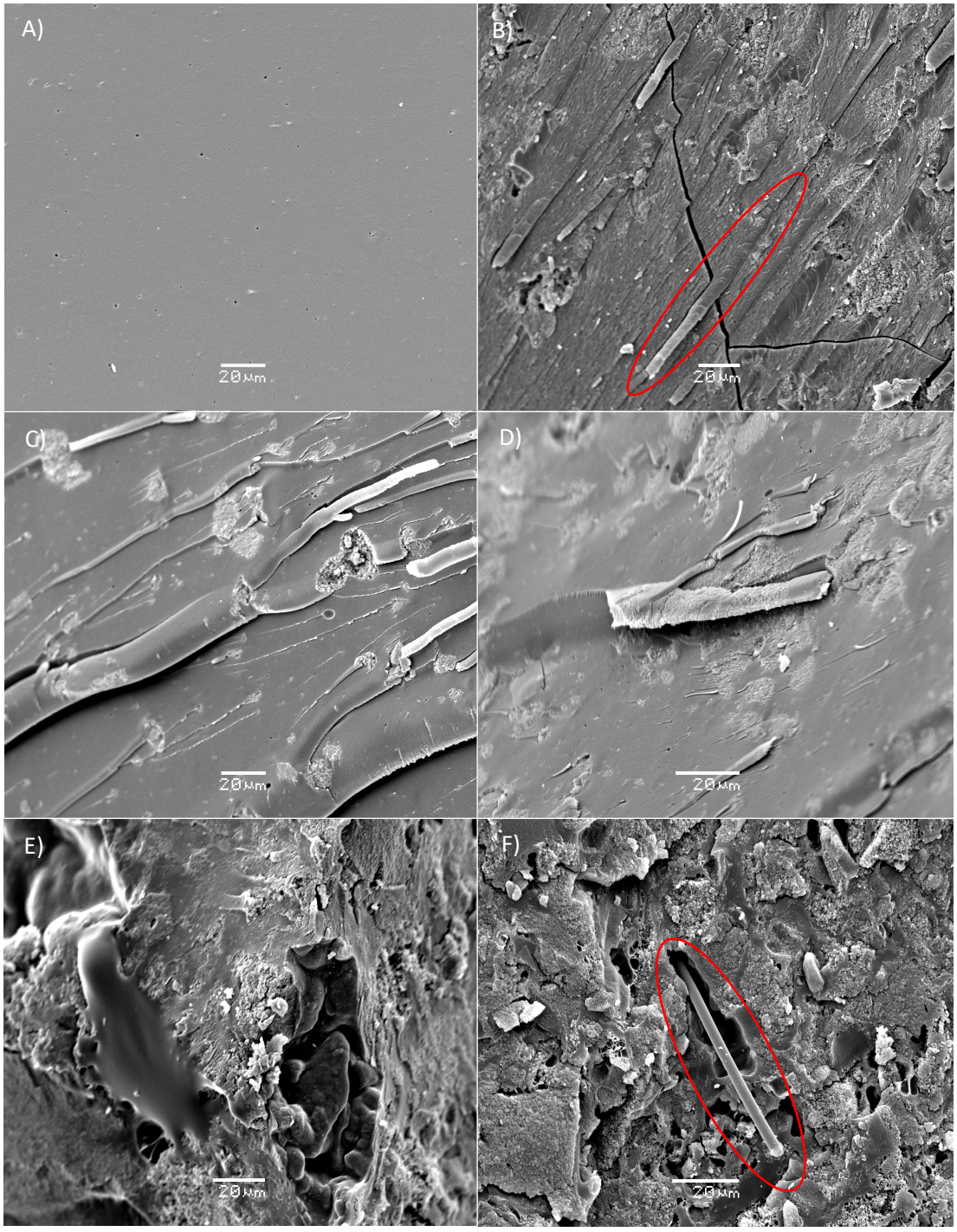

Figure 20: SEM images of WPI hydrogels containing varying CNT concentrations. *0% (A), 2.5% (B), 5% (C), 10% (D), 20% (E) and 40% (F). Images illustrate scale bar (20µm)*

9.3 Fourier Transmission Infrared Spectroscopy (FT-IR)

FT-IR spectra of CNT samples displayed a wide, symmetric band at approximately 3443 cm^{-1}, which is representative of the presence of hydroxyl groups. A cluster of bands was also present in the region of 1750 and 1000 cm^{-1} which are generally attributed to bonds between Carbon and Oxygen or Hydrogen (C=O, C-O and C-H). The complex band between 3000 and 2800 cm^{-1} also suggests the presence of bonds between Carbon and Hydrogen, as this is representative of CH_2 and CH_3 groups.

Spectra for the WPI and WPI-CNT hydrogels, as expected, illustrated features typical of proteins. A wide, complex band representative of the presence of a carboxyl group was observed between 3800 and 2300 cm^{-1}. Within this band, numerous shoulders were observed that may be attributed to a variety of interactions, including C-O, hydroxyl, amide A and B and =C-H in alkenes (Garidel and Schott, 2006). In the region below 1800 cm^{-1}, bands characteristic of amide I, amide II and amide III with different wavelengths attributed to vibrations of multiple functional groups were observed (Barth, 2007). It was also documented that the shape and relative intensities of bands observed on WPI spectra were impacted, in a dose dependent manner, by increasing CNT concentration. This is clearest to see in the altered shape of the complex band between 3800 and 2300 cm^{-1} and the narrowing of the band at 1642 cm-1.

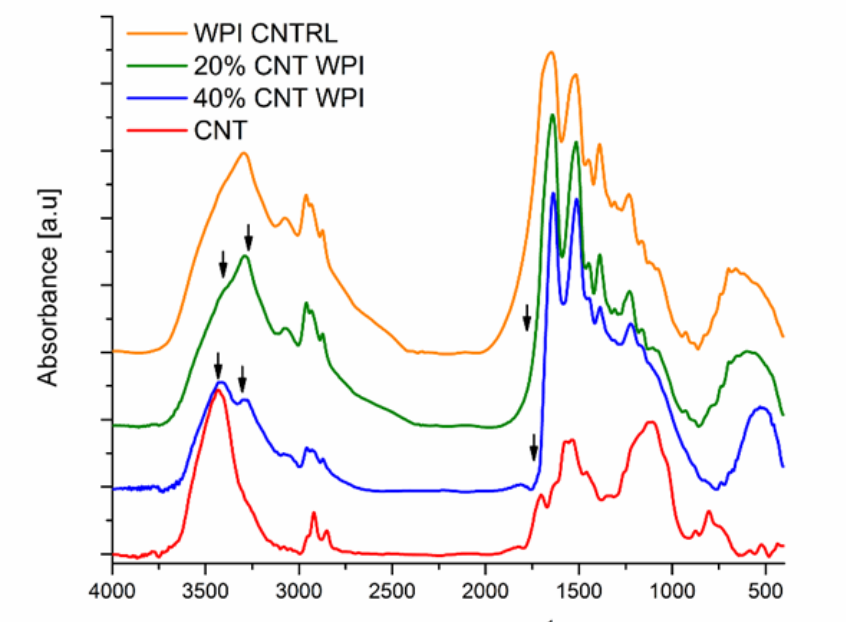

Figure 21: FTIR spectra of WPI-CNT hydrogel samples, presented in the region between 4000-400 cm-1. *The spectra are offset and maximized for better clarity. Regions of most significant changes induced by the presence of CNTs are indicated by arrows*

9.4 Cell Culture

9.4.1 Fluorescent Microscopy

The interaction of WPI-CNT hydrogels with a human osteoblast-like (MG-63) cell line was evaluated at intervals of 1, 4 and 7 days. The adhesion, proliferation, and morphology of cells present on the samples was assessed by fluorescent microscopy, as illustrated in figure 22. Cell nuclei were successfully stained (blue) with Hoechst, while the cytoplasmic regions of cells were successfully stained (red) with Texas Red.

Following the first 24 hours of cell culture, fluorescent microscopy (figure 22) illustrated that MG-63 cells were present on all WPI hydrogels (0, 5, 10, 20 and 40% CNTs). The WPI control (0% CNT), 5% and 10% CNT samples all displayed good cell coverage across the hydrogel samples. Observed cells also presented a seemingly healthy morphology. However, samples with elevated CNT concentrations (20 and 40%) exhibited reduced cell coverage and less defined cytoplasmic regions.

On the 4th day of cell culture, the cell coverage on both the WPI control and 5% CNT samples appeared to be reduced, with regions of little to no cell coverage identified. Despite this, clusters of MG-63 cells were still identified with clearly defined cytoplasmic regions and well spread morphologies on both samples. The cell coverage on the remaining sample groups (10, 20 and 40% CNT) appeared to increase in comparison to the observations following the first 24 hours. Again, the 10 and 20% CNT samples displayed seemingly healthy morphologies, while the 40% sample group remained somewhat less defined.

Following the 7th day of cell culture, good cell coverage was identified via fluorescent microscopy for sample groups containing 0 to 20% CNT. Again, the nuclei and cytoplasmic regions of observed MG-63 cells were well defined. However, as with the previous time points, the presence of MG-63 cells with seemingly healthy morphologies appeared reduced when the CNT concentration was increased to 40%, as seen in figure 22.

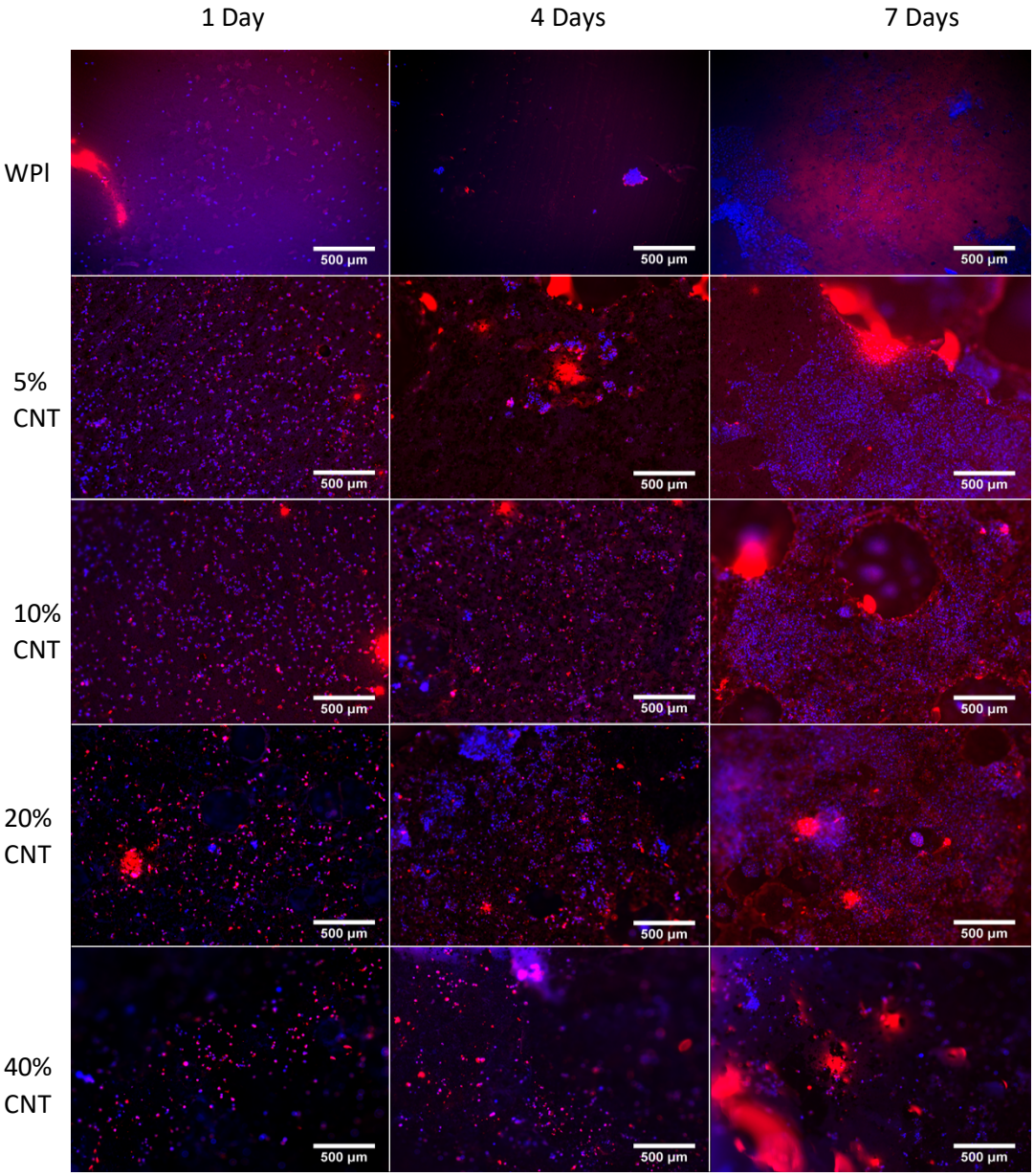

Figure 22: Fluorescent microscopy of MG-63 osteoblast-like cells cultured on WPI hydrogels supplemented with CNTs at concentrations of 0, 5, 10, 20 and 40% at 1, 4 and 7 days. *Cells stained by Hoechst (nuclei, blue) and Texas Red (cell cytoplasm, red). Scale bar indicates 500µm.*

9.4.2 Proliferation (MTS) Assay

The previously discussed MTS assay, which measures the extent to which metabolically active cells convert a soluble tetrazolium salt into insoluble formazan; thus, indirectly indicating proliferation, cell viability and cytotoxicity of samples, was repeated following WPI-CNT cell culture (Figure 23)

After 24 hours, no statistically significant reduction ($P<0.05$) in metabolic activity from the cultured MG-63 cells was observed for cells cultured on the WPI control (0%) or 5% CNT samples compared to the polystyrene control, although the absorbance recorded for the polystyrene control was more than double that of the WPI control. The absorbance values recorded for the 10 and 20% CNT samples, although significantly reduced compared to the polystyrene control, demonstrated no statistically significant reduction when compared to the remaining sample groups.

After 4 and 7 days of cell culture, the absorbance values recorded for all sample groups, including the WPI control, displayed a statistically significant reduction in intensity compared to the polystyrene control at the corresponding time point. Despite this, after 4 days of cell culture, there was no statistically significant difference between the absorbance values for the 10 or 20% CNT samples, compared with that of the WPI control. Interestingly, the 5% CNT samples showed a statistically significant increase of 0.23 a.u compared to the WPI control.

Following 7 days of cell culture, the absorbance value recorded for the WPI control (0.604a.u.) were significantly ($P<0.05$) elevated compared to the remaining sample groups. The lowest absorbance value within CNT supplemented hydrogels was from the 20% CNT group (0.247) and the highest for 10% CNT samples (0.449). Despite this, it is important to note that all sample groups displayed a statistically significant increase in absorbance after 7 days of cell culture than that observed after 24 hours.

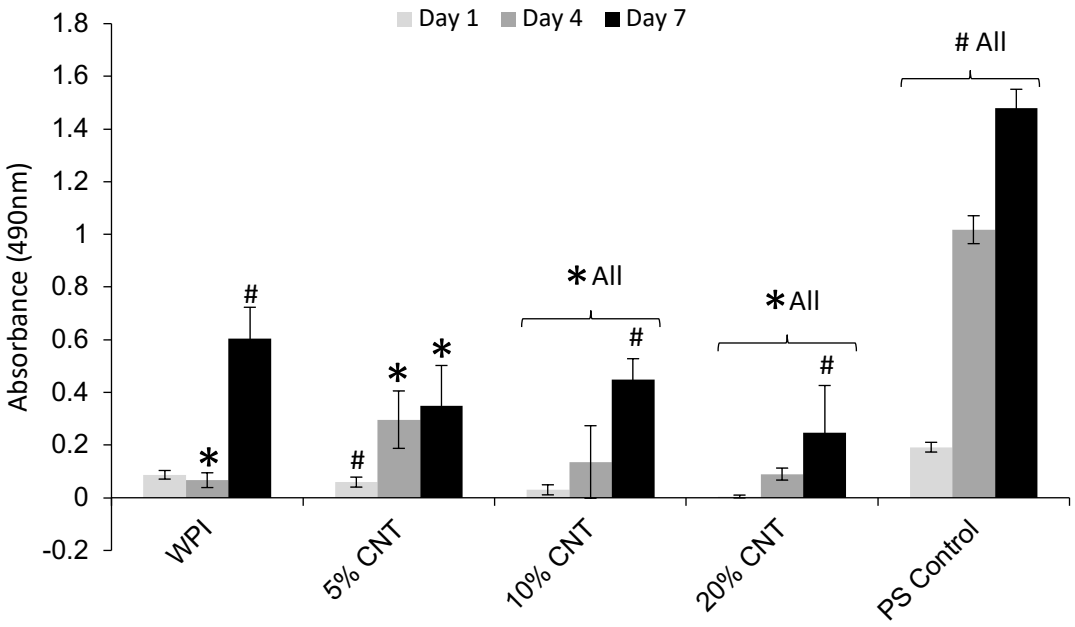

Figure 23: Proliferation of MG-63 osteoblast-like cells on 40% WPI hydrogels with CNT concentrations 0 (WPI control), 5, 10 and 20%, assessed at 1, 4 and 7 days, via the MTS assay*. As per method, Hydrogels were placed in 500µl of MTS solution and incubated for 2 hours. Absorbance was then measured via a spectrophotometer (at 490nm). Polystyrene control also included. * indicates statistical significance compared to the polystyrene control at the corresponding time point (P<0.05). # indicates statistical significance within sample groups (P<0.05). Error bars show standard deviation.*

9.5 Cell Culture Scanning Electron Microscopy

To supplement the previously described methods to evaluate the ability of WPI-CNT hydrogels to support the growth of MG-63 cells, SEM was utilised to provide enhanced detail into the extent of attachment and the topography of cultured cells on the surface of hydrogel samples (figure 24).

Consistent with the previous analysis, SEM analysis of 5% CNT-WPI hydrogels presented large areas of cell coverage on the hydrogel surface. Cells appeared well spread with clearly defined boarders, and visible filopodia, suggesting successful attachment. However, rounded cells were also visible in places (figure 24A). Additionally, CNTs were visibly integrated into the MG-63 cell layers and could be observed within them, as well as protruding from them.

Similarly, when 10% CNT-WPI hydrogels were imaged following 7 days of cell culture (figure 24C and D), large layers of cell coverage were observed, with a spread morphology and filopodia once again visible on the hydrogel surface. Despite this, the visible layers of MG-63 cells appeared to present areas with cells debris and gaps within them on a more frequent basis than the 5% CNT samples (D). When imaged at higher magnification, the boarders of cells could be seen detaching from one-another and peeling away from the layer (D).

As the CNT concentration was elevated, first to 20% (figure 24E and F) and then to 40% (figure 24G and H), the areas of hydrogel presenting MG-63 cell coverage was visibly reduced. On both 20% and 40% CNT samples, imaging revealed layers of cells which may previously have been confluent. Cells with a spread morphology remained visible, however, these were somewhat sporadic and vastly outnumbered by cells presenting unhealthy morphologies. The frequency of observable cell debris from cells which appear to have been lysed was also increased.

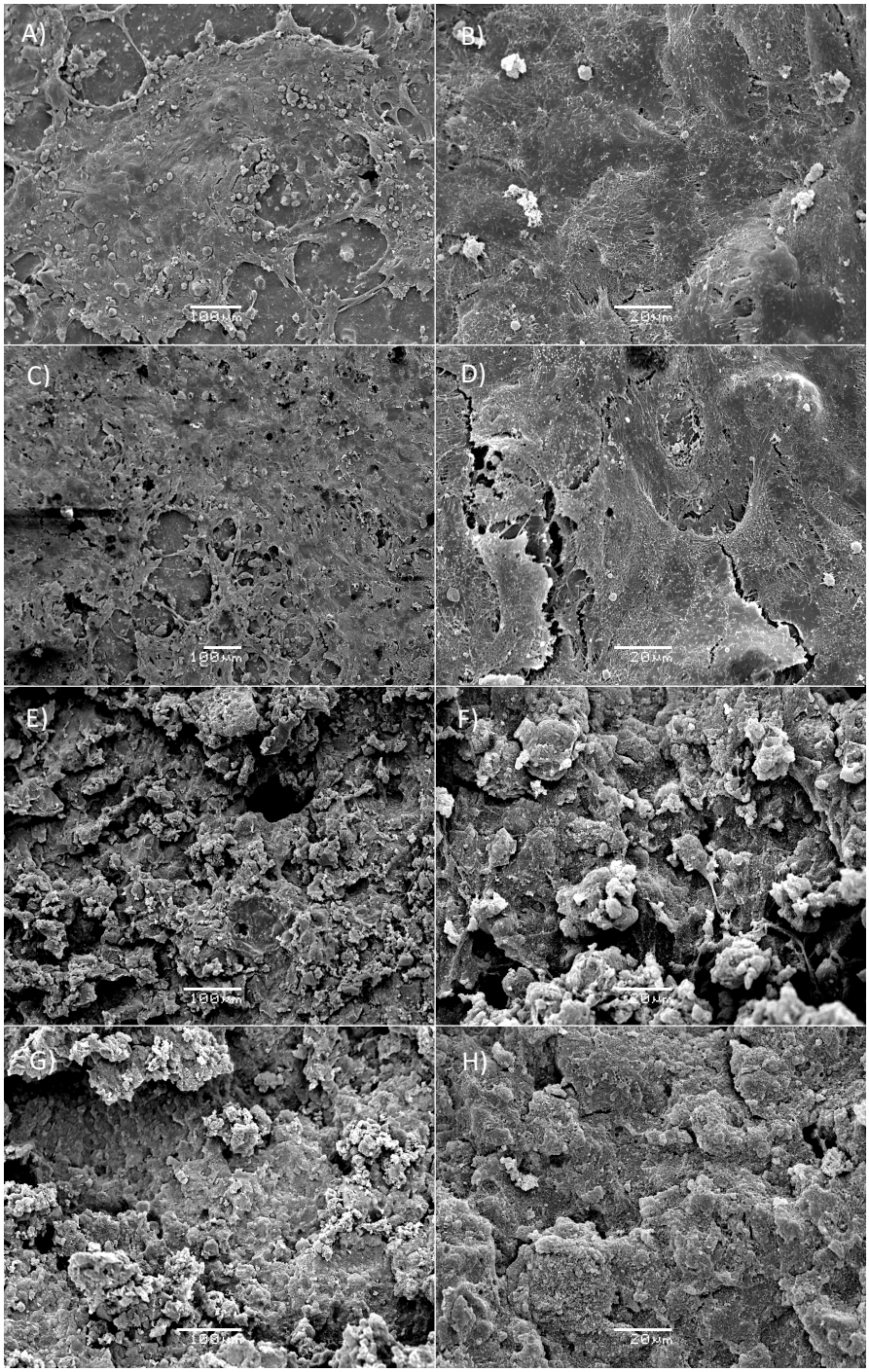

Figure 24: SEM images of WPI hydrogels containing CNT concentrations of 5% CNT (A and B), 10% CNT (C and D), 20% CNT (E and F) and 40% CNT (G and H) after the 7th day of cell culture. *Images show scale bars (left = 100 µm, right = 20 µm).*

9.6 Cell viability

The Crystal Violet assay is often utilised as an indirect measurement of cell death. When adherent cells die, they detach from the surface and are therefore not stained with Crystal Violet, whereas live cells remain adhered to the surface and are subject to staining. Therefore, the higher the absorbance observed when read with a spectrophotometer, the greater the presumed biomass.

When hFOB cells cultured in wells containing WPI hydrogels supplemented with CNTs were subjected to this assay, each of the experimental groups (0%, 20% and 40% CNT) displayed an absorbance below that of the polystyrene control after 24 hours. The observed absorbance values were elevated for both 20 and 40% CNT hydrogels compared to the WPI control. However, the only statistically significant difference ($P<0.05$) after 24 hours was between the WPI and Polystyrene control. On the fourth day, the absorbance values reduced for all sample groups. Statistically significant differences were observed between both CNT supplemented hydrogels compared to the polystyrene control, but not the WPI control. Although the absorbance values increased to beyond those observed on day four after seven days in all sample groups, the only statistically significant elevation was in the WPI control. Interestingly, this value was also elevated in comparison to that of the polystyrene control.

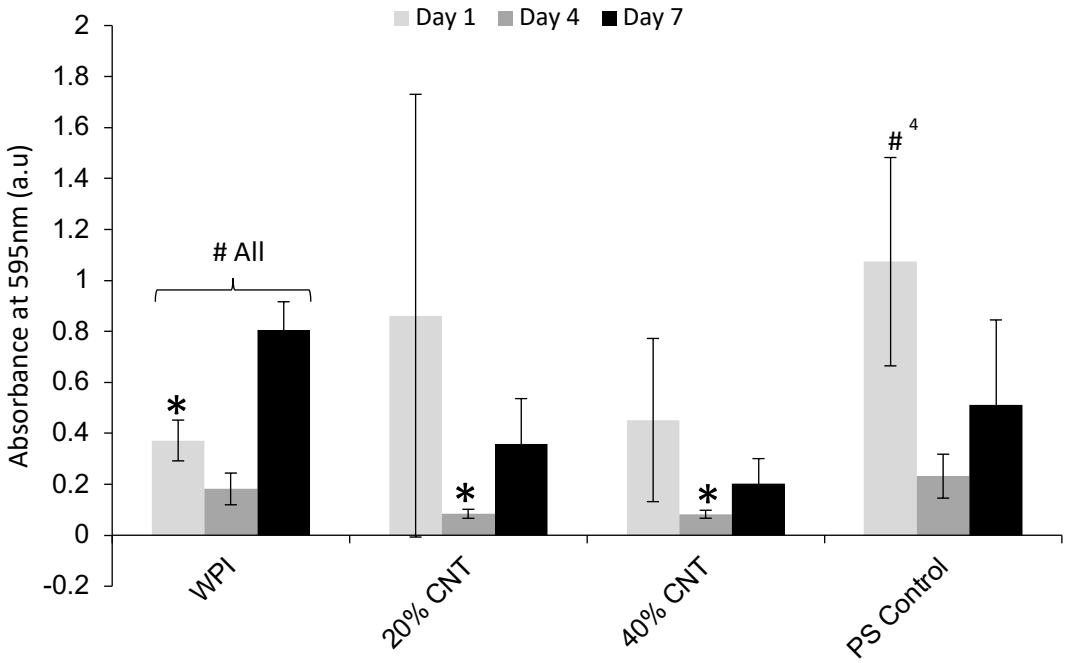

Figure 25: A Crystal Violet assay of the well in which hydrogel cell culture samples had been removed*. As per method. hFOB cells that remained on the base of the well were fixed using 4% paraformaldehyde (PFA). Crystal Violet dye was applied to each well, washed with distilled water 3 times and treated with 0.5% acidified methanol. Plates were read using a Tecan GENios multi-scan spectrophotometer at 595nm. Wells that contained 0 (WPI Control), 20 and 40% CNT samples were evaluated alongside a polystyrene (PS) control. Error bars show standard deviation. * indicates a statistically significant difference compared to the PS control at the corresponding time point (P<0.05). # indicates a statistically significant difference within sample groups (P<0.05).*

9.7 Antibacterial Testing – Colony Forming Unit Assay

The potential antibacterial properties of the WPI-CNT hydrogels were evaluated in conjunction with Doctor Raechelle D'Sa and Doctor Jenny Hanson at the University of Liverpool. This was conducted via three runs of a CFU assay, each time in triplicate.

9.7.1 Experiment One

Following 24 hours of incubation with each sample group, serial dilutions of the bacterial solutions and subsequent analysis of agar plates following overnight incubation at 37 ˚C, it was observed that the presence of CNTs reduced the number of bacterial colonies formed.

The control WPI hydrogels (0% CNT) displayed no antibacterial activity, in fact, a statistically significant increase ($P<0.05$) in the number of bacterial colonies was observed compared to the blank control (no hydrogel added during incubation). However, the 20% CNT hydrogels reduced the number of colonies observed, in a statistically significant manner, by 76%, compared to the WPI control group. This reduction was elevated to 86.7% when CNT concentration was increased to 40%, as illustrated in figure 26A.

Additionally, both the 20% and 40% CNT sample groups reduced the number of colonies observed compared to the blank control (45.4 and 69.6%, respectively), however, this was not deemed statistically significant ($P<0.05$) by a one-way ANOVA.

9.7.2 Experiment Two

Contrastingly, experiment two demonstrated no statistically significant difference ($P<0.05$) in the number of colonies present between the 20% CNT, WPI or blank control sample groups. Despite this, the 40% CNT displayed a statistically significant reduction of approximately 72% compared to the other sample groups (figure 26B).

9.7.3 Experiment Three

In the final experiment performed, the blank control group displayed confluent bacterial growth, meaning colonies were too dense for statistical analysis to be performed – therefore, the blank control was excluded from figure 26C.

Consistent with experiment one, the addition of CNTs to the WPI hydrogels reduced the number of colonies observed following bacterial incubation, compared to the WPI control. The addition of 20% CNTs resulted in a statistically significant reduction of 38%, which was elevated to 49.3% when the CNT concentration was increased to 40%.

Overall, the supplementation of WPI hydrogels with CNTs appears to provide them with antibacterial activity. The control WPI samples alone, however, do not exhibit antimicrobial activity.

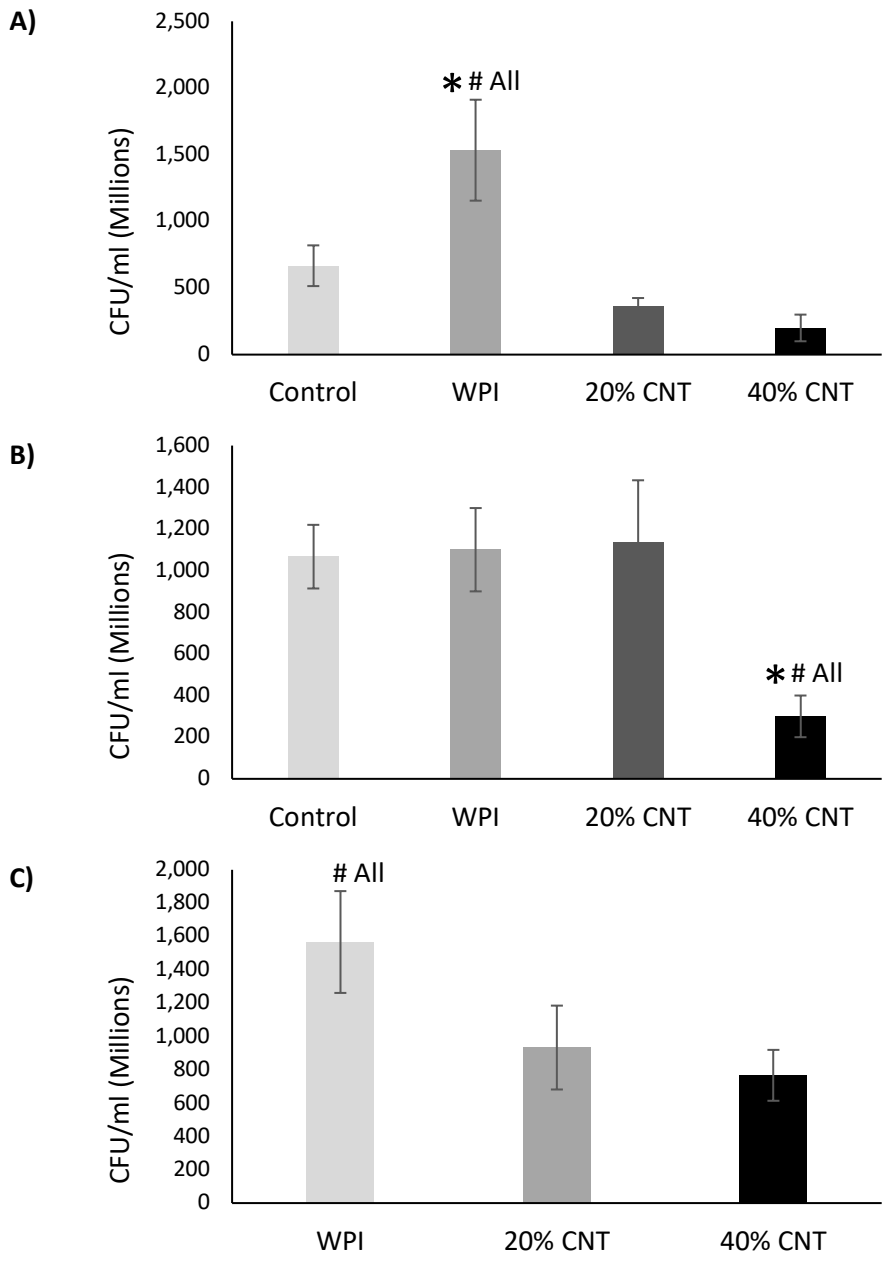

Figure 26: 3 runs of a Colony forming Unit Assay illustrating the number of surviving bacterial cells following 24 hours of incubation with WPI hydrogels supplemented with 0%, 20% and 40% CNTs. 'Blank' control also shown in experiment 1 and 2 (A and B). ** indicates statistical significance (P<0.05) compared to the blank control. # indicates statistical significance between hydrogel groups. Broth missing from run 3 as statistical analysis could not be performed due to density. Error bars display standard deviation.*

9.8 Mechanical Testing

The effects of adding CNT to WPI hydrogels on the hydrogels mechanical properties were evaluated using a Zwick 1435 Universal Testing Machine – these studies focused on the higher CNT concentrations, namely, 20 and 40% as shown in figure 27.

9.8.1 Compressive Strength

Addition of CNTs to WPI hydrogels resulted in a decrease in compressive strength (figure 27A). The control WPI samples (0% CNTs) demonstrated a mean compressive strength of 4.11Mpa which reduced by approximately 50%, in a statistically significant manner, as a result of CNT supplementation (both 20 and 40%). Although not statistically significant, the compressive strength of the 40% CNT sample group demonstrated a mean increase of 0.17MPa compared to the 20% sample group (1.84 to 2.01MPa).

9.8.2 Young's Modulus

Supplementing WPI hydrogels with CNTs (both 20 and 40%) increased the Young's Modulus of samples in a dose-dependent manner compared to the WPI controls (figure 27B). Specifically, the addition of 20% CNTs increased the Young's Modulus from approximately 2.57MPa (WPI control) to 3.28MPa. This was elevated further to approximately 4.39MPa when the CNT concentration was increased to 40%. Both increases were deemed to be statistically significant compared to the WPI control ($P<0.05$).

9.8.3 Strain at Break

Finally, the addition of CNTs resulted in a decrease in the strain at break of the hydrogel samples (figure 27C). WPI control samples deformed by a mean 5.69mm (71.14%) before breaking. The mean strain at break decreased to 44.67% in the 20% CNT experimental group, and further to approximately 28.13% in the WPI hydrogels supplemented with 40% CNTs. Statistical significance was confirmed compared to the WPI control and between 20 and 40% sample groups ($P<0.05$).

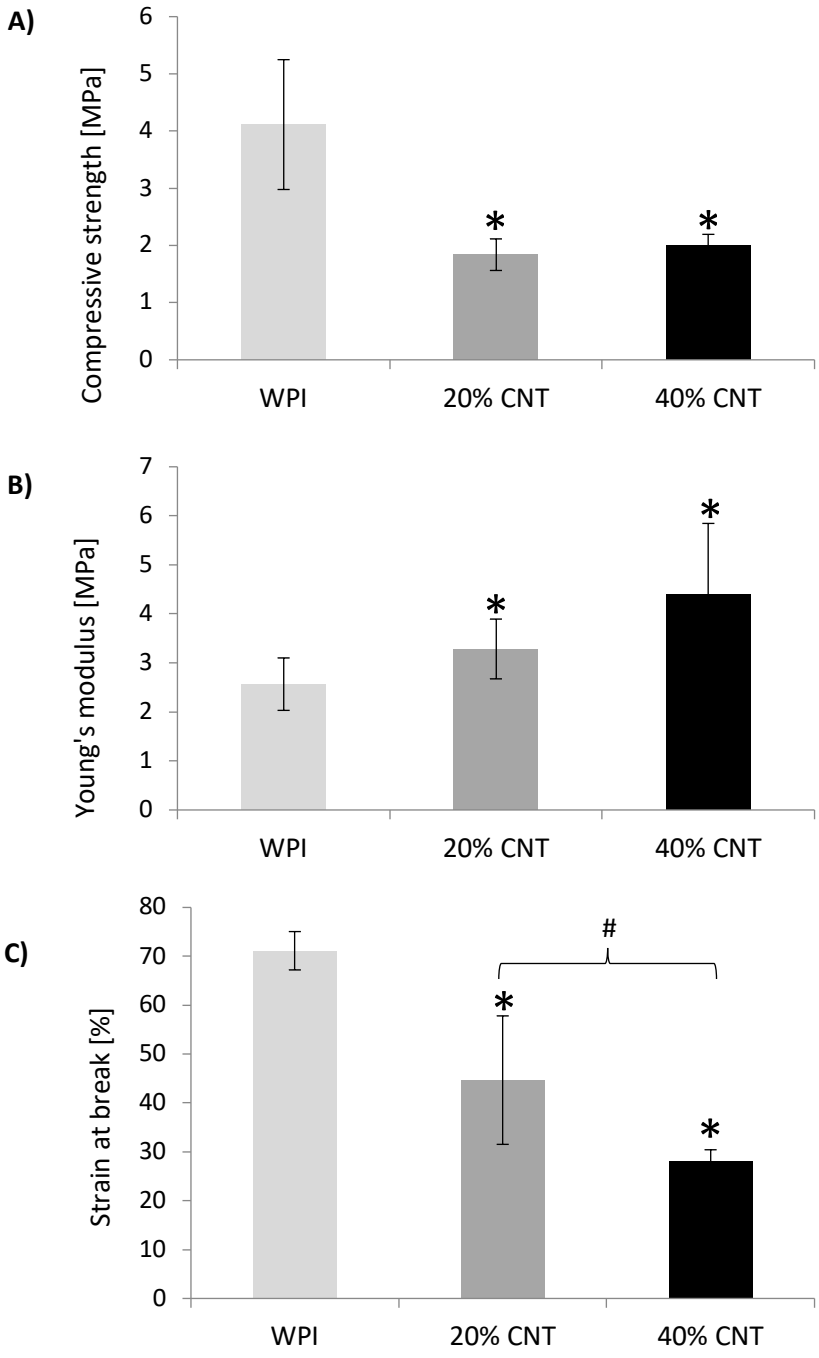

Figure 27: Mechanical testing of cylindrical WPI hydrogels containing 0, 20 and 40% CNT, with a Zwick 1435 Universal Testing Machine. *A) Compressive strength, B) Young's Modulus, C) Strain at break. * indicates statistical significance compared to the WPI control (P<0.05). # indicates statistical significance between WPI-CNT groups (P<0.05).*

9.9 Dry Mass

The dry mass percentages of WPI hydrogels (the mass of the hydrogel not attributable to water) containing CNTs at quantities of 0 to 40% are illustrated in figure 28.

The addition of lower concentrations of CNTs (2.5, 5, and 10%) to the hydrogels appeared to have no effect on the dry mass percentage, compared to the control WPI hydrogels (0% CNT). The mean dry mass percentage for each of these 4 groups was approximately 33%. An increase to 44% was observed when CNT concentration was increased to 20%, however, this was not deemed to be significant. Compared to the control, the mean dry mass percentage approximately doubled for the 40% CNT samples (65%). This value, as demonstrated by figure 28, showed statistical significance when compared to each of the other sample groups ($P<0.05$).

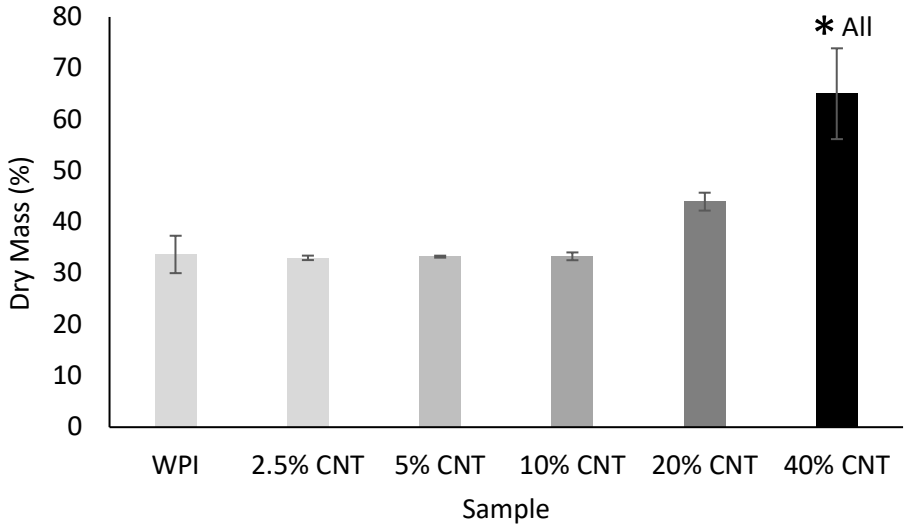

Figure 28: Dry Mass percentages of 40% WPI hydrogels with CNT concentrations of 0, 2.5, 5, 10, 20 and 40%. Samples were weighed in the hydrated state, dried for 24 hours at 60°C, and weighed again for the dry mass % to be calculated. *Error bars display standard deviation. Differences considered significant if p < 0.05. '*' relates to the significant difference compared to the WPI control (* P<0.05). 'All' relates to the significant difference between the 40% CNT group compared to the remaining groups.*

10.0 Discussion

As previously discussed, research has elucidated unique properties which implicate CNTs in numerous applications. Specific to bone tissue engineering, hydrogels supplemented with CNTs have demonstrated enhanced mechanical properties (Tozzi et al., 2016 and Usui et al., 2008) and reduced gelation time as a result of the thermal properties demonstrated by CNTs (Yasmeen et al., 2014). Furthermore, CNTs have been shown to promote the formation of mineralised bone (Zhao et al., 2005). However, the antimicrobial activity which they have demonstrated against a range of pathogens is the primary reason for their selection in the present study.

Similarly, WPI is a 'green' material with low production costs and multiple potential advantages in the bone tissue engineering space. As gelation is induced by heat, hydrogels comprised of WPI possess the benefit of simultaneous fabrication and sterilisation. Furthermore, WPI has been shown to enhance the growth of both human osteoblast-like Saos-2 cells and human neonatal dermal fibroblasts (FIB), in addition to inducing the expression of markers characteristic of osteogenic cell differentiation by human adipose tissue derived stem cells (ASC). This, along with the availability and low cost of WPI, implicates it in bone tissue engineering applications and underpins the decision to evaluate WPI based hydrogels in the present study.

Therefore, the purpose of the current study was to supplement WPI hydrogels with CNTs, with the intention of conveying the advantages of their unique properties onto the hydrogels. Subsequently, the efficacy of WPI-CNT hydrogels as materials with potential implications in bone tissue engineering was evaluated. Areas of specific interest were the potential mechanical reinforcement and antibacterial properties induced by CNT supplementation.

Firstly, the laser diffractometry measurements indicated that there were no CNTs below 1.95µm, with only a negligible proportion between 1.95µm and 5.69µm. As CNTs are known to measure only a few nanometres in diameter, these results may represent agglomerates, rather than individual CNTs. CNTs tend to agglomerate due to strong van der Waals forces, meaning that surfactants or ultrasonication are required to aid their dispersion in solution (Krause et al, 2010). An alternative technique, such as Transmission Electron Microscopy (TEM), may be more appropriate to evaluate the size of the CNTs used in this study.

As expected, increasing the CNT concentration of WPI hydrogels resulted in considerably rougher microstructures. When WPI-CNT composites were examined by SEM, CNTs were visible both encapsulated within the hydrogels and penetrating through the exterior coated in protein. At the highest CNT concentrations examined (20 and 40%), homogeneity of the hydrogels was notably reduced. Areas of exceedingly increased porosity were visible, as were CNTs attached to the hydrogels but not coated in protein.

Subsequent imaging of cross-sectional samples of WPI-CNT hydrogels should be conducted for the homogeneity of CNT dispersion to be evaluated more accurately. This will also confirm the efficacy of the vortexing, and sonication steps carried out prior to gelation, which, as discussed by Foldvari and Bagonluri (2008), is one of the easiest methods to achieve dispersion of CNTs. However, it is also important to note that the concentrations of CNTs used (20% and 40%) are particularly high in this study as the intention was to maximise biological and mechanical effects as a result of CNT supplementation. For example, previous studies, such as that by Seo et al (2014), evaluated composites supplemented with only 2% functionalised CNTs.

10.1 Fourier-Transform Infrared Spectroscopy (FT-IR)

Further to visual analysis, FT-IR analysis evaluated the interaction between the CNTs and WPI in the hydrogel at a molecular level. Rather than simple encapsulation, a direct interaction

between CNTs and the protein phase of the hydrogels was confirmed by this technique. Functional groups of CNTs were found to chemically interact with functional groups of the WPI, break intermolecular bonds between peptide chains and, ultimately, force the transition from Beta pleated sheets to alpha helices. Importantly, as the effect on the shape and intensity of the spectra was exaggerated at higher doses, it is suggested that this interaction occurs in a dose-dependent manner.

10.2 Mechanical testing

As previously stated, one of the primary motives for the inclusion of CNTs in WPI hydrogels was the hypothesised mechanical reinforcement that would accompany it. This theory was investigated in conjunction with AGH University of Science and Technology.

Consistent with the suggestion of a dose-dependent interaction between CNTs and the WPI hydrogel, the Young's moduli of these composites elevated with the inclusion of CNTs, in a similarly dose-dependent manner. However, a decrease in both compressive strength and strain at break was observed in CNT supplemented hydrogels compared to the control. Therefore, CNT addition to WPI hydrogels was demonstrated to result in stiffer, but not compressively stronger, hydrogels. This is inconsistent with studies such as that by Seo et al (2014) who observed an increase in compressive strength of chitosan hydrogels supplemented by CNTs, and Tozzi et al (2016) and Usui et al (2008) who demonstrated considerable increases in the tensile strength and elastic moduli of chitosan and silica membranes augmented with CNTs. However, lower concentrations of CNTs were used in these studies. Consistent with FT-IR analysis, this suggests that the presence of CNTs in higher quantities interferes with the proteinaceous interactions of the WPI hydrogels, ultimately having a negative impact on hydrogel integrity. Therefore, in line with the CNT concentrations used in previous studies, subsequent mechanical testing should be completed with the 2.5 and 5% CNT hydrogels to confirm the ability of CNTs to increase the

compressive strength of WPI hydrogels. However, irrespective of the *in-vitro* decrease in mechanical strength observed in this study, CNT supplemented hydrogels may increase the mechanical strength *in-vivo.* Specifically, as observed by Usui et al (2008) in a mouse model, the CNTs would remain and be able to integrate with the bone tissue after the hydrogel is naturally broken down.

10.3 Antibacterial

The remaining primary motive for the inclusion of CNTs in WPI hydrogels, hypothesised CNT induced antibacterial properties, was confirmed by way of the colony forming unit assay.

As the bacterial colonies observed following incubation with WPI hydrogels were more numerous than those observed in the blank control (no hydrogel present during incubation), the present study suggests that WPI hydrogels provide an environment which may encourage the growth of *Staphylococcus aureus*, in the absence of CNTs. This may not be surprising, as milk proteins are known to function as delivery mechanisms for essential micronutrients (Douglas et al., 2018).

However, the successful dose-dependent reduction in the number of *Staphylococcus aureus* colonies which accompanied the supplementation of WPI hydrogels with CNTs confirms the hypothesis. Therefore, the current study suggests that the supplementation of WPI hydrogels with CNTs does impart antibacterial activity, at least in the case of *Staphylococcus aureus*.

As previously discussed, implant related microbial infections caused by bacteria and fungi, such as *Staphylococcus aureus,* are one of the primary causes of wound healing complications and failure of orthopaedic implants (Romanò et al., 2015; Salomé Veiga and Schneider, 2013). Both the incidence and socio-economic cost of these complications continue to rise (Aggarwal et al., 2014; Romanò et al., 2015). Therefore, the apparent antibacterial properties of WPI-CNT hydrogels are desirable in potential tissue engineering

applications and, therefore, may implicate them in bone tissue regeneration. However, as the size and type of CNT (SWNT or MWNT) is known to influence the potency of their antibacterial effect in isolation (Kang et al., 2008), this should be examined in composites (such as those in the present study) in future research.

10.4 Cell Culture

However, the mechanism by which CNT conveys antibacterial properties must not elicit cytotoxic effects, should they be used in these applications. Therefore, the ability of a human osteosarcoma (MG-63) cell line to adhere and proliferate on WPI-CNT hydrogels was an important aspect of the present study.

Although cells were present on all sample groups following 4 hours of cell culture, good cell coverage was observed on hydrogels with 0, 5 and 10% CNT, with reduced cell coverage exhibited for hydrogels with elevated CNT concentrations. On the 4th day of cell culture, cells on both the WPI control and the 5% CNT hydrogel had been visibly removed due to mechanical interference when manipulating samples. This could be because samples had reached confluency and had become more susceptible to damage of this nature. Following the 7th day of cell culture, seemingly good cell coverage was observed on samples ranging from 0 to 20% CNT, with visibly fewer cells on the 40% hydrogels. However, the reduction in cells on the 40% CNT samples suggests that higher concentrations of CNTs have a negative impact on the viability of MG-63 cells.

It is important to note that 40% CNT hydrogels were not subject to the MTS assay because the samples had become exceedingly ‘powdery’ and could not withstand the manipulation necessary to complete the assay. Once again, this supports the suggestion that the presence of CNTs in higher quantities interferes with the proteinaceous interactions of the WPI hydrogels, resulting in a loss of integrity. This ‘powdery’ nature may also be the reason for

the reduction in cell number observed on 40% samples after cell culture, as stiffer surfaces are known to promote the differentiation of cells.

Despite this, following the 7th day of cell culture, even though CNT supplemented hydrogels all demonstrated a significantly lower absorbance than that of the control, the absorbance for each sample group was elevated in a statistically significant manner compared to that observed after 24 hours. This supports the findings from fluorescent microscopy and suggests that cells remained both viable and metabolically active after 7 days exposure to CNT supplemented hydrogels, even at concentrations of 20%. However, it should not go unnoticed that the 40% CNT samples displayed considerably reduced cell coverage when subject to fluorescent microscopy. It can, therefore, only be assumed that this reduction would also be seen in the MTS assay.

It should also be noted that, although cell culture-based toxicity assays are popular methods for investigating the toxicity of nanotubes (Wang et al., 2012), the results are often inconsistent between research groups. This may be due to the interaction of the CNTS with the dyes used in the cytotoxicity assays, ultimately altering the colour emitted and resulting in false readings (Liu et al., 2009). However, it would be expected that these effects would be greatest at the highest concentrations, whereas in the current study, the absorbance was lowest for the samples with the highest CNT concentration.

10.5 Cell culture Scanning Electron Microscopy

SEM enabled the morphology of MG-63 cells cultured on the WPI-CNT hydrogels to be examined in greater detail. Due to time constraints, this method was only utilised to image 5 to 40% CNT hydrogels.

Although large areas of cell coverage could be observed, particularly on the 5% CNT hydrogels, with clearly defined boarders and visible filopodia. SEM also allowed rounded

cells to be imaged. Importantly, even at 5%, CNTs were visibly integrated into the MG-63 cells, observed both within and protruding from them.

With increasing CNT concentration, cells could be seen detaching from the surface, coverage reduced and cell debris from cells which appear to have been lysed increased in frequency. Thus, suggesting that CNT supplemented hydrogels have cytotoxic effects on MG-63 cells.

As previously stated, it has been suggested that CNT mediated toxicity varies based upon several factors, including method of exposure, shape, size, and composition (Madani et al., 2013). Specific to the effects of CNTs on bone tissue, multiple *in-vivo* studies combining MWCNTs in combination with chitosan or hyaluronate (rather than WPI) have indicated enhanced bone tissue growth in the absence of a notable immune response (Abarrategi et al., 2008; Mendes et al., 2010; Saito et al., 2001; Usui et al., 2008; Wang et al., 2007).

An important factor to consider is the purity of MWCNTs. Metals such as Cobalt (Co), Iron (Fe), Nickel (Ni), and Molybdenum (Mo) are used as a catalyst during CNT synthesis (Donaldson et al., 2006). Residues of these metals can become encapsulated within the graphene layers and remain as impurities, which have been implicated to induce cell death via mechanisms such as mitochondrial destruction and oxidative stress (Pichardo et al., 2012).

Methods of purification have been shown to reduce CNT mediated toxicity significantly. As Toh et al (2012) demonstrated with CNTs exposed to ultrasonication for as few as 5 minutes. In the current study, CNTs were sonicated once in the WPI solution to aid dispersion. However, a proposed alteration to the experimental technique would be to sonicate the CNTs individually, before adding them to the solution.

Furthermore, as 2.5% CNT samples were absent from some of the primary tests due to time constraints, these should be repeated with the lower concentrations of CNTs. Overall, the unique properties which CNTs possess implicate them in numerous clinical applications.

However, additional research into WPI-CNT hydrogels, and CNTs alone must be conducted for their toxicity to be fully understood and their potential in biomedical applications to be realised. Furthermore, the ability to simultaneously fabricate and sterilise relatively low cost 'green' WPI hydrogels provides an interesting platform for further research. For example, WPI hydrogels could be supplemented with alternative antimicrobials, or exposed to ALP-induced mineralisation to optimise their properties for potential use in bone tissue regenerative applications.

11.0 Conclusion

The present study demonstrated that the incorporation of CNTs successfully increased the Young's modulus, demonstrated satisfactory cytocompatibility towards MG63 cells and provided WPI hydrogels with antibacterial activity against *Staphylococcus aureus.* Therefore, CNT reinforced WPI hydrogels may provide promising candidates for bone tissue engineering applications.

Chapter 4: Phloroglucinol-WPI Hydrogels

12.0 Introduction

Phenolic compounds, subunits of polyphenols, have also been implicated as components of an antimicrobial hydrogel. Polyphenols are derived from plants and, as well as their antibacterial effects, are known to possess antioxidative properties. This is beneficial in terms of bone tissue engineering, as oxidative stress has been indicated to impede both the differentiation of osteoblasts and the resorption of bone by osteoclasts, *in-vitro* (Bax et al., 1992*;* Mody, 2001). The ability of phenolic compounds such as gallic acid (GA), isolated from terrestrial plants, and phloroglucinol (PG), found in seaweeds, to ameliorate oxidative stress has been documented on numerous occasions (Kim et al., 2012; Queguineur et al., 2012; Umadevi et al., 2012). Similarly, a study conducted by Lišková et al (2015) demonstrated that GA and PG both increased the antioxidant activity of chitosan hydrogels and decreased the colony forming ability of *Escherichia coli*. However, hydrogels containing GA (but not PG) were also found to be cytotoxic in cell culture, due to the release of toxic substances from the hydrogel into the culture medium.

Therefore, in addition to the previously described CNT supplemented hydrogels, the present study incorporated PG into WPI hydrogels with the intention to create a biomaterial with antibacterial properties in the absence of cytotoxic effects.

13.0 Methods

13.1 Hydrogel Preparation:

Stock solutions of 40% w/v whey protein isolate were prepared by dissolving WPI powder in deionised H_2O. A sonicator was used to facilitate dissolution and minimise foaming. Subsequently, 500µl of stock solution was added to Eppendorf tubes alongside the required amount of Phloroglucinol (Sigma-Aldrich, Germany) to make 0 (control), 2.5, 5, 10, and 20% PG samples. Once in Eppendorf tubes, samples were vortexed until mixed homogenously.

Samples were then autoclaved at 134°C for 20 minutes, to simultaneously sterilise and induce gelation of the samples.

13.2 Scanning Electron Microscopy (SEM):

Samples were prepared for SEM as previously described in chapter 3 section 8.4.

13.3 Mechanical Testing:

The effects of adding PG to WPI hydrogels on the hydrogels mechanical properties were evaluated in collaboration with Krzysztof Pietryga (AGH University of Science and Technology, Poland). Cylindrical samples of 2.5, 5, 10 and 20% PG, measuring 10mm in height and 8mm in diameter, were subject to compressive testing using a Zwick 1435 Universal Testing Machine. Test parameters were set at a speed of 10mm per minute, and a test range of 0-95% strain.

13.4 Cell Culture:

To evaluate the interaction of the WPI-PG hydrogels with bone cells, a human osteosarcoma (MG-63) cell line was seeded on to the hydrogels as per method in chapter 3, section 8.7.

13.4.1 Fluorescent Microscopy:

At intervals of 1, 4 and 7 days, the adhesion, proliferation, and morphology of cells was assessed by fluorescent microscopy as per the method in chapter 3 section 8.7.1.

13.4.2 Proliferation Assay (MTS)

At intervals of 1, 4 and 7 days, MG-63 cell viability was evaluated via the MTS assay, as per method in chapter 3, section 8.7.2.

14.0 Results

Sample Abbreviation	Description
WPI Control	40% WPI - 0% PG hydrogel
2.5% PG	40% WPI - 2.5% PG hydrogel
5% PG	40% WPI - 5% PG hydrogel
10% PG	40% WPI - 10% PG hydrogel
20% PG	40% WPI - 20% PG hydrogel
40% PG	40% WPI - 40% PG hydrogel

Table 3: The different sample groups examined in Chapter 4

14.1 Scanning Electron Microscopy (SEM)

The microstructures of WPI-PG hydrogels with concentrations ranging from 0 to 20% PG were analysed via SEM. The WPI control (0% PG) sample (Figure 29A) presented a consistently smooth surface topography. As expected, the observed microstructure of samples became increasingly rougher as the PG concentration increased

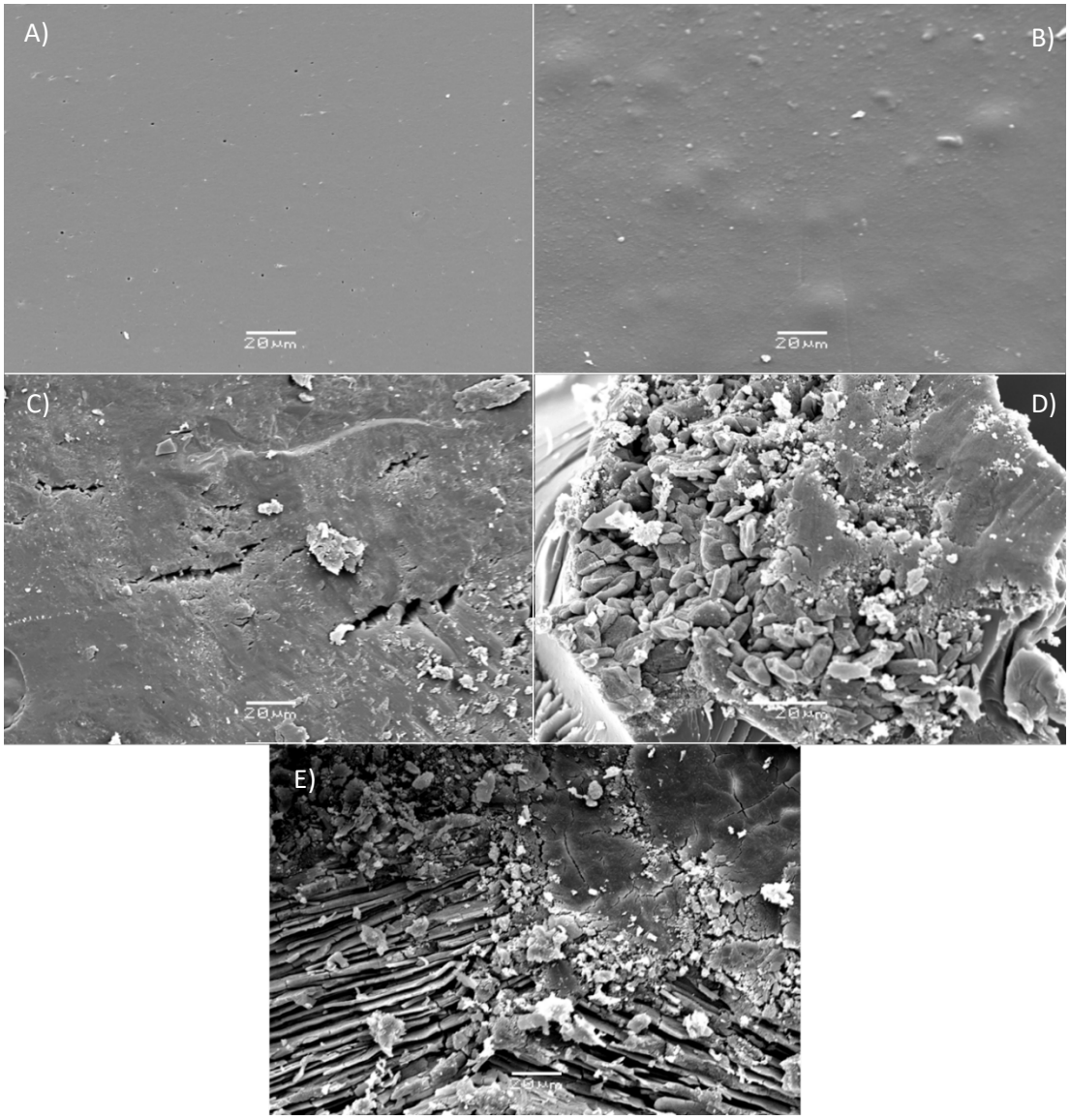

Figure 29: SEM images of WPI hydrogels containing PG at concentrations of 0% (A), 2.5% (B), 5% (C), 10% (D) and 20% (E). *Scale bar indicates 20µm*

14.2 Mechanical Testing

It is important to note that, due to high friction, the WPI samples supplemented with 20% PG were stuck in the jaws of the Zwick testing machine, meaning values for strength, modulus and strain at break were overestimated.

14.2.1 Compressive Strength

No statistically significant difference in compressive strength was observed between the WPI control (0% PG) and the 2.5% PG sample group (mean values of 4.26 and 4.34MPa respectively). However, increasing the PG concentration to 5% resulted in the compressive strength decreasing by 1.35MPa to a mean of 2.91MPa. This reduction was deemed to be statistically significant compared to both the WPI control and the 2.5% PG sample group ($P<0.05$). Increasing the PG concentration to 10% demonstrated a mean compressive strength of 5.06MPa. However, values were inconsistent within this group and no statistical significance was proven.

14.2.2 Young's Modulus

Except for the 20% PG sample group for which values were overestimated, no statistically significant difference in Young's Modulus was observed between PG supplemented sample groups compared to the WPI control (Figure30B). The addition of 2.5% PG resulted in a negligible increase in Young's Modulus, while 5% resulted in a negligible decrease. A statistically significant increase of 0.43MPa was observed when PG concentration was increased from 5% to 10%. However, all samples demonstrated a Young's modulus between 3 and 4MPa.

14.2.3 Strain at Break

Finally, the mean deformation observed for the WPI control (0% PG) sample group was 7.09mm (70.92%). The addition of 2.5% PG to WPI hydrogels resulted in a slight increase in the strain a break (72.31%) while supplementation of 10% decreased this value to 70.14%.

However, except for the overestimate in the 20% PG samples, the only statistically significant difference ($P<0.05$) observed for strain at break coincided with addition of 5% PG (61.78%).

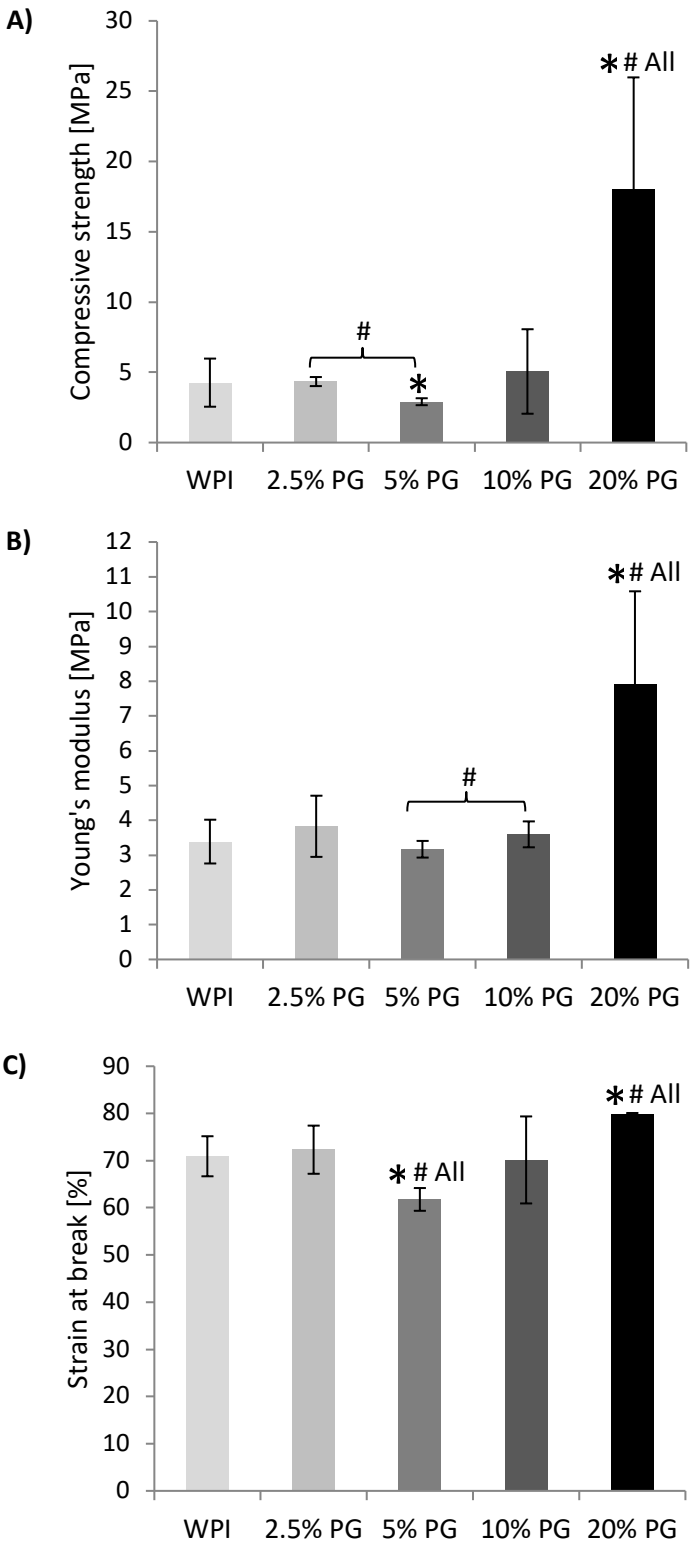

Figure 30: Mechanical testing ol WPI hydrogels containing 0, 2.5, 5, 10 and 20% PG*. A) Compressive strength, B) Young's Modulus, C) Strain at break. * indicates statistical significance compared to the WPI control (P<0.05). # indicates significance between WPI-PG groups (P<0.05). Error bars show standard deviation.*

14.3 Cell Culture:

14.3.1 Fluorescent Microscopy:

The adhesion, proliferation, and morphology of MG-63 cells cultured on WPI hydrogels supplemented with PG was evaluated, at intervals of 1, 4 and 7 days, by fluorescent microscopy (Figure 31). Prior to imaging, Hoechst stain was used to stain cell nuclei (blue), and Texas Red was utilised to stain the cytoplasmic regions (red).

Imaging of the samples suggested that PG was leaching out of the hydrogels and having a negative impact on cell viability. This is evidenced in figure 31, as cells were visible on the hydrogels containing the lowest concentration of PG (2.5%); with the number of observable cells reducing with increasing PG concentration, to almost no cell coverage at 20% PG. These observations were consistent at all three time points (1, 4, and 7 days). However, despite the presence of cells on the 2.5 and 5% PG samples, none of the observed cells displayed a healthy morphology – cells were rounded rather than spread and well defined.

Interestingly, what appeared to be crystalline structures were also observed on the surface of the 20% PG samples.

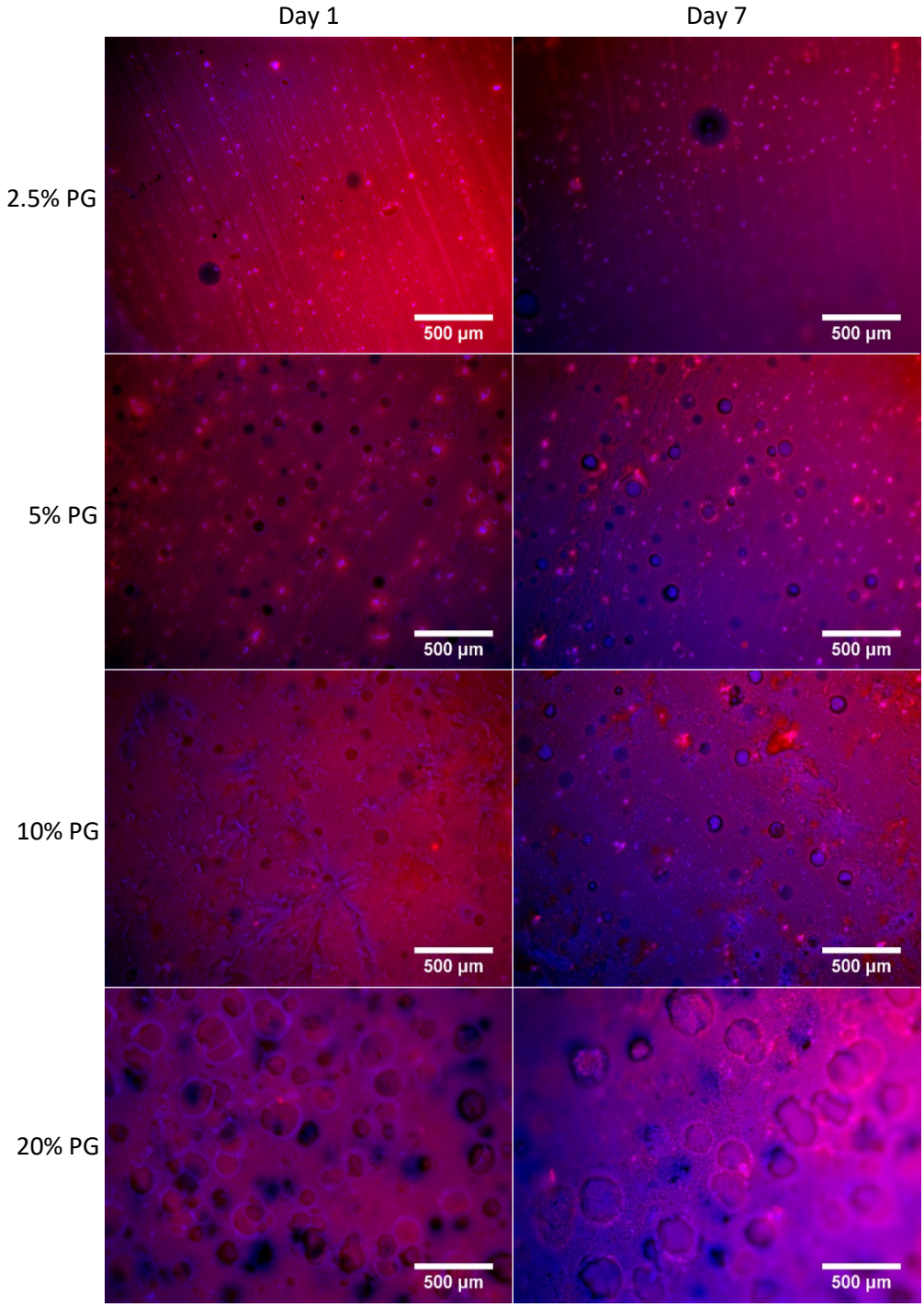

Figure 31: Fluorescent microscopy of MG-63 osteoblast-like cells cultured on WPI hydrogels supplemented with PG at concentrations of 2.5%, 5%, 10% and 20% after 1 and 7 days*. Cells stained by Hoechst (nuclei, blue) and Texas Red (cell cytoplasm, red). Scale bar 500µm.*

14.3.2 Proliferation (MTS) Assay:

Again, the MTS assay was utilised to allow the quantitative evaluation of cell metabolic activity – indirectly, proliferation, cell viability, and cytotoxicity of WPI-PG hydrogels.

Prior to the subtraction of the absorbance value for the background (samples in the absence of cells), the MTS assay produced false positive results for WPI-PG hydrogels. The uncorrected absorbance values indicated high levels of cell proliferation, elevated compared to the polystyrene control, and increasing with increasing PG concentration. However, this was also observed for the unseeded samples, indicating that PG interferes with the MTS assay.

When this was corrected for (background absorbance values subtracted), the values were close to 0, as displayed in figure 32. For each of the WPI-PG sample groups, the observed absorbance values were highest 24 hours after cell culture. No correlation between PG concentration and absorbance was observed - no statistically significant difference between 2.5 or 20% PG samples was detected compared to the polystyrene control at the same time point, whereas 5 and 10% samples were significantly lower. Following the 4^{th} and 7^{th} day of cell culture, no obvious trend in absorbance was visible as all groups were close to 0, significantly reduced compared to the polystyrene controls.

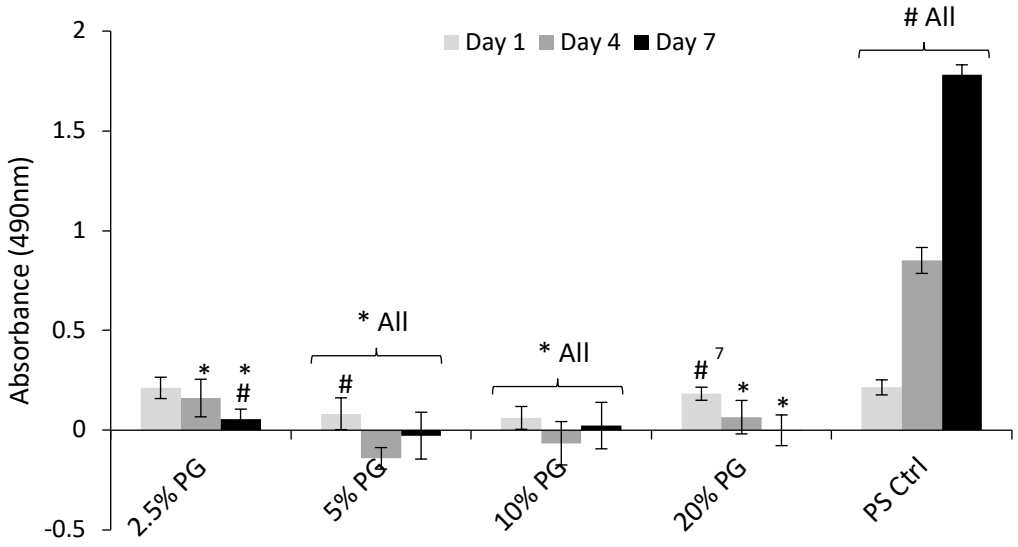

Figure 32: Proliferation of MG-63 osteoblast-like cells on 40% WPI hydrogels with PG concentrations 2.5, 5, 10 and 20% was assessed at 1, 4 and 7 days, via the MTS assay. *As per method, hydrogels were placed in 100µl of MTS solution and incubated for 2 hours. Absorbance was then measured via a spectrophotometer (at 490nm). # indicates statistical significance within sample groups (7) indicates the time period with the difference to. * indicates statistical significance compared to the polystyrene control at the corresponding time point (P<0.05). Polystyrene control also included. Error bars show standard deviation.*

15.0 Discussion

The purpose of current study was to evaluate the efficacy of WPI hydrogels supplemented with PG as materials with implications in bone tissue engineering applications. Alike gelatin hydrogels which can be simultaneously crosslinked and sterilised by electron irradiation, WPI hydrogels possess the advantage of simultaneous fabrication and sterilisation, as gelation is induced by heat. Furthermore, as WPI is a by-product when producing foods such as Greek yoghurt, it is a readily available low-cost material.

Specific to bone tissue engineering, WPI has been shown to enhance human osteoblast-like Saos-2 (for which calcium deposition was also stimulated) and human neonatal dermal fibroblast (FIB) cell growth. Additionally, human adipose tissue derived stem cells (ASC) demonstrated WPI induced expression of markers characteristic of osteogenic cell differentiation (Douglas et al., 2018). All of which contributed to the decision to utilise WPI hydrogels in this study.

Similarly, PG, a phenolic compound isolated from seaweed, was identified as a supplementary component of the experimental hydrogels due to their known antimicrobial and antioxidative properties. Specifically, the colony forming ability of *Escherichia coli* was reduced in chitosan hydrogels supplemented with PG (Lišková et al., 2015).

15.1 Scanning Electron Microscopy (SEM)

The effects of PG supplementation on the microstructure of WPI hydrogels was examined using SEM. As expected, the control WPI hydrogels (0% PG) displayed a homogenously smooth surface topography. With increasing PG concentration, hydrogels were observably rougher. This may be an advantage for their potential applications in bone tissue engineering as both stiffer and rougher surfaces are known to promote the differentiation of cells towards the osteoblastic phenotype. Although seemingly ‘free’ PG could be observed on the surface of the hydrogels, SEM also demonstrated that PG had become encapsulated inside

the WPI hydrogel. However, cross-sectional samples of these hydrogels must be imaged to confirm homogeneity of distribution and, therefore, the efficacy of vortexing the WPI/PG mixture before gelation.

15.2 Mechanical Testing

Minimal increases in both Young's modulus and percentage strain at break were found to accompany PG supplementation at lower concentrations (2.5%). Since stiffer surfaces are known to promote the differentiation of cells towards the osteoblastic phenotype, PG imparted stiffness would improve the compatibility of these hydrogels with bone tissue. However, this effect was not observed in a dose-dependent manner.

The values for Young's modulus, compressive strength and percentage strain at break remained relatively consistent throughout sample groups, even when the concentration of PG was increased to 10%. This suggests that the incorporation of PG into the WPI hydrogels has no significant impact on the overall structural function of WPI hydrogels. However, it is important to note that, due to high friction, the WPI hydrogels supplemented with 20% PG remained stuck in the jaws of the testing machine. As such, it is suggested that PG supplementation at higher concentration may alter the mechanical properties of WPI composites, resulting in 'stickier' hydrogels.

15.3 Fluorescent Microscopy

Although PG was identified to supplement hydrogels due to its antimicrobial activity, this must be achieved in the absence of cytotoxic effects, should these hydrogels be implicated in bone tissue regeneration.

Thus, the ability of PG supplemented WPI hydrogels to support the adhesion and proliferation of MG-63 cells was evaluated. Cell viability appeared to reduce with increasing PG concentration. Interestingly, crystalline structures were also observed on the surface of hydrogel samples containing 20% PG. This suggests that PG has cytotoxic effects in cell

culture, potentially due to the release of cytotoxic substances from the hydrogel into the culture medium. These observations contradict those by Lišková et al (2015) who found no cytotoxic effects of PG in cell culture. However, the same study documented the cytotoxic effects of gallic acid (Ga; an alternative phenolic compound). Therefore, future research is necessary to elucidate the mechanism of this apparent cytotoxicity.

It should be noted that no control WPI (0% PG) sample was evaluated alongside the PG supplemented samples as they were subject to contamination prior to the cell culture procedure.

15.4 Proliferation (MTS) Assay

The MTS assay, which is a measure of cell metabolic activity, produced false positive results indicating high levels of cell proliferation even for unseeded WPI-PG hydrogels. This interference increased alongside increasing PG concentrations. Therefore, supporting the theory that substances are leached from the hydrogels into the cell culture medium.

With the background corrected for, the observed absorbance values for each sample group was close to 0. Thus, providing further evidence for the cytotoxic effects of WPI-PG hydrogel leachables.

15.5 Future

Time constraints limited the number of analytical methods utilised to evaluate WPI-PG hydrogels. However, in the future degradation studies should be carried out and the substances leaching out of the hydrogels should be identified and evaluated. In the case of GA, previous research has reported that toxicity is concentration dependent and occurs via apoptosis as a result of elevated levels of reactive oxygen species (Lišková et al., 2015). Therefore, the concentration dependent cytotoxicity of PG should be examined.

As the antimicrobial properties of PG were the primary reason for incorporating it into the WPI hydrogels, antibacterial studies should also be carried out. For example, it should be elucidated whether PG supplemented hydrogels decrease the colony forming ability of *E. coli* as seen in chitosan hydrogels.

16.0 Conclusion

PG supplementation at lower concentrations demonstrated minimal impact on the mechanical properties of WPI hydrogels. Similarly, on the contrary to previous research PG appeared to be cytotoxic in cell culture, in a dose-dependent manner. Despite this, if the concentration dependent cytotoxicity of PG is clarified and future research demonstrated the ability of concentrations below this to provide antibacterial effects, WPI-PG hydrogels may still provide opportunities in the bone tissue engineering space.

17.0 General Discussion

The present study evaluated the extent to which physiochemical and biological properties desirable of materials for applications in bone tissue engineering were met by three hydrogels differing in composition:

1. Electron irradiated Gelatin hydrogels supplemented with Alkaline Phosphatase (ALP)
2. WPI hydrogels supplemented with Phloroglucinol (PG)
3. WPI hydrogels supplemented with Carbon Nanotubes (CNTs)

Previously, surgery took place in the absence of additives, such as implants, which are now available to facilitate surgical interventions. The demand for medical implants has been driven by advancements in the understanding of human anatomy and the identification of materials compatible with the body (Axinte et al., 2019; Saptaji et al., 2018). Implanted

materials may be utilised as short term, long term, or permanent aids to treat, repair or replace biological tissue in numerous applications.

As the average life-expectancy and chronological age of the human population rises, the incidence of bone related disorders and conditions has increased. Particularly in populations where obesity and insufficient physical activity coincides with aging. Even though bone is a dynamic vascularised tissue with the capability to heal naturally in response to damage, hundreds of millions of surgical procedures are performed, each year, to correct severe bone lesions (Maisani et al., 2017). Research into bone tissue engineering (BTE) has led to improvements in both surgical techniques and orthopaedic implants. However, skeletal conditions remain undertreated. Therefore, coinciding with the aging population, orthopaedic trauma and resultant orthopaedic surgery is becoming more frequent. Thus, highlighting the increasing need for cost efficient and effective treatments (Pilia et al., 2013).

Conventional treatments of bone tissue defects include autografts, allografts, xenografts, and the implantation of exogenous biomaterials, such as metal or ceramics. All of which have considerable disadvantages. Although autologous bone grafts, where the recipient is also the donor, remain the 'gold standard' to augment bone tissue healing, their autologous nature means the supply of appropriate bone is limited. Similarly, there are multiple other concerns including donor site morbidity, surgical limitations, and elevated bone resorption during healing (Banwart et al., 1995; Sheikh et al., 2015).

Allografts, the transfer of bone tissue sourced from a genetically different human donor, and xenografts, the transfer of bone tissue sourced from a different species, negate the concerns regarding donor site morbidity and allow greater quantities of bone tissue to be transplanted. However, due to the necessary sterilisation and purification processes that must precede transplantation, the osteoinductive properties that accompany autografts are lost (Schroeder and Mosheiff, 2011). Additionally, both methods (particularly xenografts),

elicit a significant immune response in the host tissue, ultimately leading to rejection unless immunosuppressive medication is received. Similarly, grafts of this nature are accompanied by the risk of bacterial, viral, and prion transmission (Mankin et al., 2005). Finally, allografts/xenografts rarely integrate fully with host tissue. Most transplants result in only the periphery of the graft substituting successfully, leading to a subsequent graft fracture in as many as 60% of cases after 10 years (Wheeler and Enneking, 2005).

The use of large prostheses, such as metals and metal alloys, is an additional method to remedy bone tissue defects. However, prostheses of this kind are usually a temporary solution, with 30% of recipients requiring a revision 7 years after the original procedure (Mittermayer et al., 2001). This is because metal/metal alloy implants lack a biological interface. As they do not interact, either chemically or biologically, with the surrounding tissue, there is minimal osteointegration or interfacial bonding. Therefore, over time, chronic wear or loosening renders the implant ineffective (Schroeder and Mosheiff, 2011). Additionally, 'stress shielding' which occurs due to the mismatch in mechanical properties between metallic implants and natural bone tissue results in unwanted bone resorption and implant loosening (Alexander and Theodos, 1993). Similarly, implants of this nature are known to damage host tissue due to their weight and robustness, release toxic ions and particles via corrosion and cause allergic reactions and inflammatory cascades (Mediaswanti et al., 2013 and Poinern et al., 2013).

Despite the varying advantages which accompany each of these conventional techniques, their overall effectiveness remains inadequate. In the USA alone, projections for the demand of hip and knee implants were estimated to increase by 174% and 673%, respectively, between 2005 and 2030 (Kurtz et al., 2007). Similarly, in Australia, primary and revision hip surgery numbers were elevated by approximately 17% in 2008 compared to the previous year (Mediaswanti et al, 2013). Therefore, highlighting the need for more effective

biomechanically and biocompatible materials for use in orthopaedic applications – a space which the materials evaluated in this study show promise.

Like allografts and xenografts, the materials examined in the present study negate the concerns with donor site morbidity and limited material supply associated with autografts. However, in contrast, the hydrogels utilised in this study avoid the risk of bacterial, viral, and prion transmission in the absence of a pre-implantation purification processes known to diminish the osteoinductive properties of the implant (Schroeder and Mosheiff, 2011). Specifically, simultaneous formation and sterilisation is achieved via electron irradiation (Gelatin hydrogels) and by autoclaving (WPI hydrogels).

Similarly, as preliminary *in-vitro* studies demonstrated that CNT supplemented WPI hydrogels and electron beam-crosslinked hydrogels, both mineralised and unmineralized, displayed satisfactory cytocompatibility towards human osteoblast-like MG-63 cells, these materials show promise as potential scaffolds for autologous cells. Therefore, as well as the absence of an elicited immune response that accompanies allografts, potential scaffolds constructed from these materials may possess the ability to induce the osteogenic differentiation of local stem cells that is observed following autografts (Goldberg, 2000; Shen et al., 2005; Urist, 1980). PG supplemented hydrogels, however, demonstrated cytotoxicity in a dose-dependent manner. As such, WPI-PG hydrogels (currently) do not show promise in this space.

Compared to metal/metal alloy implants, the primary advantages suggested of electron irradiated gelatin hydrogels is, in fact, mineralisation. Whereas metal/metal alloy implants do not possess a biological interface capable of effective osteointegration (Schroeder and Mosheiff, 2011), mineralisation is known to enhance the biological performance of bone-substituting materials by a phenomenon of bioactivity (LeGeros, 1991). Additionally, CaP ceramics are known to possess an intrinsic affinity for biologically active proteins, such as

growth factors, which are necessary for the natural healing process of bone tissue (Ruhe et al., 2005). Therefore, the successful CaP mineralisation of gelatin hydrogels is promising. However, as with the study by Osathanon et al., (2009) that demonstrated the ability of a fibrin gel to enhance bone tissue formation in a mouse calvarial defect following ALP mediated mineralisation, this material must be evaluated *in-vivo*.

WPI based hydrogels were not subject to this mineralisation process. However, a study conducted by Douglas et al (2018) demonstrated that, in addition to stimulating calcium deposition by Saos-2 cells and elevating the expression of type I collagen by FIB, WPI induced the expression of markers characteristic of osteogenic cell differentiation by human adipose tissue derived stem cells (ASC). Furthermore, increased ALP activity was observed. Similarly, Zhao et al (2005) noted that CNTs promoted the formation of mineralised bone while Usui et al (2008) demonstrated that, in a mouse model, MWCNTs were biocompatible, permitted bone repair, and became integrated with bone tissue.

ALP mediated mineralisation was also demonstrated to elevate the compressive modulus of gelatin hydrogels. The effect of supplementing WPI hydrogels with CNTs or PGs on their compressive strength was inferior to that of gelatin mineralisation, however, increases in Young's modulus were observed, in a dose-dependent manner, following CNT reinforcement. Typically, hydrogels possess weak mechanical properties, meaning that, without reinforcement, their implications are somewhat restricted to soft tissue engineering. However, as noted by Douglas et al (2013), the mechanical reinforcement brought about by mineralisation enables them to be considered for bone tissue regeneration (Douglas et al., 2013). The elevated mechanical properties may also improve the compatibility of the hydrogels with bone tissue, as both stiffer and rougher surfaces are known to promote the differentiation of cells towards the osteoblastic phenotype. Therefore, the increase in

mechanical properties observed, particularly in the mineralised gelatin hydrogels, implicates them in bone tissue engineering applications.

Implant-related microbial infections remain one of the primary causes of wound healing complications and failure of orthopaedic implants (Romano et al., 2015; Salomé Veiga and Schneider, 2013). Specifically, pathogenicity at the tissue-implant interface can compromise wound healing and lead to the failure of orthopaedic implants (Salomé Veiga and Schneider, 2013). Importantly, pathogens that possess multi-resistance are also frequently isolated from complication sites (Aggarwal et al., 2014).

CNTs are known to possess antimicrobial activity against a broad spectrum of microorganisms. The first evidence of this was documented by Kang et al (2007) who observed antimicrobial activity of both SWNTs and MWNTs against Escherichia coli. Since this time, numerous studies have implicated CNTs in applications for the inactivation of pathogens (Liu et al., 2018). Similarly, a study conducted by Lišková et al (2015) demonstrated that PG decreased the colony forming ability of *Escherichia coli*. Thus, the present study aimed to evaluate the antibacterial properties of WPI hydrogels supplemented with CNT and PG.

Antibacterial testing was only performed on WPI-CNT hydrogels. However, CNT inclusion successfully provided WPI hydrogels with antibacterial effects against *Staphylococcus aureus*.

Ultimately, the present study concludes that hydrogels comprised of both gelatin and WPI show promise in this field. Specifically, the composites examined in this study, except for PG supplemented WPI hydrogels, show potential as candidates for use in bone tissue engineering applications. However, further research must be conducted with lower CNT concentrations to identify whether an increase in compressive strength can be supplied, without detracting from the observed antibacterial activity. Similarly, further research regarding the safety of CNTs is required prior to the realisation of potential benefits in bone

tissue engineering. WPI hydrogels could also be supplemented with alternative additives to optimise their properties for application in this space. Furthermore, prior to their use in bone tissue engineering applications, the long-term activity of hydrogel composites, specifically *in-vivo*, should be elucidated. Cytotoxicity, biocompatibility, biodegradability, and osteogenicity should all be established (Zhao et al. 2015).

References

Abarrategi, A., Gutiérrez, M., Moreno-Vicente, C., Hortigüela, M., Ramos, V., López-Lacomba, J., Ferrer, M. and del Monte, F. (2008). Multiwall carbon nanotube scaffolds for tissue engineering purposes. *Biomaterials*, 29(1), 94-102.

Aggarwal, V., Bakhshi, H., Ecker, N., Parvizi, J., Gehrke, T. and Kendoff, D. (2014). Organism Profile in Periprosthetic Joint Infection: Pathogens Differ at Two Arthroplasty Infection Referral Centres in Europe and in the United States. *Journal of Knee Surgery*, 27(05), 399-406.

Aguirre, J., Plotkin, L., Stewart, S., Weinstein, R., Parfitt, A., Manolagas, S. and Bellido, T. (2006). Osteocyte Apoptosis Is Induced by Weightlessness in Mice and Precedes Osteoclast Recruitment and Bone Loss. *Journal of Bone and Mineral Research*, 21(4), 605-615.

Ahmed, E. (2015). Hydrogel: Preparation, characterization, and applications: A review. *Journal of Advanced Research*, 6(2), 105-121.

Alexander, R. and Theodos, L. (1993). Fracture of the bone-grafted mandible secondary to stress shielding: Report of a case and review of the literature. *Journal of Oral and Maxillofacial Surgery*, 51(6), 695-697.

Amini, A., Laurencin, C. and Nukavarapu, S. (2012). Bone Tissue Engineering: Recent Advances and Challenges. *Critical Reviews in Biomedical Engineering*, 40(5), 363-408.

Ara, M., Watanabe, M. and Imai, Y. (2002). Effect of blending calcium compounds on hydrolytic degradation of poly(dl-lactic acid-co-glycolic acid). *Biomaterials*, 23(12), 2479-2483.

Athanasiou, K., Zhu, C., Lanctot, D., Agrawal, C. and Wang, X. (2000). Fundamentals of Biomechanics in Tissue Engineering of Bone. *Tissue Engineering*, 6(4), 361-381.

Axinte, D., Guo, Y., Liao, Z., Shih, A., M'Saoubi, R. and Sugita, N. (2019). Machining of biocompatible materials — Recent advances. *CIRP Annals*, 68(2), 629-652.

Baino, F., Verné, E. and Vitale-Brovarone, C. (2009). 3-D high-strength glass–ceramic scaffolds containing fluoroapatite for load-bearing bone portions replacement. *Materials Science and Engineering: C*, 29(6), 2055-2062.

Baldini, N, Cenni, E, Ciapetti, G. (2009). Bone repair and regeneration. In:Planell, JA, Best, SM, Lacroix, D. (eds) *Bone repair biomaterials*. Amsterdam: Elsevier, 69–105.

Banwart, J., Asher, M. and Hassanein, R. (1995). Iliac Crest Bone Graft Harvest Donor Site Morbidity. *Spine*, 20(9), 1055-1060.

Barth, A. (2007). Infrared spectroscopy of proteins. Biochimica et Biophysica Acta (BBA) - *Bioenergetics*, 1767(9), 1073-1101.

Bartolo, P., Kruth, J., Silva, J., Levy, G., Malshe, A., Rajurkar, K., Mitsuishi, M., Ciurana, J. and Leu, M. (2012). Biomedical production of implants by additive electro-chemical and physical processes. *CIRP Annals*, 61(2), 635-655.

Baughman, R. H., Cui, C., Zakhidov, A. A., Iqbal, Z., Barisci, J. N., Spinks, G. M., Wallace, G. G., Mazzoldi, A., De Rossi D, Rinzler, A. G., Jaschinski, O., Roth, S., & Kertesz, M. (1999). Carbon nanotube actuators. *Science* (New York, N.Y.), 284(5418), 1340–1344.

Bax, B., Alam, A., Banerji, B., Bax, C., Bevis, P., Stevens, C., Moonga, B., Blake, D. and Zaidi, M. (1992). Stimulation of osteoclastic bone resorption by hydrogen peroxide. *Biochemical and Biophysical Research Communications*, 183(3), 1153-1158.

Beertsen, W. and van den Bos, T. (1992). Alkaline phosphatase induces the mineralization of sheets of collagen implanted subcutaneously in the rat. *Journal of Clinical Investigation*, 89(6), 1974-1980.

Best, S., Porter, A., Thian, E. and Huang, J. (2008). Bioceramics: Past, present and for the future. *Journal of the European Ceramic Society*, 28(7), 1319-1327.

Bonewald L. (2007). Osteocytes as Dynamic Multifunctional Cells. *Annals of the New York Academy of Sciences*, 1116(1), 281-290.

Bottini, M., Rosato, N. and Bottini, N. (2011). PEG-Modified Carbon Nanotubes in Biomedicine: Current Status and Challenges Ahead. *Biomacromolecules*, 12(10), 3381-3393.

Byrne, D., Lacroix, D., Planell, J., Kelly, D. and Prendergast, P. (2007). Simulation of tissue differentiation in a scaffold as a function of porosity, Young's modulus and dissolution rate: Application of mechanobiological models in tissue engineering. *Biomaterials*, 28(36), 5544-5554.

Campbell, A. (2003). Bioceramics for implant coatings. *Materials Today*, 6(11), 26-30.

Cao, W. and Hench, L. (1996). Bioactive materials. *Ceramics International*, 22(6), 493-507.

Cooke, F.W., Lemons, J.E. and Ratner, B.D. (1996). Properties of materials, in *biomaterials science: An introduction to materials in science*, B.D. Ratner, A.S. Hoffman, F.J. Schoen, J.E. Lemons, Editors: Academic Press, San Diego USA, 11-35.

Crane, N., Popescu, V., Morris, M., Steenhuis, P. and Ignelzi, M. (2006). Raman spectroscopic evidence for octacalcium phosphate and other transient mineral species deposited during intramembranous mineralization. *Bone*, 39(3), 434-442.

Dale, H., Hallan, G., Espehaug, B., Havelin, L. and Engesæter, L. (2009). Increasing risk of revision due to deep infection after hip arthroplasty. *Acta Orthopaedica*, 80(6), 639-645.

De Volder, M., Tawfick S., Baughman, R., Hart, J. (2013). Carbon Nanotubes: Present and future commercial applications. *Sci*. 339(6119), 535-539.

Delaisse, J. (2014). The reversal phase of the bone-remodeling cycle: cellular prerequisites for coupling resorption and formation. *BoneKEy Reports*, 3.

Diarrassouba, F., Garrait, G., Remondetto, G., Alvarez, P., Beyssac, E. and Subirade, M. (2015). Food protein-based microspheres for increased uptake of vitamin D3. *Food Chemistry*, 173, 1066-1072.

Do, A., Williams, K. and Toomer, O. (2016). In vitro digestibility and immunoreactivity of bovine milk proteins. *Food Chemistry*, 190, 581-587.

Doblaré, M., García, J. and Gómez, M. (2004). Modelling bone tissue fracture and healing: a review. *Engineering Fracture Mechanics*, 71(13-14), 1809-1840.

Donaldson, K., Aitken, R., Tran, L., Stone, V., Duffin, R., Forrest, G. and Alexander, A. (2006). Carbon Nanotubes: A Review of Their Properties in Relation to Pulmonary Toxicology and Workplace Safety. *Toxicological Sciences*, 92(1), 5-22.

Dorozhkin, S. and Epple, M. (2002). Biological and Medical Significance of Calcium Phosphates. *Angewandte Chemie International Edition*, 41(17), 3130-3146.

Douglas, T., Messersmith, P., Chasan, S., Mikos, A., de Mulder, E., & Dickson, G., Schaubroeck, D., Balcaen, L., Vanhaecke, F., Bubruel, P, Jansen, J and Leeuwenburgh, S.C. (2012). Enzymatic Mineralization of Hydrogels for Bone Tissue Engineering by Incorporation of Alkaline Phosphatase. *Macromolecular Bioscience*, 12(8), 1077-1089.

Douglas, T., Pamula, E., & Leeuwenburgh, S. C. (2013). Biomimetic mineralization of hydrogel biomaterials for bone tissue engineering. M. Ramalingam, X. Wang, G. Chen, P. Ma, & F.-Z. Cui (Eds.), *Biomimetics: advancing nanobiomaterials and tissue engineering*, 51–67.

Douglas, T., Krawczyk, G., Pamula, E., Declercq, H., Schaubroeck, D., Bucko, M., Balcaen, L., Van Der Voort, P., Bliznuk, V., van den Vreken, N., Dash, M., Detsch, R., Boccaccini, A., Vanhaecke, F., Cornelissen, M. and Dubruel, P. (2016). Generation of composites for bone tissue-engineering applications consisting of gellan gum hydrogels mineralized with calcium and magnesium phosphate phases by enzymatic means. *Journal of Tissue Engineering and Regenerative Medicine*, 10(11), 938-954.

Douglas, T., Vandrovcová, M., Kročilová, N., Keppler, J., Zárubová, J., Skirtach, A. and Bačáková, L. (2018). Application of whey protein isolate in bone regeneration: Effects on growth and osteogenic differentiation of bone-forming cells. *Journal of Dairy Science*, 101(1), 28-36.

Driessens, F., Dijk, J. and Borggreven, J. (1978). Biological calcium phosphates and their role in the physiology of bone and dental tissues I. Composition and solubility of calcium phosphates. *Calcified Tissue Research*, 26(1), 127-137.

Drosse, I., Volkmer, E., Capanna, R., Biase, P., Mutschler, W. and Schieker, M. (2008). Tissue engineering for bone defect healing: An update on a multi-component approach. *Injury*, 39, S9-S20.

Du, C., Cui, F., Zhang, W., Feng, Q., Zhu, X. and de Groot, K. (2000). Formation of calcium phosphate/collagen composites through mineralization of collagen matrix. *Journal of Biomedical Materials Research*, 50(4), 518-527.

Eddy Jai Poinern, G., Brundavanam, S. and Fawcett, D. (2013). Nanometre Scale Hydroxyapatite Ceramics for Bone Tissue Engineering, *American Journal of Biomedical Engineering*, 3(6), 148-168.

Eddy Jai Poinern, G., Brundavanam, S. and Fawcett, D. (2013). Biomedical Magnesium Alloys: A Review of Material Properties, Surface Modifications and Potential as a Biodegradable Orthopaedic Implant. *American Journal of Biomedical Engineering*, 2(6), 218-240.

Everts, V., Delaissé, J., Korper, W., Jansen, D., Tigchelaar-Gutter, W., Saftig, P. and Beertsen, W. (2002). The Bone Lining Cell: Its Role in Cleaning Howship's Lacunae and Initiating Bone Formation. *Journal of Bone and Mineral Research*, 17(1), 77-90.

Fedorovich, N., Alblas, J., de Wijn, J., Hennink, W., Verbout, A. and Dhert, W. (2007). Hydrogels as Extracellular Matrices for Skeletal Tissue Engineering: State-of-the-Art and Novel Application in Organ Printing. *Tissue Engineering*, 13(8), 1905-1925.

Foldvari, M. and Bagonluri, M. (2008). Carbon nanotubes as functional excipients for nanomedicines: II. Drug delivery and biocompatibility issues. *Nanomedicine: Nanotechnology, Biology and Medicine*, 4(3), 183-200.

Garidel, P. and Schott, H. (2006). Fourier-transform midinfrared spectroscopy for analysis and screening of liquid protein formulations. Part 1: understanding infrared spectroscopy of proteins. *BioProcess Int*. 4. 40-46.

Gasperini, L., Mano, J. and Reis, R. (2014). Natural polymers for the microencapsulation of cells. *Journal of The Royal Society Interface*, 11(100), 20140817.

Gawel, K., Barriet, D., Sletmoen, M. and Stokke, B. (2010). Responsive Hydrogels for Label-Free Signal Transduction within Biosensors. *Sensors*, 10(5), 4381-4409.

Gbureck, U. (2003). Mechanical activation and cement formation of β-tricalcium phosphate. *Biomaterials*, 24(23), 4123-4131.

Geckil, H., Xu, F., Zhang, X., Moon, S. and Demirci, U. (2010). Engineering hydrogels as extracellular matrix mimics. *Nanomedicine*, 5(3), 469-484.

Ghasemi-Mobarakeh, L. (2015). Structural properties of scaffolds: Crucial parameters towards stem cells differentiation. *World Journal of Stem Cells*, 7(4), 728.

Gkioni, K., Leeuwenburgh, S., Douglas, T., Mikos, A. and Jansen, J. (2010). Mineralization of Hydrogels for Bone Regeneration. *Tissue Engineering Part B: Reviews*, 16(6), 577-585.

Goldberg, V. (2000). Selection of Bone Grafts for Revision Total Hip Arthroplasty. *Clinical Orthopaedics and Related Research*, 381, 68-76.

Gómez-Barrena, E., Rosset, P., Lozano, D., Stanovici, J., Ermthaller, C. and Gerbhard, F. (2015). Bone fracture healing: Cell therapy in delayed unions and nonunions. *Bone*, 70, 93-101.

Griffith, L. (2000). Polymeric biomaterials. *Acta Materialia*, 48(1), 263-277.

Gröger, A., Kläring, S., Merten, H., Holste, J., Kaps, C. and Sittinger, M. (2003). Tissue Engineering of Bone for Mandibular Augmentation in Immunocompetent Minipigs: Preliminary Study. *Scandinavian Journal of Plastic and Reconstructive Surgery and Hand Surgery*, 37(3), 129-133.

Guo, H., Su, J., Wei, J., Kong, H., & Liu, C. (2009). Biocompatibility and osteogenicity of degradable Ca-deficient hydroxyapatite scaffolds from calcium phosphate cement for bone tissue engineering. *Acta Biomaterialia*, 5(1), 268-278.

Ha, H., Kim, J., Lee, M. and Lee, W. (2013). Formation and characterization of quercetin-loaded chitosan oligosaccharide/β-lactoglobulin nanoparticle. *Food Research International*, 52(1), 82-90.

Harrington, W. and Von Hippel, P. (1962). The Structure of Collagen And Gelatin. *Advances in Protein Chemistry*, 1-138.

Heino, T., Hentunen, T. and Väänänen, H. (2002). Osteocytes inhibit osteoclastic bone resorption through transforming growth factor-β: Enhancement by estrogen*. *Journal of Cellular Biochemistry*, 85(1), 185-197.

Hench, L. (1991). Bioceramics: From Concept to Clinic. *Journal of the American Ceramic Society*, 74(7), 1487-1510.

Hench, L.L. and Wilson, J. (1993) *An introduction to bioceramics*, Hench L.L, Wilson J Editors: World Scientific Publishing Co Pte Ltd: Singapore, 1-24.

Hoffman, A. (2002). Hydrogels for biomedical applications. *Advanced Drug Delivery Reviews*, 54(1), 3-12.

Hong, L., Wang, Y., Jia, S., Huang, Y., Gao, C. and Wan, Y. (2006). Hydroxyapatite/bacterial cellulose composites synthesized via a biomimetic route. *Materials Letters*, 60(13-14), 1710-1713.

Hutchens, S., Benson, R., Evans, B., O'Neill, H. and Rawn, C. (2006). Biomimetic synthesis of calcium-deficient hydroxyapatite in a natural hydrogel. *Biomaterials*, 27(26), 4661-4670.

Jayakrishnan, A. and Jameela, S. (1996). Glutaraldehyde as a fixative in bioprostheses and drug delivery matrices. *Biomaterials*, 17(5), 471-484.

Kang, S., Pinault., M., Pfefferle, ,L. D. & Elimelech, ,M. (2007). Single-walled carbon nanotubes exhibit strong antimicrobial activity. *Langmuir* 23, 8670–8673.

Kang, Y., Scully, A., Young, D., Kim, S., Tsao, H., Sen, M. and Yang, Y. (2011). Enhanced mechanical performance and biological evaluation of a PLGA coated β-TCP composite scaffold for load-bearing applications. *European Polymer Journal*, 47(8), 1569-1577.

Kazanci, M., Fratzl, P., Klaushofer, K. and Paschalis, E. (2006). Complementary Information on In Vitro Conversion of Amorphous (Precursor) Calcium Phosphate to Hydroxyapatite from Raman Microspectroscopy and Wide-Angle X-Ray Scattering. *Calcified Tissue International*, 79(5), 354-359.

Khan W., Muntimadugu E., Jaffe M., Domb A.J. (2014) Implantable Medical Devices. In: Domb A., Khan W. (eds) *Focal Controlled Drug Delivery. Advances in Delivery Science and Technology*. Springer, 33-59.

Kim, K., Piao, M., Cho, S., Lee, N. and Hyun, J. (2012). Phloroglucinol protects human keratinocytes from ultraviolet B radiation by attenuating oxidative stress. Photodermatology, *Photoimmunology & Photomedicine*, 28(6), 322-331.

Kondiah, P., Choonara, Y., Kondiah, P., Marimuthu, T., Kumar, P., du Toit, L. and Pillay, V. (2016). A Review of Injectable Polymeric Hydrogel Systems for Application in Bone Tissue Engineering. *Molecules*, 21(11), 1580.

Kontopidis, G., Holt, C. and Sawyer, L. (2004). Invited Review: β-Lactoglobulin: Binding Properties, Structure, and Function. *Journal of Dairy Science*, 87(4), 785-796.

Krause, B., Mende, M., Pötschke, P., & Petzold, G. (2010). Dispersability and particle size distribution of CNTs in an aqueous surfactant dispersion as a function of ultrasonic treatment time. *Carbon*, 48(10), 2746-2754.

Kretlow, J. and Mikos, A. (2007). Review: Mineralization of Synthetic Polymer Scaffolds for Bone Tissue Engineering. *Tissue Engineering*, 13(5), 927-938.

Kurtz, S., Ong, K., Lau, E., Mowat, F. and Halpern, M. (2007). Projections of Primary and Revision Hip and Knee Arthroplasty in the United States from 2005 to 2030. *The Journal of Bone and Joint Surgery-American Volume*, 89(4), 780-785.

Lacerda, L., Bianco, A., Prato, M., & Kostarelos, K. (2006). Carbon nanotubes as nanomedicines: from toxicology to pharmacology. *Advanced drug delivery reviews*, 58(14), 1460–1470.

Lam, Chiu-Wing & James, John & McCluskey, Richard & Hunter, Robert. (2004). Pulmonary Toxicity of Single-Wall Carbon Nanotubes in Mice 7 and 90 Days After Intratracheal Instillation. *Toxicological sciences: an official journal of the Society of Toxicology*. 77. 126-34.

Lamoureux, F., Baud'huin, M., Duplomb, L., Heymann, D. and Rédini, F. (2007). Proteoglycans: key partners in bone cell biology. *BioEssays*, 29(8), 758-771.

LaStayo, P., Winters, K. and Hardy, M. (2003). Fracture healing: Bone healing, fracture management, and current concepts related to the hand. *Journal of Hand Therapy*, 16(2), 81-93.

Leeuwenburgh, S., Jansen, J. and Mikos, A. (2007). Functionalization of oligo(poly(ethylene glycol)fumarate) hydrogels with finely dispersed calcium phosphate nanocrystals for bone-substituting purposes. *Journal of Biomaterials Science, Polymer Edition*, 18(12), 1547-1564.

Leeuwenburgh, S., Ana, I. and Jansen, J. (2010). Sodium citrate as an effective dispersant for the synthesis of inorganic–organic composites with a nanodispersed mineral phase. *Acta Biomaterialia*, 6(3), 836-844.

Le Geros, R. (1991). *Calcium phosphates in oral biology and medicine*. Basel: Karger.

Lentino, J. (2003). Prosthetic Joint Infections: Bane of Orthopedists, Challenge for Infectious Disease Specialists. *Clinical Infectious Diseases*, 36(9), 1157-1161.

Leontieva, O., Demidenko, Z. and Blagosklonny, M. (2014). Contact inhibition and high cell density deactivate the mammalian target of rapamycin pathway, thus suppressing the senescence program. *Proceedings of the National Academy of Sciences*, 111(24), 8832-8837

Iijima, S. (1991). Helical microtubules of graphitic carbon. *Nature*, 354(6348), 56-58.

Lišková, J., Douglas, T., Beranová, J., Skwarczyńska, A., Božič, M., Samal, S., Modrzejewska, Z., Gorgieva, S., Kokol, V. and Bačáková, L. (2015). Chitosan hydrogels enriched with polyphenols: Antibacterial activity, cell adhesion and growth and mineralization. *Carbohydrate Polymers*, 129, 135-142.

Liu, D., Mao, Y., & Ding, L. (2018). Carbon nanotubes as antimicrobial agents for water disinfection and pathogen control. *Journal Of Water And Health*, 16(2), 171-180.

Liu, Z., Tabakman, S., Welsher, K. and Dai, H. (2009). Carbon nanotubes in biology and medicine: In vitro and in vivo detection, imaging and drug delivery. *Nano Research*, 2(2), 85-120.

Lu, Z., Roohani-Esfahani, S., Wang, G. and Zreiqat, H. (2012). Bone biomimetic microenvironment induces osteogenic differentiation of adipose tissue-derived

mesenchymal stem cells. *Nanomedicine: Nanotechnology, Biology and Medicine*, 8(4), 507-515.

Madani, S., Mandel, A. and Seifalian, A. (2013). A concise review of carbon nanotube's toxicology. *Nano Reviews*, 4(1), 21521.

Maisani, M., Pezzoli, D., Chassande, O. and Mantovani, D. (2017). Cellularizing hydrogel-based scaffolds to repair bone tissue: How to create a physiologically relevant micro-environment?. *Journal of Tissue Engineering*, 8, 204173141771207.

Mandair, G. and Morris, M. (2015). Contributions of Raman spectroscopy to the understanding of bone strength. *BoneKey Reports*, 4.

Mankin, H., Hornicek, F. and Raskin, K. (2005). Infection in Massive Bone Allografts. *Clinical Orthopaedics and Related Research*, (432), 210-216.

Marsell, R. and Einhorn, T. (2011). The biology of fracture healing. *Injury*, 42(6), 551-555.

Martin, I., Muraglia, A., Campanile, G., Cancedda, R. and Quarto, R. (1997). Fibroblast Growth Factor-2 Supportsex VivoExpansion and Maintenance of Osteogenic Precursors from Human Bone Marrow. *Endocrinology*, 138(10), 4456-4462.

Marzona, L, Pavolini, B. (2009). Play and players in bone fracture healing match. *Clin Cases Miner Bone Metab*; 6: 159–162.

Mediaswanti K, Wen C, Ivanova EP, Berndt CC, Malherbe F, et al. (2013) A Review on Bioactive Porous Metallic Biomaterials. *Journal of Biomimetics Biomaterials and Tissue Engineering*, 18: 104.

Mendes, R., Silva, G., Caliari, M., Silva, E., Ladeira, L. and Ferreira, A. (2010). Effects of single wall carbon nanotubes and its functionalization with sodium hyaluronate on bone repair. *Life Sciences*, 87(7-8), 215-222.

Miller, SC, de Saint-Georges, L, Bowman, BM and Jee, WS. (1989). Bone lining cells: structure and function. *Scanning Microscopy*, 3(3): 953–960.

Mitchell, L., Gao, J., Wal, R., Gigliotti, A., Burchiel, S. and McDonald, J. (2007). Pulmonary and Systemic Immune Response to Inhaled Multiwalled Carbon Nanotubes. *Toxicological Sciences*, 100(1), 203-214.

Mitsuishi, M., Cao, J., Bártolo, P., Friedrich, D., Shih, A., Rajurkar, K., Sugita, N. and Harada, K. (2013). Biomanufacturing. *CIRP Annals*, 62(2), 585-606.

Mittermayer, F., Krepler, P., Dominkus, M., Schwameis, E., Sluga, M., Heinzl, H. and Kotz, R. (2001). Long-Term Followup of Uncemented Tumor Endoprostheses for the Lower Extremity. *Clinical Orthopaedics and Related Research*, 388, 167-177.

Mody, N. (2001). Oxidative stress modulates osteoblastic differentiation of vascular and bone cells. *Free Radical Biology and Medicine*, 31(4), 509-519.

Moshiri, A. and Oryan, A. (2012). Role of tissue engineering in tendon reconstructive surgery and regenerative medicine: Current concepts, approaches and concerns. *Hard Tissue*, 1(2).

Moshiri, A. and Oryan, A. (2013). Role of platelet-rich plasma in soft and hard connective tissue healing: an evidence-based review from basic to clinical application. Hard Tissue, 2(1).

Murray, A., Kisin, E., Leonard, S., Young, S., Kommineni, C., Kagan, V., Castranova, V. and Shvedova, A. (2009). Oxidative stress and inflammatory response in dermal toxicity of single-walled carbon nanotubes. *Toxicology*, 257(3), 161-171.

Neumann, M. and Epple, M. (2006). Composites of Calcium Phosphate and Polymers as Bone Substitution Materials. *European Journal of Trauma*, 32(2), 125-131.

Nichol, J., Koshy, S., Bae, H., Hwang, C., Yamanlar, S. and Khademhosseini, A. (2010). Cell-laden microengineered gelatin methacrylate hydrogels. *Biomaterials*, 31(21), 5536-5544.

Nunes, A., Bussy, C., Gherardini, L., Meneghetti, M., Herrero, M., Bianco, A., Prato, M., Pizzorusso, T., Al-Jamal, K. and Kostarelos, K. (2012). In vivodegradation of functionalized carbon nanotubes after stereotactic administration in the brain cortex. *Nanomedicine*, 7(10), 1485-1494.

Orimo, H. (2010). The Mechanism of Mineralization and the Role of Alkaline Phosphatase in Health and Disease. *Journal of Nippon Medical School*, 77(1), 4-12.

Oryan, A. and Moshiri, A. (2012). Recombinant fibroblast growth protein enhances healing ability of experimentally induced tendon injuryin vivo. *Journal of Tissue Engineering and Regenerative Medicine*, 8(6), 421-431.

Osathanon, T., Giachelli, C. and Somerman, M. (2009). Immobilization of alkaline phosphatase on microporous nanofibrous fibrin scaffolds for bone tissue engineering. *Biomaterials*, 30(27), 4513-4521.

Paderni, S., Terzi, S. and Amendola, L. (2009). Major bone defect treatment with an osteoconductive bone substitute. *Musculoskeletal Surgery*, 93(2), 89-96.

Parizi, A., Oryan, A., Shafiei-Sarvestani, Z. and Bigham, A. (2011). Human platelet rich plasma plus Persian Gulf coral effects on experimental bone healing in rabbit model: radiological, histological, macroscopical and biomechanical evaluation. *Journal of Materials Science: Materials in Medicine*, 23(2), 473-483.

Partridge, N., Jeffrey, J., Ehlich, L., Teitelbaum, S., Fliszar, C., Welgus, H. and Kahn, A. (1987). Hormonal Regulation of the Production of Collagenase and a Collagenase Inhibitor Activity by Rat Osteogenic Sarcoma Cells*. *Endocrinology*, 120(5), 1956-1962.

Patel, M., Patel, K., Caccamese, J., Coletti, D., Sauk, J. and Fisher, J. (2010). Characterization of cyclic acetal hydroxyapatite nanocomposites for craniofacial tissue engineering. *Journal of Biomedical Materials Research Part A*, 94(2), 408-18

Peppas, N. (2000). Hydrogels in pharmaceutical formulations. *European Journal of Pharmaceutics and Biopharmaceutics*, 50(1), 27-46.

Pichardo, S., Gutiérrez-Praena, D., Puerto, M., Sánchez, E., Grilo, A., Cameán, A. and Jos, Á. (2012). Oxidative stress responses to carboxylic acid functionalized single wall carbon nanotubes on the human intestinal cell line Caco-2. *Toxicology in Vitro*, 26(5), 672-677.

Pilia, M., Guda, T. and Appleford, M. (2013). Development of Composite Scaffolds for Load-Bearing Segmental Bone Defects. *BioMed Research International*, 2013, 1-15.

Pittenger, M. (1999). Multilineage Potential of Adult Human Mesenchymal Stem Cells. *Science*, 284(5411), 143-147.

Poinern, G.E.J., Brundavanam, R.K. and Fawcett, D. (2013) Nanometre scale hydroxyapatite ceramics for bone tissue engineering. *American Journal of Biomedical Engineering*, 3 (6). 148-168.

Poland, C., Duffin, R., Kinloch, I., Maynard, A., Wallace, W., Seaton, A., Stone, V., Brown, S., MacNee, W. and Donaldson, K. (2008). Carbon nanotubes introduced into the abdominal cavity of mice show asbestos-like pathogenicity in a pilot study. *Nature Nanotechnology*, 3(7), 423-428.

Raggatt, L. and Partridge, N. (2010). Cellular and Molecular Mechanisms of Bone Remodeling. *Journal of Biological Chemistry*, 285(33), 25103-25108.

Rajan, N., Habermehl, J., Coté, M., Doillon, C. and Mantovani, D. (2006). Preparation of ready-to-use, storable and reconstituted type I collagen from rat tail tendon for tissue engineering applications. *Nature Protocols*, 1(6), 2753-2758.

Rea, S., Best, S. and Bonfield, W. (2004). Bioactivity of ceramic–polymer composites with varied composition and surface topography. *Journal of Materials Science: Materials in Medicine*, 15(9), 997-1005.

Romanò, C., Scarponi, S., Gallazzi, E., Romanò, D. and Drago, L. (2015). Antibacterial coating of implants in orthopaedics and trauma: a classification proposal in an evolving panorama. *Journal of Orthopaedic Surgery and Research*, 10(1).

Ruhé, P., Boerman, O., Russel, F., Spauwen, P., Mikos, A. and Jansen, J. (2005). Controlled release of rhBMP-2 loaded poly(dl-lactic-co-glycolic acid)/calcium phosphate cement composites in vivo. *Journal of Controlled Release*, 106(1-2), 162-171.

Saito, G., Nakasugi, Y., Yamashita, T. and Akiyama, T. (2014). Solution plasma synthesis of bimetallic nanoparticles. *Nanotechnology*, 25(13), 135603.

Saito, N., Okada, T., Horiuchi, H., Murakami, N., Takahashi, J., Nawata, M., Ota, H., Nozaki, K. and Takaoka, K. (2001). A biodegradable polymer as a cytokine delivery system for inducing bone formation. *Nature Biotechnology*, 19(4), 332-335.

Salomé Veiga, A. and Schneider, J. (2013). Antimicrobial hydrogels for the treatment of infection. *Biopolymers*, 100(6), 637-644.

Saptaji, K., Gebremariam, M. and Azhari, M. (2018). Machining of biocompatible materials: a review. *The International Journal of Advanced Manufacturing Technology*, 97(5-8), 2255-2292.

Sasaki, N., Matsushima, N., Ikawa, T., Yamamura, H. and Fukuda, A. (1989). Orientation of bone mineral and its role in the anisotropic mechanical properties of bone—Transverse anisotropy. *Journal of Biomechanics*, 22(2), 157-164.

Schieker, M., Seitz, H., Drosse, I., Seitz, S. and Mutschler, W. (2006). Biomaterials as Scaffold for Bone Tissue Engineering*. European Journal of Trauma*, 32(2), 114-124.

Schindeler, A., McDonald, M., Bokko, P. and Little, D. (2008). Bone remodeling during fracture repair: The cellular picture. *Seminars in Cell & Developmental Biology*, 19(5), 459-466.

Schroeder, J. and Mosheiff, R. (2011). Tissue engineering approaches for bone repair: Concepts and evidence. Injury, 42(6), pp.609-613.

Seo, S., Kim, J., Kim, J., Lee, J., Shin, U., Lee, E. and Kim, H. (2014). Enhanced mechanical properties and bone bioactivity of chitosan/silica membrane by functionalized-carbon nanotube incorporation. *Composites Science and Technology*, 96, 31-37.

Sfeir, C., Ho, L., Doll, B., Azari, K., & Hollinger, J. (2005). Fracture Repair. *Bone Regeneration and Repair*, 21-44.

Sharifi, S., Behzadi, S., Laurent, S., Laird Forrest, M., Stroeve, P. and Mahmoudi, M. (2012). Toxicity of nanomaterials. *Chemical Society Reviews*, 41(6), 2323-2343.

Sheikh, Z., Najeeb, S., Khurshid, Z., Verma, V., Rashid, H. and Glogauer, M. (2015). Biodegradable Materials for Bone Repair and Tissue Engineering Applications. *Materials*, 8(9), 5744-5794.

Shen, F., Samartzis, D. and An, H. (2005). Cell technologies for spinal fusion. *The Spine Journal*, 5(6), S231-S239.

Shi, D. and Jiang, G. (1998). Synthesis of hydroxyapatite films on porous Al2O3 substrate for hard tissue prosthetics. *Materials Science and Engineering: C*, 6(2-3), 175-182.

Siddiqui, J., & Partridge, N. (2016). Physiological Bone Remodeling: Systemic Regulation and Growth Factor Involvement. *Physiology*, 31(3), 233-245.

Silver, F.H. (1994). *Scope and markets for medical implants, biomaterials, medical devices and tissue engineering an integrated approach,* F.H. Silver Editor: Chapman & Hall, London, 1-44.

Sivashanmugam, A., Arun Kumar, R., Vishnu Priya, M., Nair, S. and Jayakumar, R. (2015). An overview of injectable polymeric hydrogels for tissue engineering. *European Polymer Journal*, 72, 543-565.

Spoerke, E., Anthony, S. and Stupp, S. (2009). Enzyme Directed Templating of Artificial Bone Mineral. *Advanced Materials*, 21(4), 425-430.

Stangenberg, L., Schaefer, D., Buettner, O., Ohnolz, J., Möbest, D., Horch, R., Stark, G. and Kneser, U. (2005). Differentiation of Osteoblasts in Three-Dimensional Culture in Processed Cancellous Bone Matrix: Quantitative Analysis of Gene Expression Based on Real-Time Reverse Transcription- Polymerase Chain Reaction. *Tissue Engineering*, 11(5-6), 855-864.

Takanashi, S., Hara, K., Aoki, K., Usui, Y., Shimizu, M., Haniu, H., Ogihara, N., Ishigaki, N., Nakamura, K., Okamoto, M., Kobayashi, S., Kato, H., Sano, K., Nishimura, N., Tsutsumi, H., Machida, K. and Saito, N. (2012). Carcinogenicity evaluation for the application of carbon nanotubes as biomaterials in rasH2 mice. *Scientific Reports*, 2(1).

Tancret, F., Bouler, J., Chamousset, J. and Minois, L. (2006). Modelling the mechanical properties of microporous and macroporous biphasic calcium phosphate bioceramics. *Journal of the European Ceramic Society*, 26(16), 3647-3656.

Teitelbaum, S. (2000). Bone Resorption by Osteoclasts. *Science*, 289(5484), 1504-1508.

Teitelbaum, S. and Ross, F. (2003). Genetic regulation of osteoclast development and function. *Nature Reviews Genetics*, 4(8), 638-649.

Toh, R., Ambrosi, A. and Pumera, M. (2012). Bioavailability of Metallic Impurities in Carbon Nanotubes Is Greatly Enhanced by Ultrasonication. *Chemistry - A European Journal*, 18(37), 11593-11596.

Tonelli, F. M., Santos, A. K., Gomes, K. N., Lorençon, E., Guatimosim, S., Ladeira, L. O., & Resende, R. R. (2012). Carbon nanotube interaction with extracellular matrix proteins producing scaffolds for tissue engineering. *International journal of nanomedicine*, 7, 4511–4529.

Tozzi, G., De Mori, A., Oliveira, A. and Roldo, M. (2016). Composite Hydrogels for Bone Regeneration. *Materials*, 9(4), 267.

Travan, A., Pelillo, C., Donati, I., Marsich, E., Benincasa, M., Scarpa, T., Semeraro, S., Turco, G., Gennaro, R. and Paoletti, S. (2009). Non-cytotoxic Silver Nanoparticle-Polysaccharide Nanocomposites with Antimicrobial Activity. *Biomacromolecules*, 10(6), 1429-1435.

Ulubayram, K., Aksu, E., Gurhan, S., Serbetci, K. and Hasirci, N. (2002). Cytotoxicity evaluation of gelatin sponges prepared with different cross-linking agents. *Journal of Biomaterials Science, Polymer Edition*, 13(11), 1203-1219.

Umadevi, S., Gopi, V., Simna, S., Parthasarathy, A., Yousuf, S. and Elangovan, V. (2012). Studies on the Cardio Protective Role of Gallic Acid Against AGE-Induced Cell Proliferation and Oxidative Stress in H9C2 (2-1) Cells. *Cardiovascular Toxicology*, 12(4), 304-311.

Urist, M.R. (1980). Bone transplants and implants. In *Fundamental and Clinical Bone Physiology*; MR, U., Ed.; JB Lippincott: Philadelphia, PA, USA, 331–368.

Usui, Y., Aoki, K., Narita, N., Murakami, N., Nakamura, I., Nakamura, K., Ishigaki, N., Yamazaki, H., Horiuchi, H., Kato, H., Taruta, S., Kim, Y., Endo, M. and Saito, N. (2008). Carbon Nanotubes with High Bone-Tissue Compatibility and Bone-Formation Acceleration Effects. *Small*, 4(2), 240-246.

van den Bos, T. and Beertsen, W. (1994). Mineralization of alkaline phosphatase-complexed collagenous implants in the rat: Relation with age, sex, and site of implantation. *Journal of Biomedical Materials Research*, 28(11), 1295-1301.

Van den Vreken, N., Pieters, I., De Maeyer, E., Jackers, G., Schacht, E., & Verbeeck, R. (2006). Apatite formation in composites of alpha-TCP and degradable polyesters. *Journal of Biomaterials Science-Polymer Edition*, 17(9), 953–967.

van Luyn, M., van Wachem, P., Damink, L., Dijkstra, P., Feijen, J. and Nieuwenhuis, P. (1992). Secondary cytotoxicity of cross-linked dermal sheep collagens during repeated exposure to human fibroblasts. *Biomaterials*, 13(14), 1017-1024.

Verborgt, O., Tatton, N., Majeska, R. and Schaffler, M. (2002). Spatial Distribution of Bax and Bcl-2 in Osteocytes After Bone Fatigue: Complementary Roles in Bone Remodeling Regulation?. *Journal of Bone and Mineral Research*, 17(5), 907-914.

Wajda, A. and Sitarz, M. (2018). Structural and microstructural comparison of bioactive melt-derived and gel-derived glasses from CaO-SiO2 binary system. *Ceramics International*, 44(8), 8856-8863.

Walzem, R., Dillard, C. and German, J. (2002). Whey Components: Millennia of Evolution Create Functionalities for Mammalian Nutrition: What We Know and What We May Be Overlooking. *Critical Reviews in Food Science and Nutrition*, 42(4), 353-375.

Wang, G., Zhang, J., Dewilde, A., Pal, A., Bello, D., Therrien, J., Braunhut, S. and Marx, K. (2012). Understanding and correcting for carbon nanotube interferences with a commercial LDH cytotoxicity assay. *Toxicology*, 299(2-3), 99-111.

Wang, W., Watari, F., Omori, M., Liao, S., Zhu, Y., Yokoyama, A., Uo, M., Kimura, H. and Ohkubo, A. (2007). Mechanical properties and biological behavior of carbon nanotube/polycarbosilane composites for implant materials. *Journal of Biomedical Materials Research Part B: Applied Biomaterials*, 82B(1), 223-230.

Webb, J. and Tricker, J. (2000). A review of fracture healing. *Current Orthopaedics*, 14(6), 457-463.

Wheeler, D. and Enneking, W. (2005). Allograft Bone Decreases in Strength In Vivo over Time. *Clinical Orthopaedics and Related Research*, 435, 36-42.

Wichterle, O. and Lim, D. (1960). Hydrophilic Gels for Biological Use. *Nature*, 185(4706), 117-118.

Wisotzki, E., Friedrich, R., Weidt, A., Alexiou, C., Mayr, S. and Zink, M. (2016). Cellular Response to Reagent-Free Electron-Irradiated Gelatin Hydrogels. *Macromolecular Bioscience*, 16(6), 914-924.

Wisotzki, E., Hennes, M., Schuldt, C., Engert, F., Knolle, W., Decker, U., Käs, J., Zink, M. and Mayr, S. (2014). Tailoring the material properties of gelatin hydrogels by high energy electron irradiation. *Journal of Materials Chemistry B*, 2(27), 4297-4309.

Yang, C., Chien, C., Yao, C., Hsiao, L., Huang, Y. and Wu, C. (2004). Mechanical Strain Induces Collagenase-3 (MMP-13) Expression in MC3T3-E1 Osteoblastic Cells. *Journal of Biological Chemistry*, 279(21), 22158-22165.

Yasmeen, S., Lo, M., Bajracharya, S. and Roldo, M. (2014). Injectable Scaffolds for Bone Regeneration. *Langmuir*, 30(43), 12977-12985.

Zhao, B., Hu, H., Mandal, S. and Haddon, R. (2005). A Bone Mimic Based on the Self-Assembly of Hydroxyapatite on Chemically Functionalized Single-Walled Carbon Nanotubes. *Chemistry of Materials*, 17(12), 3235-3241.

Zhao, F., Yao, D., Guo, R., Deng, L., Dong, A. and Zhang, J. (2015). Composites of Polymer Hydrogels and Nanoparticulate Systems for Biomedical and Pharmaceutical Applications. *Nanomaterials*, 5(4), 2054-2130.